PHOTOCATALYTIC OXIDATION OF HAZARDOUS AIR POLLUTANTS USING SILICA-TITANIA COMPOSITES IN A PACKED-BED REACTOR

By

JENNIFER MORGAN STOKKE

A DISSERTATION PRESENTED TO THE GRADUATE SCHOOL
OF THE UNIVERSITY OF FLORIDA IN PARTIAL FULFILLMENT
OF THE REQUIREMENTS FOR THE DEGREE OF
DOCTOR OF PHILOSOPHY

UNIVERSITY OF FLORIDA

2008

To my parents, Wayne and Susan

ACKNOWLEDGMENTS

I would first like to thank my parents and family for the love, guidance, and support that they have provided through the years. I would also like to thank my advisor, Dr. David Mazyck, for the guidance and opportunities that he has provided during my graduate education. I will certainly take away many lifelong lessons from this experience. I am grateful for the guidance and suggestions provided by my advisory committee, Dr. Paul Chadik, Dr. Chang-Yu Wu, and Dr. Hassan El-Shall, as well as those of Dr. Angela Lindner.

I would like to thank Rick Sheahan and Joe Sines of MicroEnergy Systems, Inc (Oakland, MD) for services related to pilot reactor fabrication and testing, Jim Stainfield from NCASI (Gainesville, FL) for providing analytical support, and Christina Akly, Heather Byrne, Teri Lierman, Paloma Rohrbaugh, Brendon Blum, Miguel Morales, Vanessa Pineda, Gustavo Avila, and Aly Byrne for their assistance in conducting laboratory studies. I am appreciative of the Department of Energy and American Forest Product Association for sponsoring a portion of this research via grant number DE-FC36-03ID14437.

Finally, I would like to thank past and present members of my research group for their support: Ameena Khan, Heather Byrne, Jennifer McElroy, Matthew Tennant, Thomas Chestnutt, Morgana Bach, Jack Drwiega, Miguel Morales, Vivek Shyamasundar, William Kostedt, IV, Christina Ludwig, and Alec Gruss.

TABLE OF CONTENTS

LIST OF TABLES

LIST OF FIGURES

Abstract of Dissertation Presented to the Graduate School
of the University of Florida in Partial Fulfillment of the
Requirements for the Degree of Doctor of Philosophy

PHOTOCATALYTIC OXIDATION OF HAZARDOUS AIR POLLUTANTS USING SILICA-TITANIA COMPOSITES IN A PACKED-BED REACTOR

By

Jennifer Morgan Stokke

May 2008

Chair: David W. Mazyck
Major: Environmental Engineering Sciences

This work centered on the optimization and scale-up of photocatalytic reactors employing silica-titania composites (STC) for two applications involving the abatement of hazardous air pollutants (HAPs) from industrial facilities: (1) degradation of HAPs, particularly methanol, emitted from pulp and paper mills; and (2) recovery of mercury emitted from chlor-alkali plants.

STC were synthesized with varying pore sizes (50 Å, 120 Å, and 260 Å) and TiO_2 loadings (0-60%) and were tested for the removal of methanol from a humid air stream. The efficiency of methanol oxidation was dependent on the surface area of the STC and the space time of the gas in the reactor. For 120 Å 12% and 260 Å 12% STC irradiated with UVA light, a lag time of 1.0 s and 1.2 s, respectively, was observed before mineralization began. After this lag time, which was zero for the 50 Å 12% STC, the data followed pseudo-first order reaction kinetics and the rate constant, k, was 0.40 s^{-1} for all pore sizes. Using the 50 Å STC, the efficiency was further improved by using a 4% TiO_2 loading and UVC lamp, which generated a higher photon flux compared to a UVA lamp. The presence of H_2S in the gas stream decreased methanol removal efficiency and resulted in SO_2 and SO_4^{2-} oxidation byproducts. When compared to other catalyst supports, the STC was more efficient in a low-humidity gas stream with a relative humidity (RH) of less than 0.22% at 23°C. In a high humidity gas stream (RH = 95% at 23°C), the efficiency of

the STC was inhibited by water vapor due to its surface chemistry and performed similarly to TiO_2-coated activated carbon. When compared to TiO_2-glass spheres, the use of an adsorbent catalyst support resulted in higher degradation efficiencies. Based on the promising bench-scale results, a 40 ACFM pilot reactor was fabricated employing a packed bed of STC and a 4.3 s space time through the packed bed. The pilot reactor achieved methanol removal rates up to 66 ± 7% with less than 1 ppm_v formaldehyde production at steady state.

A pilot-scale photocatalytic reactor packed with STC was tested at a chlor-alkali facility over a three-month period. This pilot reactor treated up to 10 ACFM of end-box exhaust and achieved 95% mercury removal. The pilot reactor was able to maintain excellent removal efficiency even with large fluctuations in influent mercury concentration (400-1600 ug/ft^3). The STC pellets were regenerated ex-situ with hydrochloric acid and performed similarly to virgin STC pellets when returned to service. Based on these promising results, two full-scale reactors with in-situ regeneration capabilities were installed and operated. After optimization, these reactors performed similarly to the pilot reactor. A cost analysis was performed comparing the treatment costs (i.e., cost per pound of mercury removed) for sulfur-impregnated activated carbon and the STC system. The STC proved to be both technologically and economically feasible for this installation.

CHAPTER 1
INTRODUCTION

Industrialized nations are faced with environmental problems related to the remediation of hazardous wastes, treatment of contaminated water, and control of air pollution from industries, military installations, and the civilian sector (Hoffmann et al., 1995). Hazardous air pollutants (HAPs) pose particular threats to human health or the environment due to their toxicity. The Clean Air Act requires the Environmental Protection Agency (EPA) to regulate emissions of 188 HAPs from industrial sources. Although a variety of technologies exist for the removal of HAPs, heterogeneous photocatalysis has the potential to offer significant benefits with respect to energy, size, and reliability compared to traditional technologies. Photocatalysis has proven effective at the bench-scale for the oxidation of a variety of organic compounds (e.g., alcohols, aliphatic compounds, aromatic compounds) to inert byproducts, such as CO_2 and H_2O (Hoffmann et al., 1995). In addition, inorganic compounds can undergo photocatalytic transformation, which can be manipulated to enhance removal by adsorption onto the catalyst surface or subsequent treatment processes (Huang et al., 1996; Nguyen et al., 2004; Pitoniak et al., 2003; Pitoniak et al., 2005; Ferguson et al., 2005).

Although much research has been devoted to photocatalysis for environmental applications, the testing and application of these systems beyond the bench-scale is limited. Photocatalytic systems for treatment of gas-phase contaminants typically employ a thin film of titania (TiO_2) on, for example, reactor walls, wire mesh, or glass beads (Alberici and Jardim, 1997; Dijkstra et al., 2002; Kim and Hong, 2002; Peral et al., 1997; Chang et al., 2000). These systems may not lend themselves well to scale up due to their low adsorption capacity, mass transfer limitations, and problems with catalyst immobilization or durability (Devilliers, 2006). In order to overcome these issues, a nano-structured silica-titania composite (STC) was

developed and has been tested at the bench-scale for the removal of mercury from synthetic flue gas (Pitoniak et al., 2003; Pitoniak et al., 2005; Li and Wu, 2006). The STC has also been tested for the degradation of organic compounds in water (Londeree, 2002; Holmes, 2003; Ludwig et al., 2008) and deactivation of pathogens (Garton, 2005). Although the results of these studies showed that the STC was capable of capturing mercury and completely degrading organic compounds, the STC had not been developed past the laboratory scale.

This work centered on the optimization and scale-up of STC for two new applications involving the abatement of HAPs emitted from industrial facilities: (1) degradation of HAPs, particularly methanol, emitted from pulp and paper mills; and (2) recovery of mercury emitted from chlor-alkali plants. These two applications are discussed in further detail below.

Degradation of HAPs Emitted from Pulp and Paper Mills

Forest products provide essential resources such as energy and materials. Compared to fossil fuels (e.g., coal and oil) the resources from forest products are more sustainable and diverse. However, the processing of forest products creates unwanted by-products including volatile organic compounds (VOCs), some of which are HAPs (Someshwar, 1994). VOCs can directly affect human health and are one of the main precursors of tropospheric ozone, a respiratory irritant in humans and a major contributor to smog formation. Maximum Achievable Control Technology (MACT) standards, as part of the 1998 Cluster Rules promulgated by the EPA, require that the concentration of HAPs in high volume low concentration (HVLC) gases emitted from pulp and paper mills be *decreased by at least 90%*.

Thermal oxidation is the most commonly applied technique for the control of VOC/HAP emissions from the forest products industry sources (Varma, 2003; Garner, 2001). While effective, these measures require a constant fuel supply to support the thermal energy requirements and create other unfavorable byproducts (such as NOx). In addition, the fans and

ductwork required for the transport of gases are costly since gas streams are usually directed to existing boilers (Varma, 2003). Thus, a cost-effective technique for in-situ treatment of these pollutants is needed.

This work focuses on optimizing the STC and reactor operating parameters for the treatment of HVLC gases emitted from pulp and paper mills, namely brown stock washers. Typical HVLC gases are composed of air saturated with water vapor and contain HAPs (such as methanol, acetaldehyde, formaldehyde), other VOCs (such as acetone and methyl ethyl ketone) and total reduced sulfur (TRS) species (Someshwar, 1994; Varma, 2003). Methanol is the primary constituent in HVLC gases and contributes to over 90% of the total HAP emissions from brown stock washer vent gases (Someshwar, 1994). A study conducted by the Someshwar (1994) at the National Council of Air and Stream Improvement found that the methanol concentration in vent gases at 16 pulp and paper mills ranged from 32 to 2,263 ppm_v. The range of concentrations was attributed to the type of washers, vent gas flow rates, and methanol concentration of the shower water. Vent gas flow rates were also found to be highly variable, ranging from 162 to 16,808 scfm (Someshwar, 1994).

This work presents the optimization of the STC properties (e.g, surface area, pore size, TiO_2 loading) and reactor parameters controlling mass transfer and photon flux to achieve 90% removal and complete oxidation of methanol, which was used as the target HAP. The competitive effects of water vapor and H_2S (a target TRS species) on methanol removal were studied since both constituents are present in HVLC gases. In addition, the removal of H_2S was investigated to understand if the STC can provide a co-benefit for odor removal. The performance of the STC was compared to that of TiO_2 coated on other catalyst supports (i.e.,

activated carbon and nonporous glass spheres). Finally, a 40 ft^3/min (ACFM) pilot reactor was designed and tested for methanol removal from a humid air stream.

The following hypotheses were investigated in this study:

- As the available total surface area of the STC increases, the rate of methanol oxidation will increase proportionally.
- The rate of methanol oxidation is limited by the resistance to mass transfer of the contaminant to the STC surface and the space time of the gas in the reactor.
- The distribution of ultraviolet (UV) light in the reactor will dictate the rate of methanol oxidation.
- The rate of methanol oxidation will be dependent on the transparency of the catalyst support, with more transparent supports achieving greater oxidation rates.
- TRS present in HVLC gases will be oxidized to sulfate on the catalyst surface, which will accumulate over time and occupy adsorption/oxidation sites thereby decreasing the rate of methanol oxidation.

The objectives of this research were as follows:

- Synthesize and characterize STC with various properties (i.e., pore size, surface area, and TiO_2 loading).
- Develop and optimize a bench-scale photocatalytic reactor using STC for the removal of VOCs/HAPs, using methanol as the target pollutant.
- Compare the silica gel to other catalyst supports with varying transparency and surface area.
- Assess the effects of water vapor and TRS on the removal of methanol.
- Design, fabricate and test a pilot-scale reactor for the optimization of VOCs/HAP removal using methanol as the target constituent.

Recovery of Mercury Vapor Emitted in End-Box Exhaust at Chlor-alkali Facilities

The release of mercury to the environment is of particular concern due to its volatility, persistence and tendency to bioaccumulate. Methylation of mercury by microbes in the environment results in the formation of methylmercury, which rapidly bioaccumulates in the cells of higher organisms in aquatic systems. Methyl mercury is magnified at each trophic level

of the food chain thereby threatening ecosystems as well as human health. The primary exposure route for humans is through the consumption of fish containing methylmercury (D'Itri et al., 1978). This exposure can lead to adverse neurological effects, particularly in the developing fetus and during early childhood (Schettler, 2001).

Mercury is released into the environment from anthropogenic sources such as coal-fired power plants, cement plants, waste incinerators, and manufacturing processes such as the chlor-alkali industry. The coal-fired power industry is the largest source of mercury in the United States, emitting about 43 tons of mercury in 1999 (Pavlish et al., 2003). Although emissions from coal-fired power plants are significant, other industries, such as the mercury-cell chlor-alkali industry, can emit more mercury on a per facility basis (EPA, 1997a). Mercury abatement from these sources is also crucial in order to protect human health and the environment. Therefore, this work focuses on the development and implementation of a photocatalytic technology for mercury recovery in the chlor-alkali industry.

The chlor-alkali industry produces valuable chemicals such as chlorine, hydrogen, and caustic soda. In 2001, between 150 and 200 chlor-alkali facilities throughout the world used the mercury-cell process. Although this process uses the mercury in a closed-loop system, mercury is released to the environment through entrainment in by-product streams, end-box ventilation systems and fugitive emissions (EPA, 1997b). According to Southworth et al. (2004), an average of about three tons of mercury per year must be added to the production process at each mercury-cell facility in the US to account for losses. The National Emissions Standard for Hazardous Air Pollutants (NESHAP) for mercury cell chlor-alkali plants requires these facilities to drastically reduce mercury emissions from their gas-phase emissions.

Due to these stricter standards, chlor-alkali facilities must either implement new control technologies or eliminate mercury from their process. A commercially-available control technology for reducing mercury emissions is activated carbon adsorption (EPA, 1997b; Anastas, 1976). While sulfur- or iodine-impregnated activated carbon may reduce mercury emissions to acceptable levels, it has a finite adsorption capacity and must be replaced and properly disposed as hazardous waste. Therefore, the mercury problem is being transferred from the air phase to the solid phase. The cost and risk associated with the continuous replacement and disposal of mercury-laden activated carbon can be limiting, as many mercury-cell facilities have chosen to convert to a mercury-free (e.g., membrane) process for manufacturing (EPA, 1997b). However, conversion to another process requires a large capital investment. Thus, a cost effective and regenerable solution is required for reducing mercury emissions.

This study focuses on the scale-up of the STC for use in the chlor-alkali industry, particularly for the recovery of mercury from end-box exhaust. The STC was originally developed at the bench-scale for mercury removal from flue gas emitted from coal-fired power plants. Pitoniak (2004) found that the adsorption capacity of the STC increased after periods of photocatalytic oxidation due to the formation of HgO on the composite surface. The total mercury (i.e., elemental and oxidized) adsorption capacity was $3\%_{wt}$, as determined by thermo gravimetric analysis. The STC could be regenerated by rinsing with acid.

The composition of end-box exhaust consists of air containing trace levels of hydrogen (< 0.02%), water vapor (saturated at 6 – 8 °C), entrained water droplets, and elemental mercury. The mercury concentration in end-box exhaust is typically two to three orders of magnitude higher than that in flue gas. The STC has the potential to be both technically and economically advantageous for the removal of mercury from end-box exhaust in chlor-alkali facilities because

of its high mercury adsorption capacity and ability to be regenerated with acid and re-used in bench-scale studies. The mercury-laden acid used for regeneration could be recycled into the mercury-cell process, thus closing the loop on mercury emissions. This work summarizes the design and performance of pilot- and full-scale reactors used to recover mercury from the end-box exhaust at a chlor-alkali facility. In addition, an economic analysis, which compares the costs of implementing this technology versus using activated carbon at the facility, is presented.

The following hypotheses were investigated in this study:

- The research involving mercury removal from simulated flue gas can be translated to mercury removal from caustic exhaust.
- Mass transfer and UV light distribution are the limiting factors for mercury removal from caustic exhaust.
- STC will be economically favorable when compared to activated carbon for the removal of mercury from end-box exhaust due to the ability of the STC to be regenerated and reused.

The objectives of this study were as follows:

- Confirm the efficacy of the technology for mercury removal from caustic exhaust and recovery of the sorbed mercury by regeneration with HCl in pilot and prototype studies at a chlor-alkali facility.
- Determine the factors that may limit mercury removal efficiency (e.g., residence time, mass transfer, and UV light distribution within the packed bed) in pilot-scale studies.
- Compare the cost of full-scale treatment units employing STC and activated carbon.

CHAPTER 2
LITERATURE REVIEW

Photocatalysis

When a semiconductor (e.g., TiO_2) is irradiated with UV light that has an energy equal to or greater than the band gap energy, an electron (e^-) is promoted from the valence band to the conduction band, leaving behind a positively charged hole (h^+) in the valence band. This reaction is shown in Equation 1 (Serpone, 1995; Hoffmann et al., 1995).

$$TiO_2 + h\nu \longrightarrow e^-_{CB} + h^+_{VB} \quad (2\text{-}1)$$

These electron-hole pairs can then recombine to generate heat or migrate to the surface and participate in redox reactions. The positively charged holes are powerful oxidants while the electrons in the conduction band can participate in reduction reactions.

Electron-hole pairs can oxidize organic pollutants directly via the electron hole or indirectly via the formation of other powerful oxidants (e.g., hydroxyl radicals). The hydroxyl radical (*OH), which has been identified as the primary oxidant in the photocatalytic oxidation of organic compounds (Turchi and Ollis, 1990) and inorganic compounds such as mercury (Pitoniak, et al. 2003; Pitoniak et al., 2005), can be generated via several pathways shown in Equations 2-2 through 2-8 (Al-Ekabi and Serpone, 1988).

$$H_2O + h_{VB}^+ \longrightarrow {}^*OH + H^+ \quad (2\text{-}2)$$

$$OH^- + h_{VB}^+ \longrightarrow {}^*OH \quad (2\text{-}3)$$

$$O_2 + 2H^+ + 2e^- \longrightarrow H_2O_2 \quad (2\text{-}4)$$

$$H_2O_2 + e^- \longrightarrow {}^*OH + OH^- \quad (2\text{-}5)$$

$$H_2O_2 \xrightarrow{h\nu} 2\,{}^*OH \quad (2\text{-}6)$$

$$O_2 + e^- \longrightarrow O_2^- \quad (2\text{-}7)$$

$$O_2^- + H_2O_2 \longrightarrow {}^*OH + OH^- + O_2 \quad (2\text{-}8)$$

Water or hydroxide ions adsorbed at the TiO_2 surface can trap electron holes (thereby preventing recombination) and form hydroxyl radicals (Equations 2-2 and 2-3). Thus, in gas-phase systems, relative humidity (RH) is often necessary for efficient oxidation of contaminants. However, some studies have shown that excess RH can decrease oxidation rates for some compounds due to the competitive adsorption between water and the target pollutant on the photocatalytic surface (Kim and Hong, 2002; Obee and Brown, 1995; Li and Wu, 2007). As shown in Equations 2-4 through 2-8, oxygen can serve as an electron acceptor (thus preventing electron-hole recombination) and create oxidative species such as the superoxide radical (O_2^-), which can also react to create hydroxyl radicals.

The photocatalytic oxidation of organic pollutants yields a series of intermediate byproducts of progressively higher carbon to oxygen ratios. If mineralization is achieved, inert byproducts, such as carbon dioxide, water, and dilute mineral acids (in the case of halogenated compounds) are formed (Ollis et al., 1991). Metals can be either oxidized or reduced via photocatalysis. This is advantageous for separation of metals from gas or liquid streams if the photocatalytically treated form of the metal is more easily removed by either sorption/deposition onto the catalyst surface or in subsequent treatment processes. For example, water entering a potable water treatment plant can be pretreated so that As(III) is oxidized to As(V), which is more easily removed by conventional water treatment processes (Ferguson et al., 2005). Removal of oxidized metals from water streams via photoreduction and subsequent deposition onto the surface of TiO_2 has proven effective for a variety of other metals such as silver (Huang et al., 1996), cadmium (Nguyen et al., 2003), and selenium (Nguyen et al., 2004). The photocatalytic oxidation of gas-phase elemental mercury (Hg^o) to HgO has resulted in enhanced

removal (Pitoniak et al., 2003). This enhanced removal of mercury via photocatalytic oxidation will be discussed in more detail later in this chapter.

Photocatalytic reactions can be catalyzed by a variety of semiconductor materials (e.g., TiO_2, ZnO, CdS, ZnS and Fe_2O_3) due to their electronic structure, which is comprised of a full valence band and empty conduction band (Hoffmann et al., 1995). TiO_2 is often used as a photocatalyst since it is commercially available, non-toxic, relatively inexpensive compared to heavy metal catalysts, and resistant to catalyst poisoning (Hurum et al., 2003). The principal catalytic phases of TiO_2 are anatase and rutile. Generally, anatase phase TiO_2 is regarded as the preferred phase due to its greater adsorption affinity for organic compounds and lower rate of electron-hole recombination (Hurum et al., 2003).

The inactivity of rutile TiO_2 is attributed to the rapid rate of electron-hole recombination. However, TiO_2 with a combination of anatase and rutile phases (such as Degussa P25) has been shown to have enhanced photocatalytic activity compared to pure anatase phase TiO_2. In mixed-phase systems, electrons generated by the rutile-phase TiO_2 can be transferred and trapped in lower energy anatase lattice sites. Degussa P25 contains unusually small nanoclusters of rutile crystallites dispersed within anatase crystallites. This morphology, which is responsible for the enhanced activity of Degussa P25, allows for the rapid transfer of electrons from rutile to anatase, resulting in catalytic "hot spots" at the rutile-anatase interface (Hurum et al., 2003). Due to its enhanced activity and commercial availability, Degussa P25 (70% anatase, 30% rutile) is frequently used in photocatalytic systems (Turchi and Ollis, 1989; Chen et al., 1999; Alberici and Jardim, 1997; Minero et al., 1992; Obee and Brown 1995).

TiO_2 is often immobilized as a thin film on various surfaces (e.g., beads, woven mesh, reactor walls) or on/in adsorbent materials (e.g., silica gel, alumina, activated carbon), which act

as catalyst supports. When TiO_2 is immobilized as a thin film, the photocatalytic reaction rate can be affected by mass transfer limitations (Ollis et al., 1991). The use of TiO_2 for practical applications is dependent on the immobilization of the TiO_2 particles onto a support such that the composite is durable, provides a reasonably high surface area, and allows accessibility to the immobilized catalyst (Shul et al., 2003). The use of adsorbent materials as catalyst supports is discussed in further detail below.

Use of Adsorbents as Catalyst Supports

By using an adsorbent catalyst support, the contaminant is concentrated around the photocatalyst. This has been shown to result in an increase in the photocatalytic reaction rate (Anderson and Bard, 1997; Tsumura et al., 2002; Vohra and Tanaka, 2003; Torimoto et al., 1996). In addition, organic contaminants are more likely to be mineralized since the intermediates, which can be toxic, can be retained and further oxidized (Torimoto et al., 1996; Lu et al., 1999).

Activated carbon is a commercially-available adsorbent material that has been studied for use as a catalyst support (Yong et al., 2005; Arana et al., 2004; Torimoto et al., 1996; Lu et al., 1999; Tsumura et al., 2002). Activated carbon is made by heating a carbonaceous precursor, usually wood or coal, in the presence of an activating agent (e.g., steam, carbon dioxide, oxygen). Properties of activated carbon such as surface area and pore size distribution are affected by the activation method (i.e., temperature, time, and activating agent). TiO_2 can be deposited onto the activated carbon by various methods such as boil deposition (Arana et al., 2004) or chemical impregnation (Yong et al., 2005). The use of activated carbon as a catalyst support has proven effective. For example, Arana et al. (2004) found that TiO_2-coated activated carbon was more efficient than bare TiO_2 for the mineralization of methanol. Lu et al. (1999) showed that granular activated carbon (GAC) was the most efficient catalyst support for the

degradation of propoxur when compared to other catalyst supports such as zeolite, brick, quartz, and glass beads. Bare TiO_2 achieved higher oxidation rates compared to the GAC/TiO_2. This was attributed to the blockage of photons by the GAC, which decreased the number of photons which reached the surface of the TiO_2 to promote oxidation reactions. Although the overall oxidation rate decreased, the mineralization rate of the TiO_2/GAC was greater than that of the bare TiO_2. The superior performance of the GAC compared to other catalyst supports and its ability to increase mineralization rates compared to bare TiO_2 were attributed to its adsorption properties.

Mixed oxide materials containing TiO_2 supported on silica (SiO_2) have also proven effective for a variety of photocatalytic reactions. SiO_2 is advantageous as a catalyst support since it has high thermal stability and excellent mechanical strength (Gao and Wachs, 1999). In addition, SiO_2 is transparent to UV light. SiO_2-TiO_2 mixed oxide materials are generally prepared by sol-gel and co-precipitation methods. The sol-gel hydrolysis route is most widely used due to the ability to control textural and surface properties of the resulting composite material (Gao and Wachs, 1999).

SiO_2- TiO_2 materials have shown superior catalytic efficiency due to quantum particle effects and the formation of Ti-O-Si linkages (Anderson and Bard, 1997; Gao and Wachs, 1999). Ti-O-Si linkages have resulted in enhanced adsorption of some contaminants (such as phenol and R6-G) via strong Bronsted acid sites, which led to enhanced degradation rates (Anderson and Bard, 1997; Yang and Chen, 2005). Yang and Chen (2005) also suggested that SiO_2 prevented electron-hole recombination by accepting electrons and providing hydroxyls for hole capture at the SiO_2-TiO_2 interface, thereby further increasing photocatalytic efficiency of SiO_2-TiO_2 composites compared to TiO_2 alone.

Shul et al. (2003) showed that the presence of SiO_2 as a catalyst support for TiO_2 helped to promote the efficiency of acetaldehyde degradation because the SiO_2 enhanced the effective surface area of the TiO_2 and increased the adsorption capacity of the composite compared to unsupported TiO_2. The photocatalytic activity of the composite increased with increasing surface area of the SiO_2 support. It was suggested that the increase in photocatalytic degradation rate was due to an increase in the concentration of reactants and intermediates near the TiO_2. Uchiyama et al. (2005) found that the incorporation of SiO_2 was also beneficial for the degradation of acetylacetone. Composites with Ti/Si ratios of 0 (pure SiO_2), 0.05, 0.25, 0.5, and 1.0 (pure TiO_2) were tested for acetylacetone adsorption and degradation. The amount of adsorbed acetaldehyde was proportional to the specific surface area of the material, whether it be unsupported TiO_2, SiO_2, or a composite of SiO_2 and TiO_2. The composite with Ti/Si = 0.05 achieved the highest rate of degradation, likely due to its high surface area (1103 m^2/g) and increased transparency compared to the other composites containing TiO_2. During the photocatalytic oxidation of acetylacetone, molecules that were adsorbed on the SiO_2 transferred to the photocatalyst, due to the concentration gradient on the surface of the composite, where they were subsequently oxidized.

Xu et al. (1997) also showed that TiO_2 supported onto a silica gel substrate resulted in higher degradation efficiencies for the oxidation of acetophenone in water compared to unsupported TiO_2. The supported TiO_2 showed higher photoactivity when supported on smaller SiO_2 particles. This suggests that the dispersing effect of the SiO_2 support on the TiO_2 particles was operative in enhancing its photoactivity.

Photocatalytic Degradation of Methanol

The photocatalytic oxidation of methanol can proceed via two pathways: (1) direct oxidation (Pathway 1), where methanol and its organic byproducts are oxidized by the electron

hole and mineralized to CO_2; and (2) indirect oxidation (Pathway 2), where methanol and its organic byproducts are oxidized by adsorbed *OH and mineralized to CO_2 and H_2O (Chen et al., 1999).

The reactions for Pathway 1 (direct oxidation) are shown in Equations 2-9 through 2-15.

$$CH_3OH + -s \longrightarrow CH_3O^-_s + H^+ \quad (2\text{-}9)$$

$$CH_3O^-_s + h^+ \longrightarrow CH_3O_s^* \quad (2\text{-}10)$$

$$CH_3O_s^* + h^+ \longrightarrow CH_2O_s + H^+ \quad (2\text{-}11)$$

$$CH_2O_s + h^+ \longrightarrow CHO_s^* + H^+ \quad (2\text{-}12)$$

$$CHO_s^* + h^+ + H_2O \longrightarrow CHOOH_s + H^+ \quad (2\text{-}13)$$

$$CHOOH_s + h^+ \longrightarrow CHOO_s^* + H^+ \quad (2\text{-}14)$$

$$CHOO_s^* + h^+ \longrightarrow CO_{2s} + H^+ \quad (2\text{-}15)$$

The reactions for Pathway 2 (indirect oxidation) are shown in Equations 2-16 through 2-22.

$$H_2O_s + h^+ \longrightarrow {}^*OH_s + H^+ \quad (2\text{-}16)$$

$$CH_3O^-_s + {}^*OH_s \longrightarrow CH_3O_s^* + OH^-_s \quad (2\text{-}17)$$

$$CH_3O_s^* + {}^*OH_s \longrightarrow CH_2O_s + H_2O_s \quad (2\text{-}18)$$

$$CH_2O_s + {}^*OH_s \longrightarrow CHO_s^* + H_2O_s \quad (2\text{-}19)$$

$$CHO_s^* + {}^*OH_s \longrightarrow CHOOH_s \quad (2\text{-}20)$$

$$CHOOHs + {}^*OH_s \longrightarrow CHOO_s^* + H_2O_s \quad (2\text{-}21)$$

$$CHOO_s^* + {}^*OH_s \longrightarrow CO_{2s} + H_2O_s \quad (2\text{-}22)$$

The H^+ product from the above reactions can react with O_2 to form H_2O via the reduction reaction shown in Equation 2-23 (Noguchi et al., 1998).

$$O_2 + 4e^- + 4H^+ \longrightarrow 2H_2O \quad (2\text{-}23)$$

It is generally reported that the degradation of organic molecules via photocatalytic oxidation proceeds by the formation and subsequent reaction with hydroxyl radicals (Pathway 2) (Turchi and Ollis, 1990; Hoffmann et al., 1995; Obee and Brown, 1996). According to Kim and Hong (2002), methanol degradation was achieved using a TiO_2 thin film in the absence of water vapor. They suggested that methanol was oxidized by hydroxyl radicals that were formed from the hydroxyl groups of the methanol. The degradation rate reached an optimum at a water vapor concentration of 0.383 mol/m^3. At water vapor concentrations higher than the optimum, the degradation efficiency decreased suggesting that water molecules competitively adsorbed to catalyst surface thereby decreasing the degradation rate.

Yamakata et al. (2003) suggested an alternative mechanism for the photocatalytic oxidation of methanol, whereby methanol is oxidized directly by the electron hole, even in the presence of water vapor. In their study, the adsorbed water vapor was responsible for the electron-consuming reaction while methanol was responsible for the hole consuming reaction. The results suggested that the hole directly reacted with methanol, which adsorbed on the TiO_2 surface as the methoxy species (CH_3O^-), and that the hydroxyl radicals did not play a role in the photocatalytic oxidation since the highest activity of hole consuming reactions was achieved in the absence of water vapor. They suggested that water vapor enhanced the photocatalytic oxidation of methanol by preventing electron accumulation, which would otherwise cause defective sites on the TiO_2 surface, and electron-hole recombination.

Literature generally suggests that methanol is degraded first to formaldehyde, then to formic acid, and finally to carbon dioxide and water (Lichtin et al., 1994; Tsuru et al., 2003; Chen et al., 1999), which corresponds to both Pathway 1 and Pathway 2 described above. Some have suggested alternative pathways that result in the formation of formates, particularly methyl

formate (Tsuru et al., 2003; Sadeghi et al., 1996; Arana et al., 2004). Tsuru et al. (2003) found low levels of methyl formate in the effluent when degrading methanol using TiO_2 membranes. They suggested that the presence of methyl formate was a result of esterification reactions between methanol and formic acid. Arana et al. (2004) studied methanol degradation using a flow-through column (4 mm diameter, 15 mm height) packed with Degussa P25 TiO_2. They observed no mineralization of methanol and concluded from FTIR studies that bare TiO_2 did not degrade methanol due to the fast production of formates that resulted from methoxide (CH_3O^-), which poisoned the active centers of the photocatalyst.

The results from Arana et al. (2004) contradict those reported by Alberici and Jardim (1997) and Kim and Hong (2002). Alberici and Jardim (1997) found that a TiO_2 thin film achieved 98% degradation of methanol with no catalyst deactivation. In addition, no intermediate oxidation byproducts were present in the effluent, which is likely a result of the long residence time (approximately 2 min) used in the experiments. Kim and Hong (2002) also observed that methanol degradation was achieved using a TiO_2 thin film.

For studies in which methanol degradation was achieved, the degradation rate of methanol depended on variables such as the influent methanol concentration (Kim and Hong, 2002; Tsuru et al., 2003), water vapor concentration (Kim and Hong, 2002), residence time (Tsuru et al., 2003) and photon flux of the UV lamp (Kim and Hong, 2002; Alberici and Jardim, 1997). Tsuru et al. (2003) reported that a decrease in flow rate yielded greater mineralization due to the resulting increase in residence time. The degradation rate of methanol generally followed Langmuir-Hinshelwood kinetics such that the reaction was first order at low concentration and zero order at high concentrations (Kim and Hong, 2002; Tsuru et al., 2003). This transition occurred at influent concentrations greater than 500 ppm_v for Kim and Hong (2002) and greater

than 4000 ppm_v for Tsuru et al. (2003). The concentration in which the reaction order transitions from first order to zero order varied based on the reactor system and experimental conditions. Tsuru et al. (2003) also found that the conversion of degraded methanol to carbon dioxide and water was not dependent on influent methanol concentration, indicating that higher levels of intermediate byproducts were formed as a result of increased influent methanol concentration.

The intrinsic rate of photocatalytic reactions is limited by the photon flux of the UV light source (Hoffmann et al., 1995). For illumination levels above one sun equivalent, the oxidation rate generally increases with the square root of the light intensity. For levels below one sun equivalent, the oxidation rate increases linearly with light intensity. One sun equivalent is about 1 to 2 mW/cm^2 (Obee and Brown, 1995). Kim and Hong (2002) reported that the degradation rate of methanol was dependent on the photon flux of UV light such that the photocatalytic degradation rate increased with the square root of the photon flux. When the degradation efficiency of methanol was tested using a black lamp (peak wavelength = 352 nm) and a germicidal lamp (peak wavelength = 254 nm), the germicidal lamp resulted in higher degradation rates. Since the band gap energy of anatase phase TiO_2 is 3.2 eV, photons with wavelengths less than 385 nm are required to excite the photocatalyst. Thus, both the black lamp and germicidal lamps can be used to promote photocatalytic reactions. It should be noted that more energetic irradiation, such as that provided by a germicidal lamp, may affect the degradation efficiency by direct photolysis of the organic compound or the formation of radicals that may alter conversion yields (Alberici and Jardim, 1997). Kim and Hong (2002) attributed the higher degradation rates observed with the germicidal lamp to the greater photon flux emitted from this lamp compared to the black lamp. They reported that the photon flux from the germicidal lamp was about two times that emitted from the black lamp. These results contrast with those reported by Alberici

and Jardim (1997), who showed that a germicidal lamp did not increase degradation rates of any VOC (including methanol) compared to a black lamp. In these studies, both the germicidal and black lamp had a nominal power rating of 30W; however, the radiant power output of the germicidal lamp was 25% greater than that of the black lamp.

Photocatalytic Oxidation of H_2S

While many studies have been performed using TiO_2 for the degradation of VOCs, few of these studies have investigated the oxidation and removal of inorganic or sulfur-containing compounds. The photocatalytic reaction of H_2S with TiO_2 has the potential to form byproducts such as SO_2, SO_4^{2-}, and elemental sulfur. In order to completely oxidize H_2S to SO_4^{2-}, an eight electron transfer is required. The formation of SO_4^{2-} would result in deposition onto the surface of the TiO_2, since this species does not exist in the gas phase (Kataoka et al., 2005). Likewise, the elemental sulfur that could be formed as a byproduct would also deposit on the surface of the catalyst. This sulfur/sulfate deposition could potentially deactivate the catalyst over time by blocking active sites. Alternatively, SO_2 that could be formed as a result of the oxidation of H_2S could desorb back into this gas stream. Since SO_2 is a toxic gas and regulated by the EPA, subsequent removal processes (e.g., wet scrubbing) would be required to remove this gas.

Canela et al. (1998) and Kataoka et al. (2005) investigated the oxidation of H_2S using a TiO_2 thin film and found that SO_4^{2-} was formed and accumulated on the TiO_2 surface without producing any gaseous intermediates (e.g., SO_2). Portela et al. (2007) studied the oxidation of H_2S using TiO_2 thin films coated on polymeric materials and found that both SO_4^{2-} and SO_2 were produced as oxidation products. The accumulation of SO_4^{2-} on the TiO_2 surface resulted in a decrease in oxidation efficiency over the 15 hour duration of the experiments. Canela et al. (1998) experienced no catalyst deactivation over a 20 hour period when the influent H_2S concentration was 217 ppm_v. However, when the inlet concentration was increased to 600 ppm_v,

catalyst deactivation occurred, decreasing the removal efficiency from 99% to 36% after 2 hours. However, it was not clear whether the decrease in efficiency was a result of the accumulation of byproducts or the reactor temperature increasing from ambient (about 22°C) to a working temperature of 52°C as a result of turning on the lamp. This increase in temperature could decrease adsorption of H_2S onto the TiO_2, which could subsequently decrease the oxidation rate.

Washing the catalyst with deionized water was sufficient to remove the majority of the accumulated SO_4^{2-} (Portela et al., 2007; Canela et al., 1998). Canela et al. (1998) recovered 95% of the SO_4^{2-} that accumulated on the catalyst. Panela et al. (2007) removed the majority of the SO_4^{2-} from the catalyst after the first rinse and tested the catalysts for their ability to oxidize H_2S after multiple regenerations. They found that the water wash restored most of the initial activity of the photocatalyst.

Variables such as residence time, humidity, and initial H_2S concentration have been found to effect the degradation efficiency of H_2S using a TiO_2 thin film. Canela et al. (1998) studied the effect of residence time on H_2S conversion efficiency. The results indicated that increasing space time between 0.27 min and 2.46 min resulted in an increase in the conversion efficiency from about 35% to 95%. In the same study, they found that the reaction exhibited a pseudo-first order dependence on H_2S concentration at influent concentrations between 30 ppm_v and 855 ppm_v.

Water vapor concentration is often an important variable when studying the efficiency of photocatalytic reactions. Portela et al. (2007) found that the optimal humidity for oxidation of H_2S was 20% when studying air containing 35 ppm_v of H_2S and various RHs between 0 and 70% (at 40°C). It was hypothesized that water vapor played a key role in the reaction due to hole

trapping and hydroxyl radical formation. However, above 20% RH, the water vapor was thought to hinder photocatalytic oxidation due to its competition with H_2S for adsorption sites.

In a study by Kato et al. (2005), the incorporation of Ag nanoparticles onto a TiO_2 filter resulted in photocatalytic oxidation rates seven times higher than that of the un-modified TiO_2. X-ray photoelectron spectroscopy showed that H_2S, elemental sulfur, AgS, and SO_2 were not present on the Ag-TiO_2 film after use. Additionally, no byproducts were identified in the effluent gas stream. SO_4^{2-}, which was trapped on the photocatalyst, was the only byproduct present. However, the efficiency of H_2S removal did not degrade over the duration of the experiment (approximately 9 hours). It was hypothesized that the deposition of a noble metal, such as Ag, would enhance photocatalytic reaction rates by increasing the charge separation efficiency and inhibiting electron-hole recombination. In addition, the Ag enhanced the adsorption capacity of the Ag- TiO_2 film, which could have also led to increased oxidation rates. There was no measurable adsorption of H_2S onto the un-modified TiO_2. The adsorption of compounds onto TiO_2, or other hydrous oxides, is most often attributed to hydrogen bonding. Hydrogen bonds form between two functional groups, one which serves as a Bronsted acid and the other as a Lewis base. According to Sopyan (2007), H_2S does not readily form bonds with the hydroxyl groups on TiO_2 surfaces and has been shown to form hydrogen bonds in only strong basic environments. In the same study, ammonia, which is a strong Lewis base, showed adsorption capacity ten times greater than that of H_2S as a result of its ability to participate in hydrogen bonding with the TiO_2 surface.

Enhanced Mercury Recovery using Photocatalysis

The removal of mercury via photocatalysis has been investigated for application in flue gases at coal-fired power plants. Under UV irradiation, TiO_2 converts Hg^o to HgO (as shown in Equations 2-24 and 2-25), which is retained on the TiO_2 surface (Rodriguez et al., 2004).

$$Hg^o + {}^*OH \longrightarrow HgOH \quad (2\text{-}24)$$

$$HgOH \longrightarrow HgO + H^+ \quad (2\text{-}25)$$

In general, two approaches have been studied for Hg removal using TiO_2: (1) Hg^o oxidation and capture on in-situ generated TiO_2 particles (Wu et al., 1998; Lee et al., 2004; Lee et al., 2001; Rodriguez et al., 2004); and (2) synergistic adsorption and oxidation of Hg^o using STC pellets in a packed bed (Pitoniak et al., 2003; Pitoniak et al., 2005; Li and Wu, 2006; Li and Wu, 2007).

In-situ generated TiO_2 particles have been created by the injection of a TiO_2 sorbent precursor into the combustor system. The precursor injection conditions were manipulated such that agglomerated nano-sized (20-30 nm) TiO_2 particles were formed. These agglomerates had a high surface area and open structure, which would allow effective UV irradiation and minimal resistance to mass transfer. The in-situ generated TiO_2 particles showed no Hg capture in the absence of UV irradiation, indicating that physical adsorption was not an effective pathway for removal (Lee et al., 2004). However, in the presence of UV irradiation, the TiO_2 particles removed greater than 98% of the influent mercury (Lee et al., 2001). Water vapor enhanced mercury removal at low concentrations by increasing hydroxyl radical generation on the TiO_2 surface, which increased the number of active sites for oxidation and capture of Hg^o. At very high water vapor concentrations, it was expected that the water vapor would inhibit Hg removal due to competition for adsorption sites, which would reduce the number of available sites for the oxidation of Hg^o (Rodriguez et al., 2004).

A novel, high surface area silica-gel impregnated with TiO_2 nanoparticles for mercury vapor control from flue gas was developed by Pitoniak et al. (2003, 2005) and has been further developed by Li and Wu (2006, 2007). In this work, this material is referred to as STC. The

STC exhibited synergistic adsorption and photocatalytic oxidation for enhanced mercury removal. Mercury vapor was adsorbed onto the STC surface and subsequently oxidized and retained after irradiation with UV light. Mercury capture was achieved with continuous or intermittent UV radiation. When intermittent UV irradiation was applied, Hg adsorption increased after the periods of UV irradiation.

The STC demonstrated a high capacity for mercury (10 - 30 mg/g) (Pitoniak et al., 2005) and achieved high levels of Hg removal (greater than 99%) when continuously irradiated with UV light using a 0.78 s residence time (Pitoniak et al., 2003). Studies investigating the impact on residence time of Hg removal revealed that the removal efficiency decreased as the residence time decreased from 0.78 s to 0.16 s. It was determined that adsorption was the rate limiting factor and that mass transfer should be improved to achieve better removal (Pitoniak et al., 2003).

Li and Wu (2007) determined that mercury removal using the STC followed Langmuir-Hinshelwood kinetics. These results suggested that the STC has a great potential for the removal of mercury from gas streams containing high levels of Hg^o. However, it was also found that water vapor significantly inhibited the capture of mercury (Li and Wu, 2006; Li and Wu, 2007). The STC achieved the highest level of mercury removal in the absence of water vapor. Li and Wu (2007) postulated that the source of hydroxyl radicals in the absence of water vapor may be the silanol groups on the SiO_2 surface, which may serve as a the source for hydroxyl radical production. The decrease in capture efficiency as the water vapor concentration increased was likely due to competitive adsorption (Li and Wu, 2007). In addition, water vapor resulted in the re-emission of captured mercury from the STC due to the repellent effect of water and the

photocatalytic reduction of HgO to Hg^o, which subsequently desorbed from the STC surface. The proposed mechanism for the reduction of HgO is show in Equation 2-26 (Li and Wu, 2006).

$$HgO + H_2O + 2e^- \longrightarrow Hg^o + 2\ OH^- \quad (2\text{-}26)$$

Although the re-emission of mercury affected the overall capture efficiency of the STC, Li and Wu (2006) concluded that re-emission could be minimized by the appropriate application of UV irradiation.

An advantage of the STC over other adsorbents is that it can be regenerated by rinsing with acid (Pitoniak et al., 2003). The acid wash removed the mercury from the surface of the STC by transferring it into the acid solution. Although the majority of the captured mercury was recovered by the acid rinse, the performance of the regenerated pellets was not reported.

CHAPTER 3
EXPERIMENTAL

Synthesis of Photocatalytic Materials

Silica-Titania Composite (STC) Pellets

The STC pellets were prepared using an acid-catalyzed, sol-gel technique with tetraethyl orthosilicate (TEOS) as the silica precursor. Degussa P25 TiO_2 was used as the TiO_2 source and was mixed into the liquid precursors before gelation. Nitric acid and hydrofluoric acid (HF) were used to catalyze hydrolysis and condensation reactions, thereby decreasing the time to gelation. The pore size of the STC was manipulated by varying the amount of HF used during synthesis.

For bench-scale studies, TEOS (Fisher Scientific, reagent grade) was added to a solution of deionized water and ethanol (Aaper Alcohol, 200 proof) using a TEOS:water:ethanol volume ratio of 7:5:10. To catalyze the reaction, 1 N nitric acid, prepared from 15.8 N nitric acid (Fisher Scientific, certified A.C.S.), and $3\%_{wt}$ HF, prepared from $48\%_{wt}$ HF (Fisher Scientific, certified A.C.S.), were added to the solution. In order to vary the pore size of the STC, either 2, 4, or 8 mL of $3\%_{wt}$ HF per 220 mL of TEOS/ethanol/water solution. For every 100 mL of TEOS, 1 to 60 g of Degussa P25 TiO_2 (Majemac Enterprises) were mixed into the solution. The ingredients were mixed via a magnetic stir plate before being transferred into 96-well assay plates, where the solution gelled as cylindrical pellets. The assay plates were sealed and the pellets aged at room temperature for 48 hours and then at 65°C for 48 hours. The pellets were then transferred to Teflon containers, whose lids had a pin-sized hole, and dried for 18 hours at 103°C followed by 6 hours at 180°C. Each lid had a small hole to allow the liquid expelled from the pores of the STC pellets to slowly escape as vapor during the drying process, thereby preventing collapse of

the pores. Finally, the STC pellets were calcined at 450°C for 2 hours. The resulting STC pellets were about 3 mm in diameter and 5 mm in length.

In order to produce a sufficient quantity of STC pellets for the pilot and full-scale studies, the bench-scale synthesis method was modified to increase production efficiency while producing composites with similar characteristics (i.e., surface area and pore size). TEOS (Silbond Condensed) was added to water, ethanol (Spectrum Chemicals), 1 N nitric acid, prepared from 15.8 N nitric acid (Fisher Scientific, certified A.C.S.), and 3%$_w$ HF, prepared from 48%$_w$ HF (Fisher Scientific, certified A.C.S.). A known mass of Degussa P25 TiO_2 (Majemac Enterprises) was mixed into the solution based on a ratio of 4 g of TiO_2 per 100 mL of TEOS. The ingredients were stirred using a paddle mixer and then transferred to molds, which were made from 5.1 cm thick polyethylene sheets drilled with 0.8 cm diameter holes. Each mold was approximately 40.6 cm by 61.0 cm and contained 2,750 holes. The molds were filled by pouring the liquid sol into the molds, which were sealed on the bottom and top with sheets of solid polyethylene. The gels were aged at 65°C for 48 hours. The lids were then loosened and the pellets dried in the molds at 103°C. The pellets were removed from the molds, transferred to Pyrex containers, and then heated to 180°C. After aging and drying, pellets were approximately 3 mm in diameter and 20 mm in length.

TiO_2-Coated Activated Carbon (AC)

TiO_2-coated AC was synthesized by coating granular BioNuchar120 (MeadWestvaco) with Degussa P25 TiO_2 via a boil deposition method. A TiO_2 slurry was made by adding 3 g of Degussa P25 TiO_2 to 200 mL of DI water. Next, 30 g of AC were added to the slurry and heated on a hot plate until all of the water evaporated, leaving the TiO_2 coated onto the outer surface of the AC. The actual quantity of TiO_2 deposited on the AC was determined by taking the difference of the measured ash content of the as-received and TiO_2-coated AC. To determine the

ash content of an AC sample, about 1 g of dry material was heated to 550°C for 24 hours to remove the carbonaceous portion of the AC. The measured TiO_2 loading on the AC was 5.0 ± 0.4 $\%_{wt}$ (error given as the standard deviation of triplicate measurements).

TiO_2-Coated Glass Spheres

Solid glass spheres (5 mm diameter) were coated with a TiO_2 slurry (20$\%_{wt}$ Degussa P25 TiO_2 dispersed in water) and then dried at 110°C. After drying, excess TiO_2 was separated from the TiO_2-coated glass spheres by gently shaking the beads on a sieve with 4 mm openings. The mass of the spheres was measured before and after the TiO_2 coating was applied. The resulting mass of TiO_2 on each glass sphere was 0.925 mg, which equates to 11.75 g of TiO_2 per m^2 of glass spheres. The BET surface area of the TiO_2 (as measured by a Quantachrome NOVA 2200e, Boynton Beach, FL) was approximately 50 m^2/g.

Characterization of Photocatalytic Materials

The STC pellets and TiO_2-coated AC were analyzed for surface area, total pore volume, and average pore size using a Quantachrome NOVA 2200e (Boynton Beach, FL). A Quantachrome Autosorb was used for nitrogen adsorption/desorption isotherms. The samples were vacuum outgassed at 180°C for 24 hours. The surface area was determined using the Brunauer-Emmett-Teller (BET) model with the nitrogen adsorption data (P/Po = 0.1 to 0.3). The total pore volume was calculated based on nitrogen adsorption at P/Po = 0.995. The average pore size was calculated using Equation 3-1, assuming non-intersecting, cylindrical pores:

$$d = 4*V_p/S \quad (3\text{-}1)$$

where d is the average pore diameter, S is the surface area, and V_p is the total pore volume. For the analysis of pore size distribution, the desorption isotherm was analyzed using the Barrett, Joyner, and Halenda (BJH) method.

Bench-scale Reactor for Methanol and H_2S Removal Studies

The adsorption and photocatalytic oxidation of HAPs in a simulated HVLC gas emitted from pulp and paper mills were tested using a bench-scale annular reactor. The reactor had an 8 mm annulus and contained an eight-watt UV bulb (Spectronics Corporation) with a peak wavelength of either 365 nm (UVA) or 254 nm (UVC). The UV bulb was surrounded by a quartz tube, which had an outside diameter of 25 mm. A schematic of the reactor is shown in Figure 3a. UV intensity measurements inside of the reactor were taken using chemical (potassium ferrioxalate) actinometry as described by Murov et al. (1993).

A known quantity of photocatalytic material (STC, TiO_2-coated AC, or TiO_2-coated glass spheres) varying between 30 and 90 cm^3 (bulk volume) was packed into the annulus of the reactor. Where specified, an annular reactor with a 25 mm annulus was used for preliminary scale-up studies. For these studies, 132 cm^3 of photocatalytic material were packed into the annulus. A schematic of the 25 mm annulus reactor is shown in Figure 3b.

The materials were tested for adsorption capacity in the dark and for simultaneous adsorption and photocatalytic activity when irradiated with UV light. The reactor was kept in the ambient atmosphere and, when irradiated with UV light, the temperature of the packed bed rose to about 50°C. In order to achieve this temperature during adsorption studies, the reactor was wrapped with heat tape and controlled using a Variac variable voltage transformer.

Compressed air containing 1000 ppm_v of methanol or H_2S was diluted with air to obtain an influent gas stream containing 50 ppm_v of methanol and/or H_2S and a RH less than 0.22%. For the experiments requiring a high humidity, the dilution air was passed through a water bubbler to obtain an influent gas stream with an RH of about 95% at 23°C. The gas stream flowed continuously through the reactor in a single pass configuration. A schematic of the reactor set-up is shown in Figure 3-1. Initial studies performed with an empty reactor showed no photolysis of

methanol or H_2S in the presence of UVA or UVC light. Similarly, adsorption of methanol and H_2S to the reactor and its appurtenances was negligible.

Various experiments were conducted to study the effects of space time and face velocity on methanol removal using STC pellets packed in the 8 mm reactor. Space time (τ) is the time required to process one bed volume of gas in an empty reactor and was calculated using Equation 3-2:

$$\tau = V/Q \quad (3\text{-}2)$$

where Q is the gas flow rate and V is the reactor volume occupied by the packed bed. The face velocity, or superficial velocity (v), was calculated using Equation 3-3:

$$v = Q/A \quad (3\text{-}3)$$

where A is the cross-sectional area of the packed bed.

Space times were varied between 1.1 s and 4.3 s in the 8 mm reactor by varying the gas flow rate (0.42 – 1.68 L/min) passing through a 30 cm^3 packed bed. The effect of face velocity on methanol removal was studied by flowing 0.42, 0.84, and 1.26 L/min of gas through STC bed volumes of 30, 60, and 90 cm^3, respectively, to achieve a constant space time of 4.3 s and face velocities of 0.093 m/s, 0.19 m/s, and 0.28 m/s.

Pilot Reactor for Methanol Removal

A 40 ACFM pilot reactor was designed and fabricated based on optimization studies conducted at the bench-scale. A water/methanol mixture was vaporized and injected into the gas stream so that the influent methanol concentration was about 50 ppm_v and RH between 95 and 99%. The static pressure and velocity pressure were monitored before the inlet to the pilot reactor. Thermocouples were used to measure inlet and outlet temperatures.

A UVP radiometer (Upland, CA) was used to measure the UV intensity through an observation window on the side of the reactor. Initial studies performed with an empty reactor showed no photolysis of methanol and that adsorption of methanol to the reactor and its appurtenances was negligible.

Analysis of Methanol and Oxidation Byproducts

Both influent and effluent methanol concentrations for bench- and pilot-scale studies were tested using the National Council for Air and Stream Improvement (NCASI) Chilled Impinger Method (NCASI, 1995). Methanol concentrations were quantified using a PerkinElmer Clarus 500 GC/FID (Wellesly, MA) with a 50 m x 320 μm polyethylene glycol column. A 1 μL volume of sample was used for analysis. The injector temperature was set to 110°C. The oven temperature was initially 40°C (1 min hold) and was ramped to 54°C at 2°C/min (2 min hold) and then to 220°C at 21°C/min (5 min hold). The minimum detection limit (MDL) for methanol in the gas phase was 0.6 ppm_v. Effluent formaldehyde concentrations were quantified colorimetrically using a Hach DR/4000U spectrophotometer (Loveland, CO) as described in the NCASI Chilled Impinger Method (NCASI, 1995). The MDL for formaldehyde was 0.014 ppm_v. In order to quantify total byproduct formation, total organic carbon (TOC) concentrations of the impinger samples were determined using a Tekmar Dohrmann Apollo 9000 TOC analyzer (Mason, Ohio). In addition to impinger measurements, real-time influent and effluent measurements were taken during the pilot studies using a ThermoElectron TVA-1000B portable FID detector (Waltham, MA).

Analysis of H_2S and Oxidation Byproducts

Air-phase concentrations of H_2S were measured by passing 100 mL of gas through pre-calibrated, direct-read Nextteq gas detection tubes (0.25 – 120 ppm_v). Air-phase concentrations

of SO_2 were measured using a Varian 2100T GC/MS (Palo Alto, CA) equipped with a Supel-Q Plot, 30 m x 0.32 mm column. Samples were collected in 1 L Tedlar bags and stored in the dark for no longer than 24 hours. A 75 um Carboxen-PDMS SPME fiber was injected into the Tedlar bag through a silicon septum for 10 min. The fiber was injected into the GC-MS for 5 min at an injection temperature of 200 °C. The oven temperature was initially 45°C and ramped to 250°C a rate of 25°C/min after an initial 0.75 min hold. The instrument detection limit for SO_2 was 1 ppm_v.

Sulfate loading on the STC pellets was measured by soaking 30 cm^3 of pellets in 500 mL of nanopure water (18.2 MΩ-cm) with gentle stirring using a magnetic stirrer for 24 hours. The water was filtered using a 0.45 μm vacuum filter. A 10 mL sample of filtered water was analyzed for sulfate using the EPA Method 9038 with a Hach DR/4000U spectrophotometer (Loveland, CO). The MDL for sulfate measurements was 1 mg/L.

Mercury Analysis

Influent and effluent mercury concentrations for pilot and full-scale mercury removal units were determined using EPA Method 101. The MDL for mercury corresponded to an air-phase concentration of 0.1 $\mu g/ft^3$.

For pilot-scale studies, STC pellets were regenerated ex-situ to remove the mercury. The pellets were removed from the reactor, placed in a bath of 37%$_{wt}$ HCl and mixed gently for 1 hour. The pellets were then rinsed with water and placed in an oven at about 70°C for 12 hours. The mercury concentration of the pellets was determined before and after regeneration by digesting 1 g of pellets in 50 mL of aqua regia solution. The mercury concentration of this solution was measured using a Hydra AA Spectrophotometer (Leeman Labs), which has an

MDL of 0.2 μg/L. The moisture content of the pellets after heat treatment at 70°C was about 60%, as determined by gravimetric analysis.

For full-scale studies, regeneration was performed in-situ by soaking the pellets inside of the reactor with $37\%_{wt}$ HCl for 30 min. After draining the mercury-laden acid from the reactor, the pellets were soaked with water for 30 min and the water was subsequently drained.

Colburn j-factor

The Colburn j-factor (j_d) is a dimensionless parameter for mass transfer based on Reynold's number (Re) and the shape, size and packing characteristics of the STC pellets. This parameter was used to assess the effects of mass transfer on the performance of the pilot reactor and as a design parameter for the full-scale reactors. The j-factor was calculated using Equations 3-4 through 3-7, where Ψ is the shape factor (0.91 for cylindrical pellets), v is the superficial velocity of the gas, a is the surface area per volume of the packing media, d_p is the particle diameter (see equation 3-6 for non-spherical particles), ε is the bed porosity, and ρ and μ are the density and viscosity of the gas (Knudsen et al., 1999).

$$Re = v*\rho/(\mu*\Psi*a) \quad (3\text{-}4)$$

$$a = 6(1-\varepsilon)/d_p \quad (3\text{-}5)$$

$$d_p = 0.567 * \text{sqrt (part. surf. area)} \quad (3\text{-}6)$$

$$j_d = 0.91*\Psi*Re^{-0.51} \quad (3\text{-}7)$$

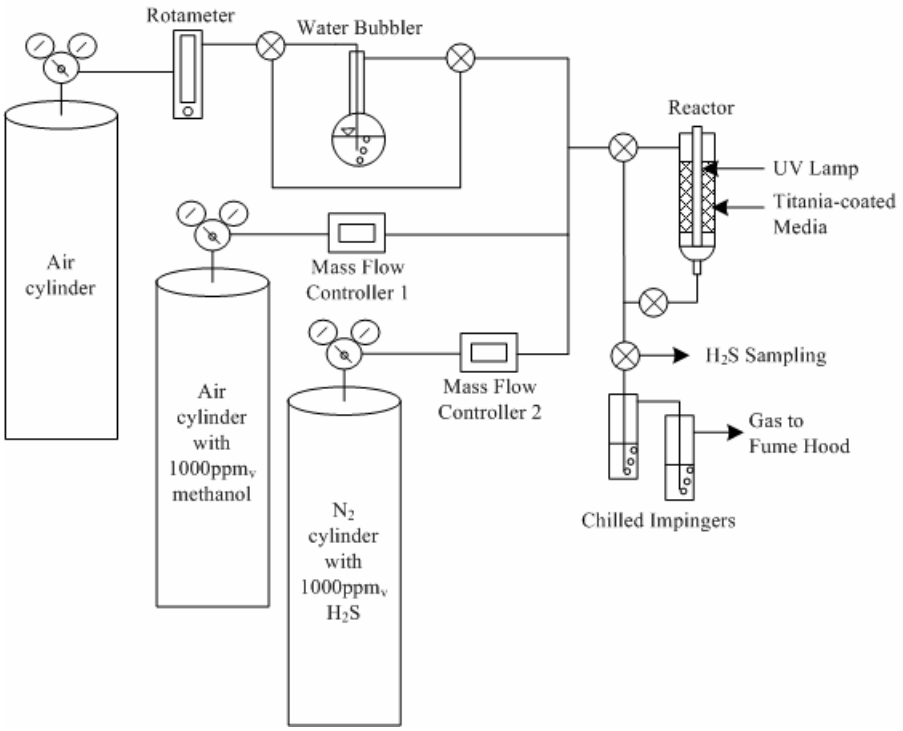

Figure 3-1. Bench-scale reactor set-up used for methanol/H_2S adsorption and photocatalytic oxidation studies.

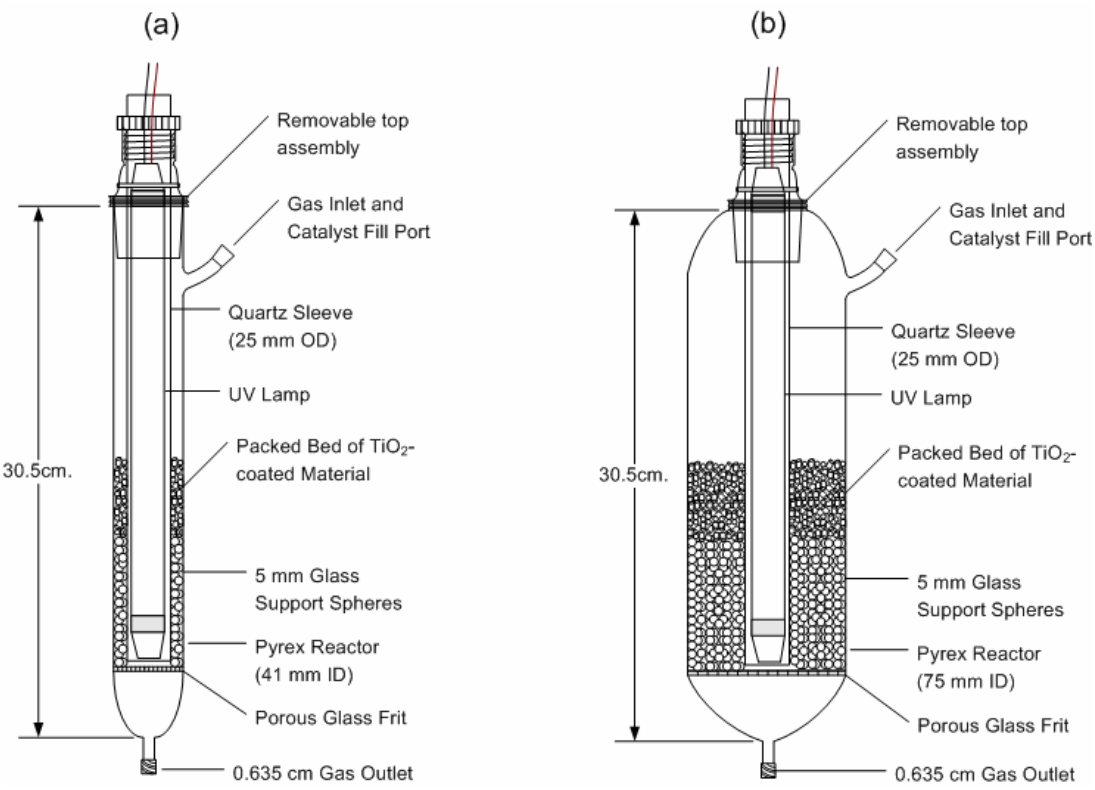

Figure 3-2. Reactor drawings. A) 8 mm annulus reactor. B) 25 mm annulus reactor.

CHAPTER 4
CHARACTERIZATION OF STC

STC pellets with three different average pore sizes and varying TiO_2 loadings were synthesized by varying the quantity of HF and TiO_2 added to the liquid precursors before gelation. BET surface area, total pore volume, and average hydraulic pore size are shown in Table 4-1. The error represents the standard deviation of grab samples taken from at least three batches of pellets. The STC pellets were labeled according to their approximate hydraulic pore size and TiO_2 loading (% mass TiO_2 per 100 mL of TEOS). Based on a mass balance of the STC synthesis from raw ingredients to the final product (i.e., dried pellets), the estimated TiO_2 mass loadings for STC labeled as 0, 1, 4, 12, and 60% were 0, 3, 12, 30, and 70%$_w$, respectively.

The surface area and total pore volume of the STC were dependent on the type of STC. The various STC labeled as "50 Å" were synthesized with a constant HF concentration and varying concentrations of TiO_2. The addition of the non-porous TiO_2 (ca. 50 m^2/g) to the porous silica gel resulted in an overall decrease in surface area and pore volume of the composite. The HF concentration also had an effect on both surface area and pore volume. For the STC synthesized with 12% TiO_2 and varying concentrations of HF (50 Å 12%, 120 Å 12%, 260 Å 12%), an increase in HF resulted in a decrease in surface area and an increase in pore volume due to the widening of the pores. The data do not suggest that significant pore blockage occurred as a result of TiO_2 addition. The change in specific surface area and pore volume was due to the addition of the non-porous TiO_2 to a porous silica gel, creating a composite material with specific surface area and pore volume values representative of a mixture of the two materials. To illustrate this, Figure 4-1 shows the actual and expected specific surface area values of the STCs. The expected values were calculated based on the mass percentage of silica in the composite multiplied by the surface area of silica gel synthesized with the same HF

concentration and no TiO_2 plus the mass percentage of TiO_2 multiplied by the surface area of TiO_2 (50 m^2/g). As shown in Figure 4-1, the measured specific surface areas of the STC are similar to the expected values. The error bars shown for the measured values were based on the measured error between multiple batches, as shown in Table 4-1. The error bars shown for the expected values were based on the error associated with the measured value of the silica gel synthesized with the same HF concentration and no TiO_2.

The nitrogen adsorption/desorption isotherms for the STC are shown in Figure 4-2. All of the STC exhibit a Type IV isotherm with H1 and H2 hysteresis loops, which is characteristic of mesoporous materials. The 50 Å STC mainly exhibited H2 hysteresis, while the 120 Å and 260 Å STC exhibited H1 hysteresis.

Although the effect of various factors on hysteresis is not fully understood, hysteresis shapes have been associated with specific pore structures. The H1 hysteresis loop, which was exhibited by the 120 Å and 260 Å STC, indicates that the material is comprised of uniform spheres arranged in a fairly regular array with a narrow distribution of pore sizes (Sing et al., 1984). H2 hysteresis, which was exhibited by the 50 Å STC, has been attributed to pores with an ink bottle shape (i.e., narrow necks and wide bodies) (Sing et al., 1984). However, poorly defined pore shape or distribution in a disordered material, which results in pore blocking and percolation, could also cause the H2 loop (Thommes, 2004). Although the 50 Å STC generally exhibited H2 hysteresis, the 50 Å 60% had a hysteresis shape more representative of H1. The 50 Å 60% hysteresis loop narrowed at a relative pressure of about 0.8, rather than 0.5 to 0.6 for the 50 Å STC of lower TiO_2 loadings (0 - 12%). This suggests that the 60% TiO_2 loading may increase the size of the pore neck, allowing the pore body to empty at higher relative pressures, or result in a less extensive pore network, as evidenced by the decrease in total pore volume.

The presence of approximately uniform spherical primary particles was confirmed by SEM images taken by Byrne et al. (2008). The SEM images showed that the spherical particles were present in all of the STC, regardless of pore size or TiO_2 loading. The size of the primary particles was smallest for the 260 Å STC and grew larger for STC synthesized with lower HF concentrations. Thus, the 50 Å STC were comprised of the largest primary particles. This was attributed to the shorter gelation times for STC with higher HF concentrations, which resulted in a shorter time for particle growth and, hence, a smaller primary particle size. The gelation time was dependent on the HF concentration used during synthesis since it catalyzes hydrolysis and condensation reactions. The 50 Å 12% STC gelled after about 12 hours while the 120 Å 12% and 260 Å 12% gelled after approximately 2.5 hours and 10 minutes, respectively. The SEM images also showed that for the 260 Å 12% and 260 Å 60% STC, the change in TiO_2 concentration did not noticeably change primary particle size or morphology.

The pore size distribution of the STC is important since it can affect the diffusivity of methanol and oxidation byproducts into and out of the STC (Satterfield, 1970). The pore size distributions of STC synthesized with various HF and TiO_2 concentrations are shown as the differential pore volume as a function of pore diameter in Figure 4-3. The hydraulic pore sizes shown in Table 4-1 are sometimes different than the average pore sizes shown in Figure 4-3. If the pores were truly cylindrical in shape, which is the assumption made for the calculation of the hydraulic pore size, the average pore size associated with the desorption isotherm would equal the hydraulic pore size. The disparity between the desorption pore size and the hydraulic pore size can be attributed to the actual shape of the pores and/or network effects.

The pore size distributions for the 50 Å 12%, 120 Å 12%, and 260 Å 12% STC, as shown in Figure 4-3a, were unimodal and the area of the peak was relative to the total pore volume of

the STC. The 50 Å 12% STC had the narrowest range of pore sizes, with about 95% of the pore volume resulting from pores between 19 Å and 56 Å. As the pore size of the STC increased due to the increased quantity of HF added to the liquid sol during synthesis, the total pore volume increased and the pore size distribution became broader. For the 120 Å 12% STC, 95% of the pore volume resulted from pores with diameters between 49 Å and 172 Å. The 260 Å 12% STC had the broadest pore size distribution, with 94% of the pore volume resulting from pores with diameters between 155 Å and 336 Å.

Pore size distributions for 50 Å STC with varying TiO_2 loadings (0-60%) are shown in Figurer 4-3b. For TiO_2 loadings between 0 and 12%, differences between the pore size distributions were mainly a result of the decrease in pore volume associated with increased TiO_2 loadings. The distributions for these STC were unimodal and the shapes of the distribution curves were similar. The 50 Å 60% STC had a much broader distribution and drastically smaller differential pore volume at the 50 Å pore diameter. The pore volume at 50 Å was approximately 0.005 cc/Å/g compared to 0.037 cc/Å/g for the 50 Å 4% STC. Although the peak differential pore volume remained at about 50 Å, pore sizes between approximately 20 and 250 Å contributed to the total pore volume for the 50 Å 60% STC.

The 50 Å 60% STC was comprised mostly of TiO_2 (i.e., about $70\%_{wt}$ of the dried product was TiO_2). Thus, the amount of shrinkage that occurred during the aging and drying process was reduced. The total volume of a dried 50 Å 60% STC pellet was about 61% less than its volume immediately after gelation. The volume of a 50 Å 12% STC pellet, for example, was reduced by 74%. This indicates that the syneresis of the SiO_2, which results in the formation of additional Si-O-Si linkages resulting in the shrinkage of the STC during aging and drying, was inhibited. This may have resulted in the formation of a broader pore size distribution by disallowing the

shrinking of the silica network and formation of additional linkages to create the smaller pores (i.e., those around 50 Å in diameter).

Table 4-1. BET surface area, total pore volume, and calculated pore size for the STC synthesized with varying concentrations of HF and TiO_2.

STC	BET surface area (m^2/g)	Total pore volume (cc/g)	Pore size (Å)
50 Å 0%	662 ± 54	0.86 ± 0.03	52 ± 3
50 Å 1%	636 ± 27	0.88 ± 0.03	55 ± 1
50 Å 4%	617 ± 19	0.76 ± 0.04	49 ± 4
50 Å 12%	532 ± 43	0.60 ± 0.06	46 ± 4
50 Å 60%	297 ± 24	0.48 ± 0.05	65 ± 5
120 Å 12%	290 ± 23	0.69 ± 0.11	123 ± 7
260 Å 12%	154 ± 18	0.99 ± 0.10	259 ± 11

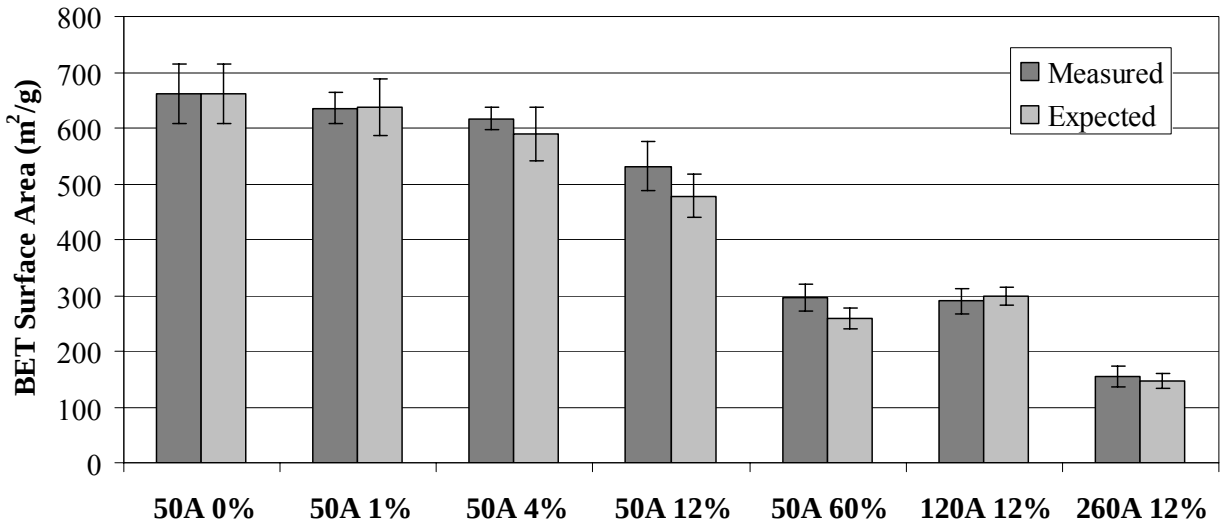

Figure 4-1. Measured and expected surface area data for STC.

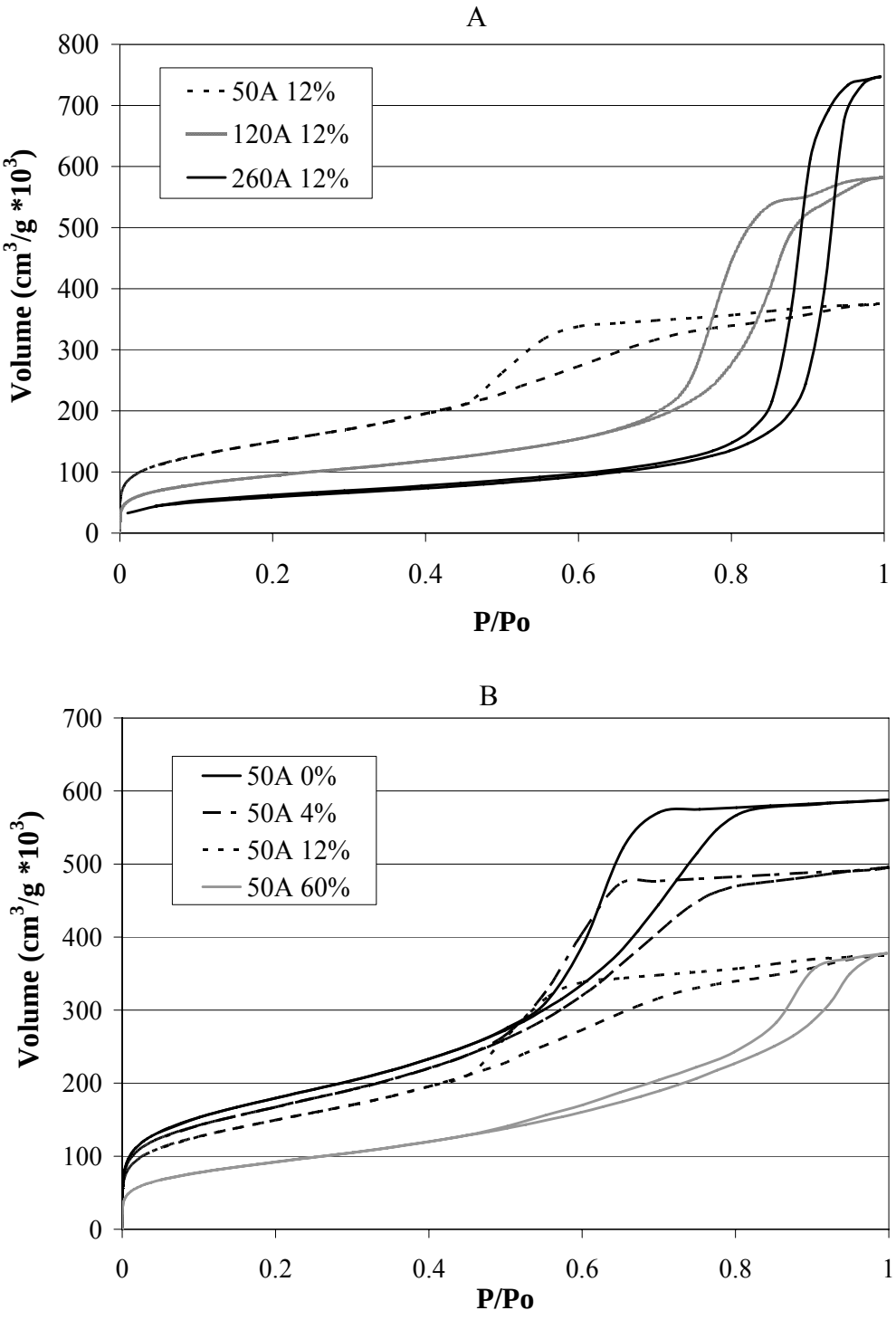

Figure 4-2. Nitrogen adsorption/desorption isotherms. A) STC with varying pore sizes and constant TiO_2 loading (12%). B) 50 Å STC with varying TiO_2 loadings (0-60%).

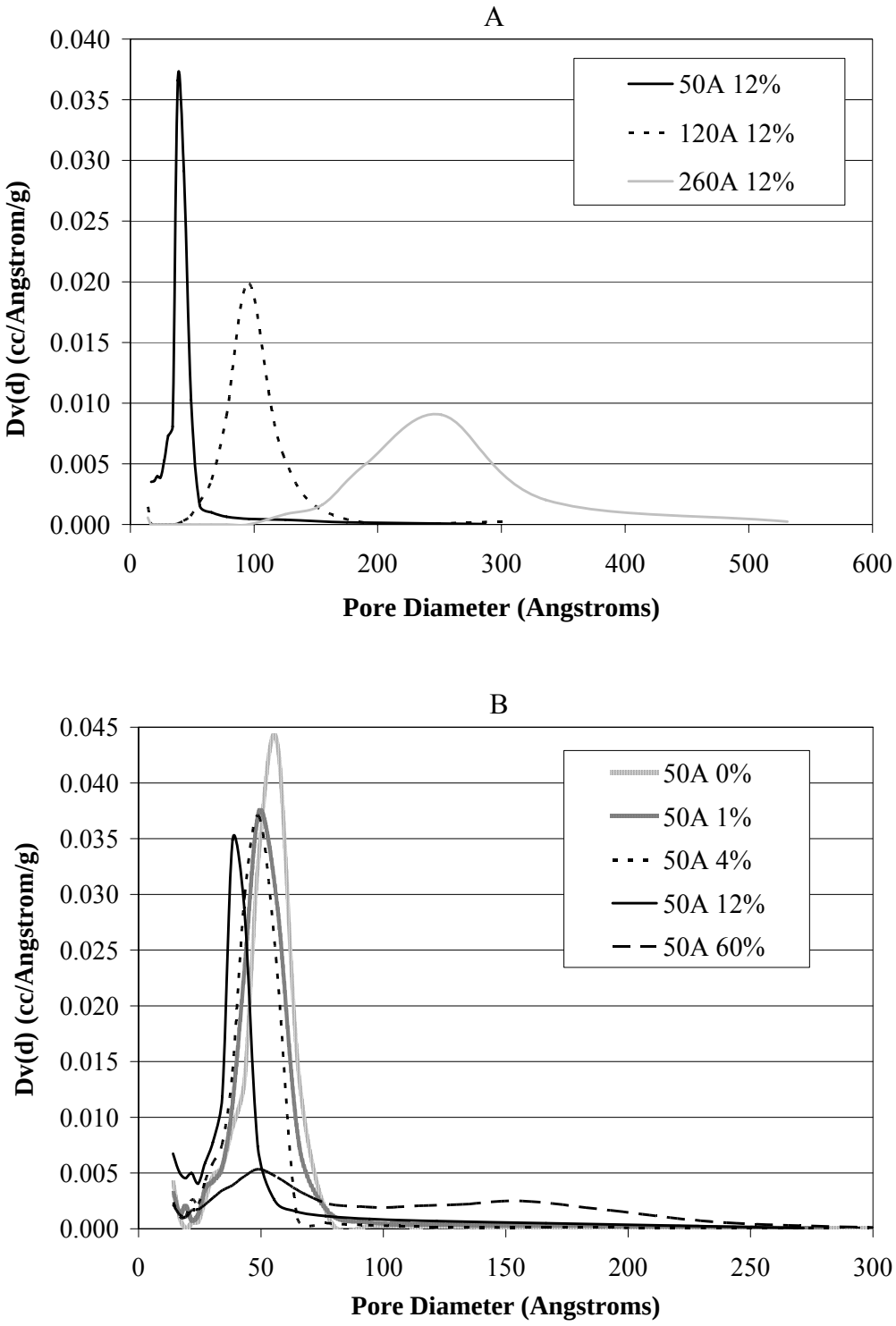

Figure 4-3. Pore size distributions. A) STC with varying pore sizes and constant TiO_2 loading (12%). B) 50 Å STC with varying TiO_2 loadings (0-60%).

CHAPTER 5
OPTIMIZATION OF METHANOL DEGRADATION USING STC PELLETS IN A BENCH-SCALE REACTOR

The use of STC pellets for VOC abatement is not widely studied since photocatalytic reactors designed to treat VOCs typically employ a TiO_2 or SiO_2-TiO_2 thin film. The objective of the work presented in this chapter was to investigate the use of the STC pellets for the removal and degradation of methanol from a high humidity air stream, specifically to determine the effects of STC pore size, TiO_2 loading, face velocity and space time on methanol degradation.

The conditions for the experiments described in this chapter are summarized in Table 5-1. An influent methanol concentration of 50 ppm_v was used for all studies. This concentration was picked based on discussions with industry. Study No. 1 represents the baseline conditions. The space time was manipulated in Study No. 2, 3, and 4 by varying the flow rate of gas containing 50 ppm_v of methanol with an influent relative humidity of about 95% (at 23°C) through the reactor packed with 30 cm^3 of pellets. For space times of 8.6 s, 2.1 s, and 1.1 s, the total flow rate through the reactor was 0.21, 0.84, and 1.68 L/min, respectively. Since the flow rate was adjusted to achieve the various space times, the face velocity, methanol loading rate (mg of methanol entering the reactor per minute) and water vapor loading rate also varied with space time, as shown in Table 5-1. Study No. 1, 5, and 6 were performed to assess the effect of varying face velocity at a constant 4.3 s space time. The bed depth was adjusted to achieve the constant space time at the varying face velocities. Flow rates of 0.42, 0.84, and 1.26 L/min containing 50 ppm_v of methanol were passed through packed beds with volumes of 30 cm^3, 60 cm^3, and 90 cm^3, respectively. This resulted in a constant 4.3 s space time and face velocities of 0.093 m/s, 0.19 m/s, and 0.28 m/s. All error bars shown in this chapter represent the standard deviation of at least triplicate measurements, unless otherwise stated.

Adsorption

STC pellets of varying pore sizes (50 Å, 120 Å, 260 Å) and constant TiO_2 loading (12%) were tested in the dark to determine methanol adsorption capacity using conditions for Study No. 1. A 12% TiO_2 loading was chosen since previous studies for the degradation of organic compounds from water have found that this TiO_2 loading was optimal (Ludwig et al., 2008; Londeree, 2002). The temperature of the reactor was kept at 50°C to simulate the reactor temperature when irradiated with UV light. As shown in Figure 5-1, the time required to reach exhaustion was dependent on the pore size of the STC pellets, with the smallest pore size (i.e., 50 Å) having the greatest methanol adsorption capacity. The total amount of methanol adsorbed by the various STC, as determined by integration of the adsorption breakthrough curves, indicated that methanol adsorption occurred via monolayer coverage versus pore filling since the adsorption trends correlated with the BET surface area data, but not with the total pore volume.

Simultaneous Adsorption and Oxidation of Methanol

The photocatalytic oxidation of methanol was tested by repeating the experiments described above in the presence of UVA light. Figure 5-2 shows the methanol removal capabilities of the 50 Å, 120 Å, and 260 Å STC pellets. Breakthrough of methanol (i.e., effluent concentration greater than the detection limit of 0.6 ppm_v or C/Co = 0.012) occurred for all STC. The time to breakthrough for the 50 Å pellets occurred after about 180 minutes in the presence of UV light, whereas in the dark the initial breakthrough occurred immediately. For the 120 Å and 260 Å STC, breakthrough occurred during the first sample period. However, the effluent concentration was lower in the presence of UV light than in the dark. For example, the normalized effluent concentration (C/Co) of the first sample from the reactor packed with 260 Å STC was about 0.65 in the dark and 0.07 when illuminated. Thus, it does not appear that a minimum surface coverage of water vapor or methanol was required for degradation to occur.

After a period of time (e.g., approximately 400 min for the 50 Å STC pellets), the system appeared to reach a pseudo-steady state (i.e., the effluent concentration was relatively constant) such that the adsorption rate was equal to the oxidation rate.

The removal efficiency of the 120 Å and 260 Å pellets at steady state was similar (about 80%). The 50 Å pellets removed greater than 90% of the methanol at steady state. The enhanced performance of the 50 Å pellets shown in Figure 5-2a is a result of the high internal surface area of these pellets. Although the UV probably does not reach the very center of each STC pellet due to the opacity of the TiO_2, these results suggest that photons do penetrate past the external surfaces of the pellets; otherwise, the performance of the pellets at steady state would be similar regardless of internal surface area.

To assess whether the system in Figure 5-2a was truly at steady state, an extended study was conducted over a period of four days using the 50 Å pellets. This study (results shown in Figure 5-2b) confirmed that the system was at steady state, achieving approximately 90% methanol removal for the duration of the experiment.

Formation of Photocatalytic Byproducts

Formaldehyde, a byproduct of the photocatalytic oxidation of methanol (Tsuru et al., 2003; Peral et al., 1997), was identified in the effluent of all studies conducted in the presence of UV light. Formaldehyde was not detected in the influent gas. The effluent formaldehyde concentration was dependent on the pore size of the STC pellets, as shown in Figure 5-3. The effluent formaldehyde concentration increased over time until a steady state was reached. The effluent formaldehyde concentration produced at steady state by the 260 Å, 120 Å, and 50 Å pellets was approximately 7, 4, and 2 ppm_v, respectively. STC pellets with a higher surface area possessed a greater number of active sites for adsorption and subsequent photocatalytic oxidation to occur. In addition, diffusion of formaldehyde out of the pellets may have depended on the pore

size of the composite (i.e., a composite with a smaller pore size had greater resistance to pore diffusion) (Chang et al., 2000). Restricted diffusion may have retained byproducts for further oxidation. The effects of mass transfer will be discussed in further detail later in this chapter.

In addition to testing effluent streams for methanol and formaldehyde, TOC analysis was performed in order to identify additional organic byproducts. For all studies, TOC analysis proved that other organic byproducts were not measurable regardless of the test parameters. For example, when 50 Å 12% STC pellets were irradiated with UVA light, methanol and formaldehyde were released in the effluent at a rate of about 0.003 mg of methanol (as carbon) per min and about 0.004 mg of formaldehyde (as carbon) per min at steady state. The results of TOC analysis showed the total rate of carbon released in the effluent was 0.007 mg/min. This mass balance shows that the TOC present in the effluent (0.007 mg C/min) was accounted for by the methanol (0.004 mg C/min) and formaldehyde (0.003 mg C/min). In addition, the absence of methyl formate, which is another byproduct that has been identified in the effluent of reactor systems that photooxidize methanol (Tsuru et al., 2003; Sadeghi et al., 1996; Arana et al., 2004), was confirmed by GC analysis.

Formic acid is a known intermediate byproduct in the oxidation from formaldehyde to carbon dioxide and water. The lack of the presence of measurable amounts of formic acid in the effluent can be attributed to the following reasons: (1) formic acid formed from the photocatalytic oxidation of methanol is strongly adsorbed to the TiO_2 surface (Lichtin et al., 1994) and (2) only one electron hole is necessary for the total degradation of formic acid, which, according to other literature values, results in a high apparent quantum yield (0.45) compared to other organic compounds (0.06-0.001) (Dijkstra et al., 2002). Since formic acid is degraded

directly to carbon dioxide and water, the balance of the effluent carbon should be present as carbon dioxide (Dijkstra et al., 2002).

Effect of Space Time on Methanol Degradation

The effect of space time on methanol removal using the 50 Å 12% STC was tested using experimental conditions 2, 3, and 4, which resulted in space times of 8.6 s, 2.1 s, and 1.1 s. The space time was controlled by adjusting the air flow rate, although the influent methanol concentration (50 ppm_v) and relative humidity (95%) remained the same. Thus, the face velocity of the air entering the packed bed and methanol and water vapor loading rate (mg/min) increased as the space time decreased. The normalized effluent methanol concentration (C/Co) is shown in Figure 5-4 for the duration of each study. Initially, the effluent methanol concentration was low, due to adsorption onto the STC. For all space times, the effluent methanol concentration increased over time until steady state removal was achieved. The effluent methanol concentration at steady state was dependent on the space time. The shortest space time (1.1 s) had the highest normalized effluent methanol concentration of about 0.52. The normalized effluent methanol concentration for the 2.1 s and 8.6 s space times were about 0.38 and 0.025, respectively. The error bars shown in Figure 5-4 represent the range of duplicate tests. Error bars are not shown for the 1.1 s residence time since the experiment was not replicated.

Formaldehyde, which is an intermediate byproduct of methanol oxidation, was identified in the effluent for all studies. Figure 5-5 shows the effluent formaldehyde concentrations for the duration of the experiments for the various space times. The effluent formaldehyde concentrations increased from time zero until reaching a steady state concentration. This concentration was also dependent on the space time. The effluent formaldehyde concentrations for the 8.6 s, 2.1 s, and 1.1 s residence times were about 0.3 ppm_v, 3 ppm_v, and 8 ppm_v, respectively. No other organic byproducts were identified in the effluent. Since one mole of

methanol is oxidized to one mole of formaldehyde and no other intermediate byproducts were identified, the difference between the influent molar flux and the total effluent molar flux of methanol and formaldehyde represents the mineralization rate of methanol.

The 120 Å 12% and 260 Å 12% STC were also tested for methanol removal using space times of 1.1, 2.1, and 8.6 s (Study Nos. 2-4). For all STC, the effluent methanol and formaldehyde concentrations at steady state are shown in Figure 5-6 for the various space times. For both the 120 Å and 260 Å STC, the effluent methanol and formaldehyde concentrations were dependent on the space time. The effluent formaldehyde and methanol concentrations for the 120 Å were less than that of the 260 Å STC for all space times studied. At a 1.1 s space time, the 260 Å STC showed no mineralization of methanol, only oxidation of methanol to formaldehyde, which then desorbed into the effluent gas stream rather than remain at the reaction site for subsequent oxidation. Thus, at the 1.1 s space time, the conversion of methanol to formaldehyde was the dominant reaction mechanism. For space times greater than 1.1 s, this mechanism no longer dominated since both methanol and formaldehyde were oxidized. The longer space times were achieved by lowering the gas flow rates, which resulted in lower methanol and water vapor loading rates (as shown in Table 5-1). The lower loading rates presumably decreased the competition for adsorption/reaction sites and the higher space times allowed more time for the subsequent adsorption and oxidation of desorbed formaldehyde to occur, thus allowing the oxidation of formaldehyde to proceed.

The greatest difference in performance between the various STC was observed at the shortest residence time studied (1.1 s). The total normalized effluent concentration ($1-X_A$), which accounts for the concentration of both methanol and formaldehyde in the effluent, was 0.68 for 50 Å, 0.91 for 120 Å, and 1.0 for 260 Å. As the space time increased, the performance of the

various STC converged so that the performance was more similar at the 8.6 s space time ($1-X_A$ was 0.035 for 50 Å, 0.045 for 120 Å, and 0.049 for 260 Å). The difference in performance between the various pore sizes was likely a result of the surface area of the STC, with the higher surface area STC (i.e., 50 Å) resulting in better performance due to the greater number of available adsorption and reaction sites. This was most pronounced at the 1.1 s space time, where the ratio of influent methanol loading to surface area was the greatest and the most significant difference in performance was observed. In addition to surface area effects, performance may also be affected by mass transfer, which is directly effected by the pore size distribution of the STC. For example, the STC with a small pore size may resist the transfer of methanol into the STC or constrain byproducts from leaving the pellet, thereby allowing for complete oxidation. This hypothesis is discussed further below.

Mass Transfer

The kinetics of the system can be limited by the effects of external and internal mass transfer of methanol into the STC and byproducts out of the STC. In order to assess the effects of external mass transfer on the methanol oxidation rate and the effluent byproduct concentration (i.e., formaldehyde concentration), Study Nos. 5-7 were conducted with 50 Å 12% STC. The 50 Å STC was chosen for these studies since it had the smallest pore size and narrowest pore size distribution. Thus, the 50 Å STC would experience the greatest resistance to mass transfer. For these studies, the face velocity was varied between 0.093 and 0.28 m/s while the space time was held constant at 4.3 s by changing the volume of the packed bed. The steady state methanol and formaldehyde concentrations in the effluent are shown in Figure 5-7. The effluent methanol concentration decreased as a result of an increase in face velocity while the effluent formaldehyde concentration was similar for all cases. This methanol removal trend was likely a result of the decrease in resistance to mass transfer from the gas stream to the media as the face

velocity increased (Satterfield, 1970). Compared to the influent concentration (50 ppm_v), the difference in methanol removal from about 5.8 ppm_v for the 0.093 m/s face velocity to 4.2 ppm_v for the 0.28 m/s face velocity was about 1.6 ppm_v. Since this difference represents only 3% of the influent concentration, the kinetic analysis presented later in this paper will neglect the effects of external mass transfer.

Using the experimental methanol mineralization rates observed at steady state, the Weisz modulus (M_w), or modified Thiele modulus, was calculated for Study Nos. 1-4, where space time was varied. The Weisz modulus is used to estimate kinetic limitations as a result of resistance to pore diffusion using the experimentally-determined rate of methanol removal at steady state. Modulus values less than 0.15 indicate that there are no kinetic limitations as a result of pore diffusion. The expression for the Weisz Modulus is shown in Equation 5-1(Levenspiel, 1999).

$$Mw = L^2 * r/(C_o * D_e) \quad (5\text{-}1)$$

where L is the characteristic length (radius/2 for cylindrical pellets); r is the mean rate of methanol oxidation per unit volume of STC; and D_e is the effective diffusion coefficient of methanol within the STC.

The effective diffusion coefficient (D_e) is a function of the diffusion coefficient of methanol (D), catalyst grain porosity (ε_c) and tortuosity of the STC (τ_c), as shown in Equation 5-2. The diffusion coefficient of methanol in air is about 15×10^{-6} and the tortuosity of the pores was assumed to be 3, which is a typical value for mesoporous silica gels (Doucet et al. 2006).

$$D_e = D * \varepsilon_c / \tau_c \quad (5\text{-}2)$$

The calculated Weisz modulus values for the various STC are shown in Table 5-2 for Study No. 1-4, where space time was varied. For each of the space times, the Weisz modulus indicated that there were no kinetic limitations as a result of pore diffusion. Although the 50 Å

12% STC exhibited the most narrow pore size distribution and smallest average pore diameter of the STC, the pore size was large enough to allow pore diffusion with very little resistance. Therefore, the rates measured in the experiments are a result of the chemical (or intrinsic) kinetics (Doucet et al., 2006).

Kinetics

The rate of reaction for gas-solid phase photocatalytic reactions can often be described by the Langmuir-Hinshelwood (L-H) model, where the rate of reaction is equal to the rate constant (k) times the surface coverage of the contaminant. Since the mineralization rate of methanol can be described by the rate equation for a single molecular reaction and the influent concentration was low, the L-H model can be simplified to the pseudo first-order equation shown in Equation 5-3 to describe the mineralization rate of methanol (Chen et al., 1999; Zou et al., 2006).

$$\ln (1-X_A) = - k\tau + A \qquad (5\text{-}3)$$

where A is a constant. Although initial rate of photocatalytic degradation is typically used for the L-H model, in this study the initial rate of photocatalytic degradation could not be easily differentiated from the removal rate due to adsorption. In addition, the inhibitory effects of water vapor may initially vary over time as the STC surface reaches its adsorption capacity for water vapor. It should be noted that water vapor adsorption tests proved that capillary condensation of water vapor did not occur in the pores of any STC studied. This data is discussed in further detail in Chapter 6. At steady state conditions, the methanol removal rate is directly related to the photocatalytic reaction rate and inhibitory effects of water vapor can be assumed to be constant for a given system. Therefore, the reaction rate was modeled using the steady state mineralization rates at the various space times studied (Study No. 1-4). The rate constant (k) was

determined for STC of the various pore sizes by a linear regression of $-\ln(1-X_A)$ versus τ, as shown in Figure 5-8.

The use of the L-H model resulted in a good fit of the data ($R^2 = 0.99$ for all STC). The rate constant was 0.40 s^{-1} for all the STC pore sizes studied. The difference in conversion rates was due to a lag time before mineralization occurred, which was observed with the 120 Å and 260 Å STC. Oxidation of methanol to intermediate byproducts occurred during the lag phase; however further oxidation required for mineralization did not proceed. A lag phase was also described by Chu and Wong (2004) in their study of the oxidation of alachlor in water, where the dominant mechanism during the lag phase was the oxidation of alachlor to intermediate byproducts with no mineralization. In this study, the lag time was expressed by the constant (A), which was 0, -0.41, and -0.49 for the 50 Å, 120 Å, and 260 Å STC, respectively. The lag times for the 120 Å and 260 Å STC are equivalent to the intercept of the regression lines in Figure 5-8 with the abscissa, which are approximately 1.0 s for 120 Å and 1.2 s for 260 Å. Thus, the L-H model is applicable to describe the mineralization of methanol for the 120 Å and 260 Å STC at times greater than these lag times. In the case of the 50 Å STC, the constant A is zero, indicating that the L-H model is applicable for all space times. The zero lag time experienced by the 50 Å STC was likely due to its high surface area, which provides more adsorption and reaction sites for the higher influent loadings associated with the low space times.

Effect of TiO_2 Loading on Methanol Degradation

STC with an average pore size of about 50 Å were tested with various TiO_2 loadings (1%, 4%, 12%, and 60%) using Study No. 1 conditions. As shown in Figure 5-9, all of the STC pellets, regardless of TiO_2 loading, removed similar amounts of methanol (ca. 90%) at steady state when continuously illuminated with UVA light. The time to initial breakthrough (i.e., time

when the effluent methanol concentration was detectable) was similar for STC pellets loaded with 1-12% TiO_2. Initial breakthrough for the pellets loaded with 60% TiO_2 occurred immediately due to the lower specific surface area of the composite (297 m^2/g) compared to that of the STC with lower TiO_2 loadings (e.g., 617 m^2/g for the 50 Å 4% STC).

TiO_2 loading did affect effluent formaldehyde concentration, as shown in Figure 5-10. This graph shows that a 4% TiO_2 loading was optimum, resulting in steady state effluent formaldehyde concentrations below 0.5 ppm_v. According to Byrne et al. (2008), the total available TiO_2 surface area for the 4%, 12%, and 60% TiO_2 loadings was 3.4 m^2/g, 8.1 m^2/g, and 13 m^2/g, respectively. Therefore, the total surface area of TiO_2 in the systems containing the STC with 4%, 12%, and 60% was 51 m^2, 137.7 m^2, and 234 m^2. Although Byrne et al. (2008) did not measure the available TiO_2 surface area for the 50 Å 1% STC, it can be assumed that the total available surface area would be lower than that for the 4% system based on the trend observed for TiO_2 loadings between 4 and 60%. Thus, the total quantity of active sites on the 1% STC was likely less than that for the 4% STC, leading to greater overall oxidation of methanol and its byproducts by the 4% STC.

Based on the total amount of available TiO_2, one may expect that the system containing the 60% STC would achieve the greatest rate of mineralization (i.e., lowest formaldehyde concentration) since it had the greatest TiO_2 surface area available. However, the overall surface area of the composite was 297 m^2/g, which was lower than that of the 50 Å STC with lower TiO_2 loadings (e.g., 50 Å 4% STC had a surface area of 617 m^2/g). Therefore, the higher total surface area of the 50 Å 4% STC may have enhanced the adsorption of the methanol such that the available TiO_2 was more efficient. In addition, increased TiO_2 loadings may have resulted in a

decrease in transparency such that total amount of irradiated TiO_2 was greater for the 4% STC compared to the 12% and 60% STC.

In order to test this hypothesis, UV transparency tests were conducted using 50 Å STC pellets of the varying TiO_2 loadings. The pellets were packed tightly into a 10 mm quartz cuvette and placed in a Hach DR4000 spectrophotometer. The % transmittance of the UV light through the packed bed was measured at a wavelength of 365 nm and the results are shown in Figure 5-11.

The % transmittance of the 50 Å 0% STC was about 8%. The 50 Å 0% STC was comprised solely of SiO_2, which is known to be highly transparent to UVA light. The low % transmittance shown in these results was likely due to the scattering of UVA light through the packed bed of pellets since the detector of the spectrophotometer measured only the UV light transmitted in a straight path through the cuvette (i.e., UV light that was scattered rather than absorbed was not measured). No significant difference was measured between the STC of varying TiO_2 loadings. The quantity of UV light transmitted through the pellets containing TiO_2 was likely a result of the light penetrating through only the interstitial space of the pellets. Based on physical observations of the pellets, the 1% STC appeared to be semi-transparent while the 60% STC appeared to be opaque. Therefore, it can be expected that the distance that the light could penetrate through the STC would be different. However, the 10 mm thickness used in this experiment was likely too large to be able to measure differences in transparency through the STC since the light would have to pass through 2-3 layers of pellets and scattering would occur. Thus, it is possible that the UV could penetrate farther into the 1% STC, but still be completely attenuated or scattered over a distance of 10 mm. Thus, the hypothesis stated above can be neither confirmed nor denied based on these data. In order to evaluate the penetration of UV

light through the STC, individual pellets or thinner layers of STC made with varying TiO_2 loadings should be measured using an integrating sphere to capture both transmitted and scattered light.

Effect of UV Wavelength on Methanol Degradation

The effect of UV wavelength on methanol oxidation was evaluated by using 50 Å 12% STC irradiated with UVA and UVC lamps using Study No. 1 conditions. The initial methanol breakthrough time (i.e., the time when the effluent concentration is measurable) was about 308 ± 28 min when the TiO_2 was activated using the UVC lamp. This time was greater than the initial breakthrough time (135± 25 min) when the UVA lamp was used. The UVA and UVC lamps performed similarly with respect to methanol removal when the reactor reached steady state, resulting in the oxidation of about 85% of the influent methanol. Figure 5-12 shows that the use of the UVC lamp resulted in lower effluent formaldehyde concentrations (i.e., more complete oxidation) compared to the UVA lamp. The total degradation efficiency was about 88% for the UVA lamp and 90% for the UVC lamp.

The UVC lamp enhanced reactor performance because the photocatalytic reaction rate is proportional to the rate of generation of electrons and holes on the TiO_2 surface, which is in turn proportional to the photon flux, or light intensity (Dijkstra, 2002). The intensity of the UVA and UVC light inside of the reactor system was 8.71E-5 and 1.13E-4 mEinsteins/s/cm^3, as determined by potassium ferroxalate actinometry. Thus, the intensity emitted by the UVC light was about 29% greater than that emitted by the UVA lamp. The increase in degradation as a result of increased light intensity can be predicted using the pseudo first order model shown in Equation 5-4.

$$C/Co = k*\tau \qquad (5\text{-}4)$$

where $k = k_o I$ for variable light intensity (I). As previously determined, the k value for Study No. 1-4 conditions when illuminated with UV light was $0.4 s^{-1}$. The predicted normalized effluent concentration as a function of adsorbed light flux is shown in Figure 5-13. According to this model, the normalized effluent concentration of the system irradiated with UVC light should be approximately 0.90. This assumed that 90% of the light emitted from the UV lamp was absorbed by the STC pellets and the remainder passed through the packed bed, which was confirmed by actinometry measurements. The actual normalized effluent concentration was indeed 0.90.

Effect of H_2S on Methanol Degradation

TRS species are often present in HVLC gases and are a major contributor to the characteristic odor associated with pulp and paper mills. The effect of H_2S, which was used as the representative TRS species, on methanol removal was studied. In addition, the removal of H_2S was investigated to understand if the STC can provide a co-benefit for odor removal. Studies were conducted using 50 Å 4% STC and Study No. 1 conditions with 50 ppm_v H_2S added to the gas stream.

In the dark, there was no measurable adsorption of H_2S onto the STC at 50°C after 10 minutes. Other studies have shown that H_2S had a weak adsorption affinity for the TiO_2 surface (Kato et al., 2005; Portela et al., 2007; Sopyan 2007). Kato et al. (2005) did not observe adsorption of H_2S onto TiO_2 coated on an alumina substrate. Portela et al. (2007) tested gases containing an influent H_2S concentration of 35 ppm_v and RH between 0 and 70%. They observed an initial decrease in effluent H_2S concentration due to adsorption for a short period of time (i.e., less than an hour); however the extent of adsorption was not quantified. The duration of H_2S adsorption was dependent on the humidity of the gas stream, since water vapor competed with H_2S for adsorption sites. In this work, water vapor competition would be expected to further

inhibit H_2S adsorption since the influent RH was about 95%. Sopyan (2007) attributed the weak adsorption affinity of H_2S for the TiO_2 surface to the difficulty of forming hydrogen bonds between H_2S and hydroxyl groups of the TiO_2 surface, which is the primary pathway for adsorption onto TiO_2 surfaces. Since adsorption via hydrogen bonding is also the primary pathway for adsorption onto the surface of SiO_2 (Travert et al., 2002), the use of a composite material containing SiO_2 and TiO_2, such as the STC, would not be expected to enhance H_2S adsorption. Sopyan (2007) concluded that the extent of adsorption of contaminants onto the TiO_2 surface was related to their ability to serve as an electron donor (i.e., Lewis basic group). Ammonia, which was reported to be a strong Lewis base, showed adsorption capacities an order of magnitude greater than that of H_2S, which has lower electron-donor ability and has been shown to adsorb via hydrogen bonding only in strongly basic environments (Sopyan, 2007).

The STC pellets were tested for oxidation of methanol and H_2S by irradiating the STC with UVC light. Note that there was no photolysis of methanol or H_2S when irradiated with UVC light alone. As shown in Figure 5-14, photocatalytic oxidation of both methanol and H_2S was achieved. The effluent H_2S concentration was about 28.4 ± 2.4 ppm_v for the duration of the experiment, which corresponds to an oxidation efficiency of approximately 43%. Effluent methanol concentrations were initially low and increased until a steady state was reached. Initial breakthrough occurred during the first sample (as opposed to occurring after about 300 minutes for the non-H_2S system). The effluent methanol concentration at steady state was about 10 ppm_v, which corresponds to a removal efficiency of about 80%. This corresponds to a decrease in removal efficiency from about 95% when H_2S was absent from the gas stream (results shown in Chapter 6). In the presence of H_2S, the decrease in methanol removal efficiency was likely due to the competition for oxidation sites on the surface of the STC. Since both the methanol and H_2S

concentrations reached a steady state, the formation of sulfur containing byproducts did not likely contribute to the deactivation of the catalyst during the experiment.

Formaldehyde, an oxidation byproduct of methanol, and SO_2, an oxidation byproduct of H_2S, were identified in the effluent. Effluent formaldehyde concentrations were about 0.9 ppm_v at steady state. This concentration was about two times greater than effluent formaldehyde concentrations at steady state when H_2S was absent from the influent gas (results shown in Chapter 6). Analysis of the STC pellets after the completion of the experiment showed that about 2.8 mg/g of SO_4^{2-} was loaded onto the surface of the pellets after approximately 3000 min. A mass balance of the reactor confirmed that SO_4^{2-} and SO_2 were the only byproducts of H_2S conversion. The SO_2 concentration increased over the duration of the experiment. This may be caused by (1) the saturation of water and methanol on the surface of the STC, which are more strongly adsorbed than the SO_2, would promote desorption of the SO_2 and inhibit its subsequent adsorption onto the STC for further oxidation and retention; and (2) the accumulation of SO_4^{2-} on the surface of the STC over time may inhibit the oxidation of SO_2 to SO_4^{2-} such that the SO_2 desorbed from the STC into the effluent before being oxidized further.

The 50 Å 4% STC were tested for H_2S removal (Co = 50 ppm_v) in the absence of methanol using Study No. 1 conditions. Both H_2S and SO_2 were present in the effluent, as shown in Figure 5-15. The effluent H_2S concentration was 27.9 ± 3.5 ppm_v for the duration of the study. This was similar to the previous study in which methanol was also present in the gas stream. In addition, the effluent SO_2 concentration also followed a trend similar to that in Figure 5-14 when methanol was present in the influent gas. Thus, oxidation of H_2S was not significantly affected by the presence of methanol. This was likely because the competition from water vapor dominated since the influent concentration of water vapor was about 28,000 ppm_v while that of

methanol was 50 ppm_v. SO_4^{2-} was identified on the surface of the STC and a mass balance showed that SO_2 and SO_4^{2-} were the only oxidation byproducts.

Table 5-1. Summary of experimental conditions.

Study No.	V (cm^3)	Q (L/min)	v (m/s)	τ (s)	C_o (ppm_v)	Methanol Loading Rate (mg/min)	Water Vapor Loading Rate (mg/min)
1	30	0.42	0.093	4.3	50	0.028	5.4
2	30	0.21	0.046	8.6	50	0.014	2.7
3	30	0.84	0.19	2.1	50	0.056	10.9
4	30	1.68	0.37	1.1	50	0.11	22.8
5	60	0.84	0.19	4.3	50	0.056	10.9
6	90	1.26	0.28	4.3	50	0.084	16.3

Table 5-2. Weisz modulus values for variable space time experiments.

Pore size (Å)	τ (s)	Weisz modulus (M_w)
Study No. 1		
50	4.3	0.058
120	4.3	0.042
260	4.3	0.036
Study No. 2		
50	8.6	0.028
120	8.6	0.028
260	8.6	0.028
Study No. 3		
50	2.1	0.077
120	2.1	0.035
260	2.1	0.033
Study No. 4		
50	1.1	0.090
120	1.1	0.009
260	1.1	0.000

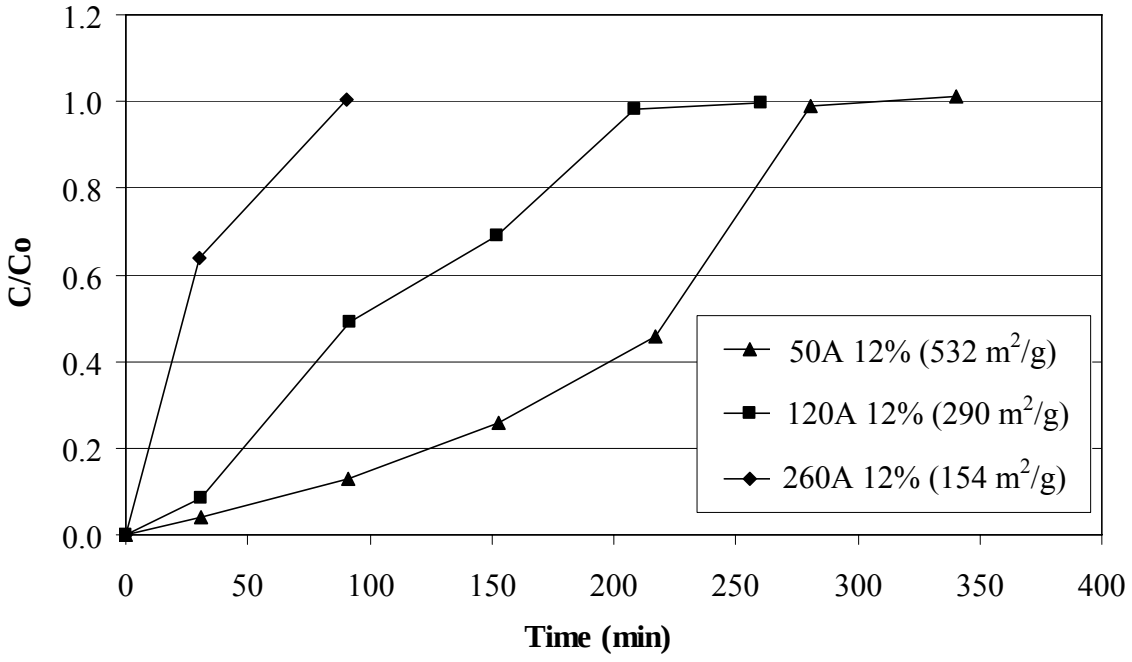

Figure 5-1. Adsorption breakthrough curves for STC pellets of varying pore sizes (50 Å, 120 Å, and 260 Å) and constant TiO_2 loading (12%).

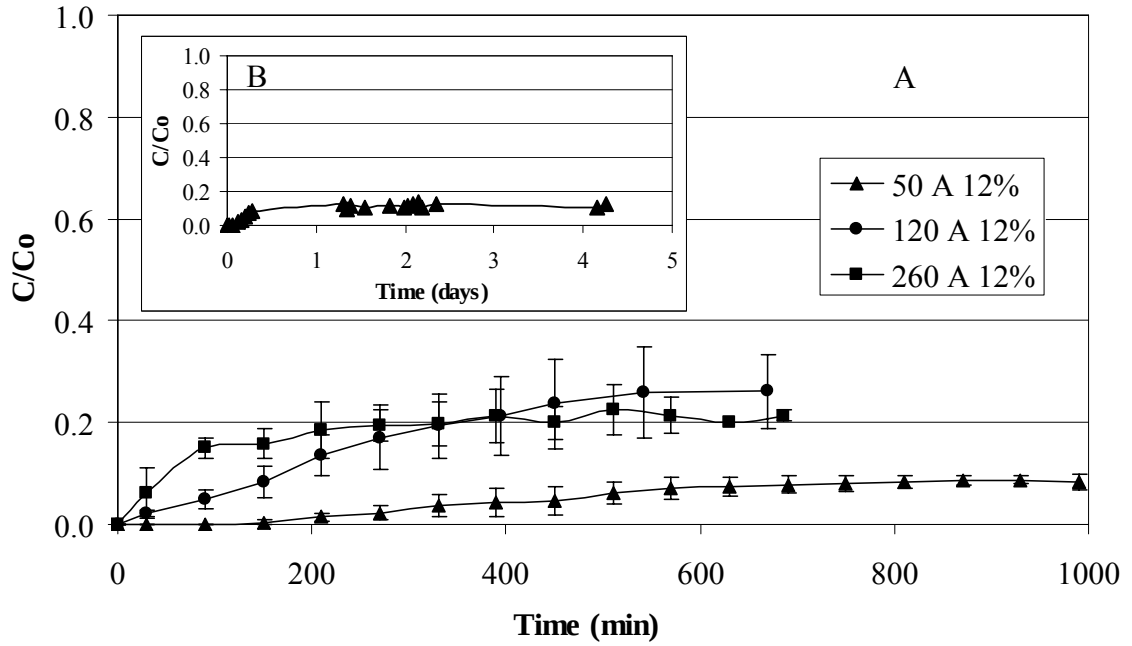

Figure 5-2. Methanol removal using STC pellets. A) Methanol removal using STC of varying pore sizes illuminated with UVA light. B) Extended study for 50 Å 12% STC pellets.

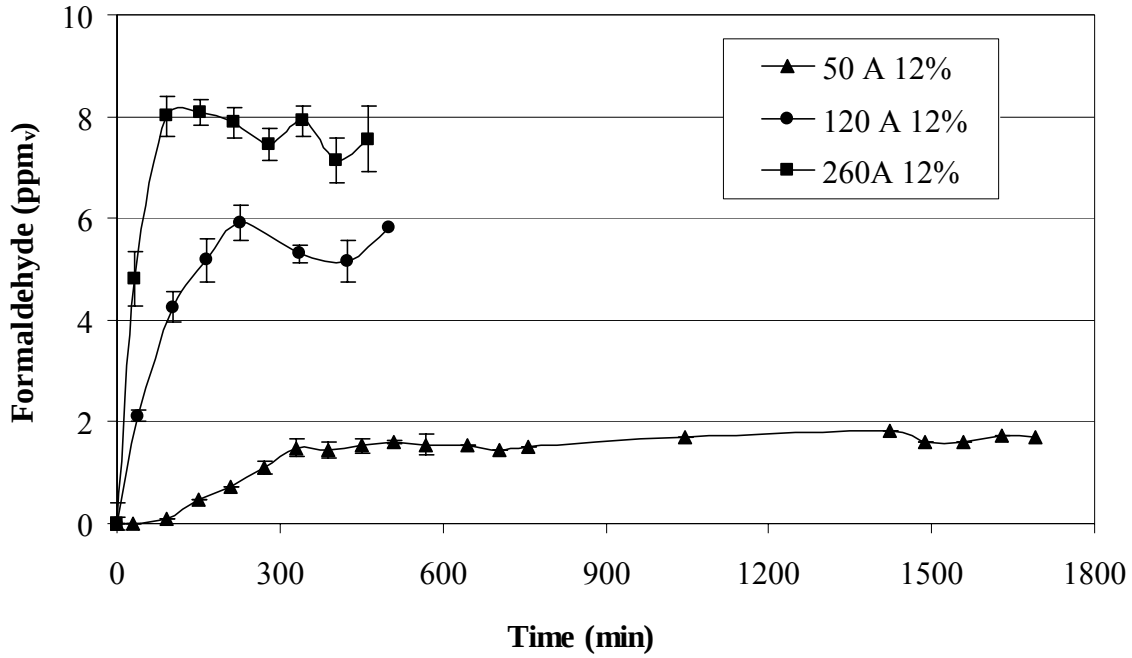

Figure 5-3. Effluent formaldehyde concentrations from STC pellets of varying pore sizes (50 Å, 120 Å, and 260 Å) when illuminated with UVA light.

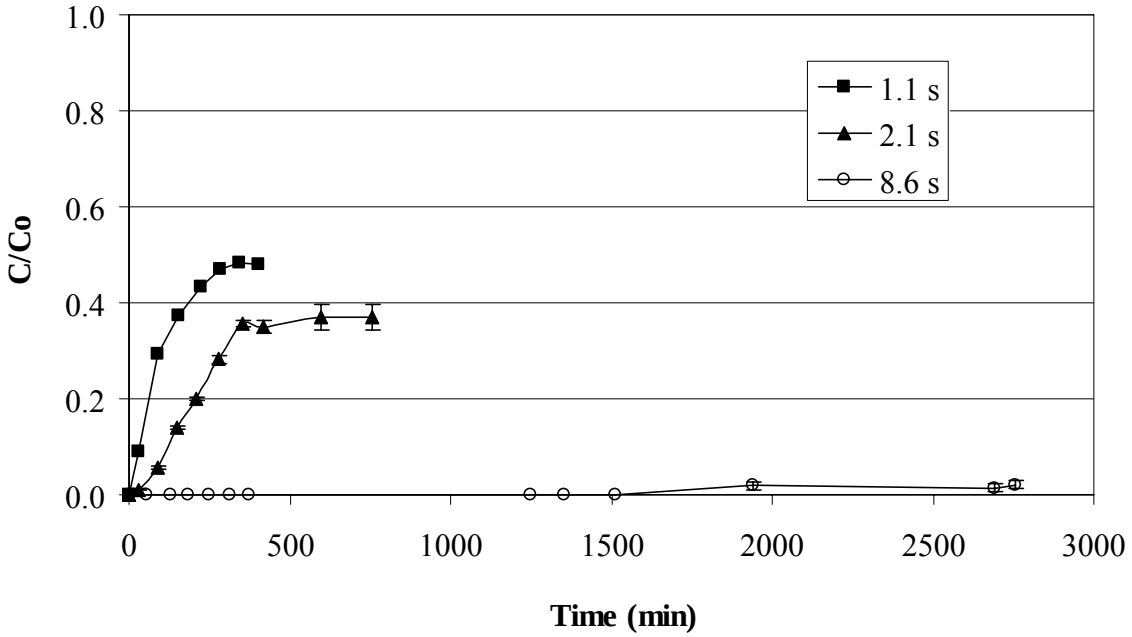

Figure 5-4. Normalized effluent methanol concentration for 50 Å 12% STC illuminated with UVA light at various space times.

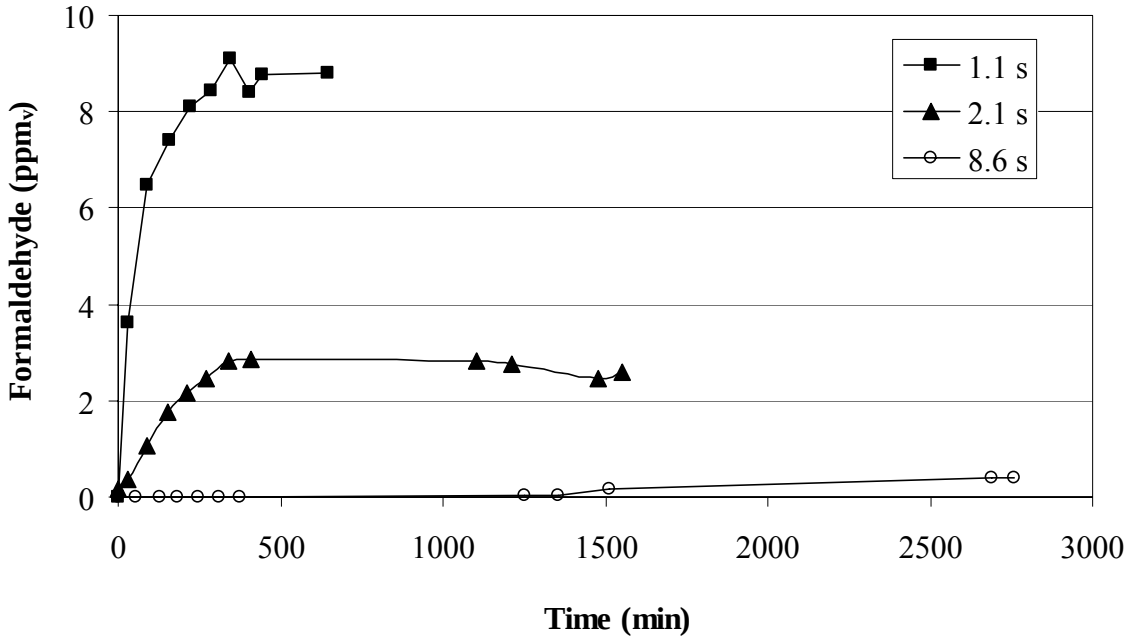

Figure 5-5. Effluent formaldehyde concentration for 50 Å 12% STC illuminated with UVA light at various space times.

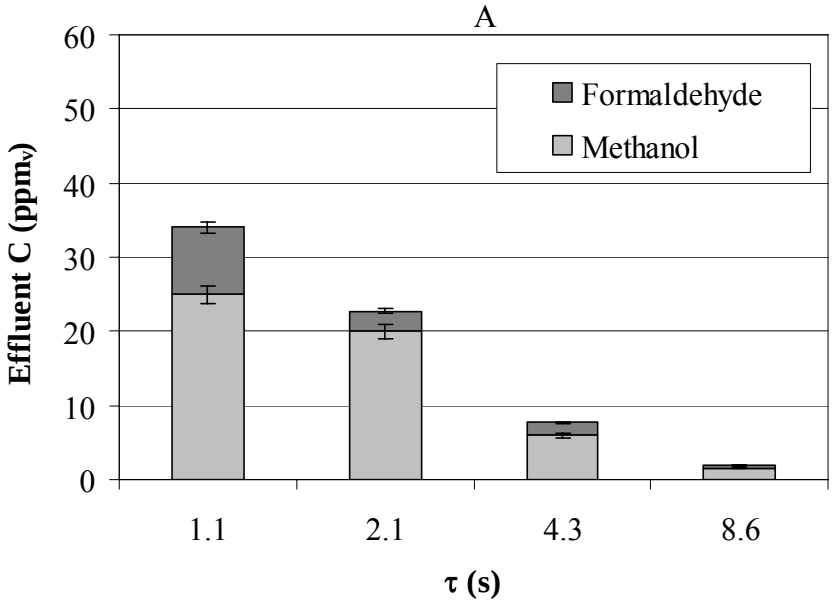

Figure 5-6. Effluent methanol and formaldehyde concentrations at steady state at varying space times. A) 50 Å. B) 120 Å. C) 260 Å STC.

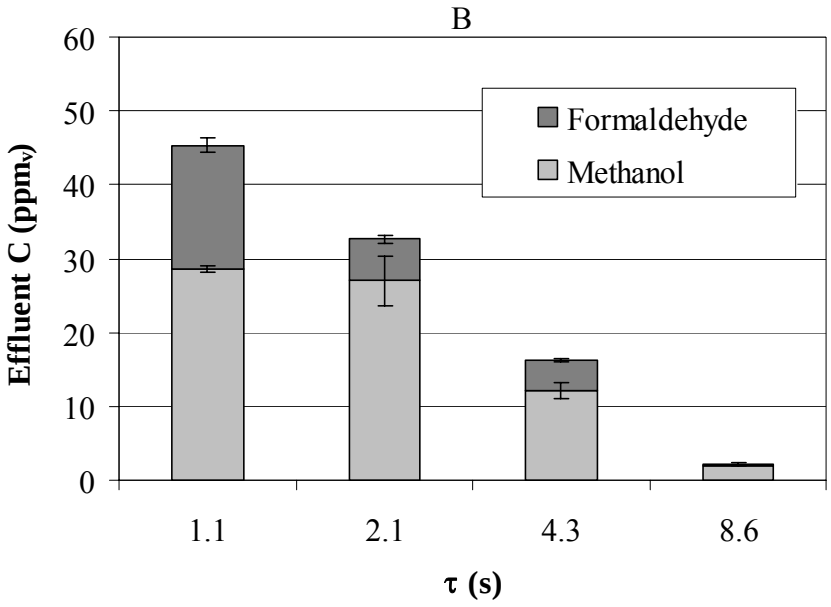

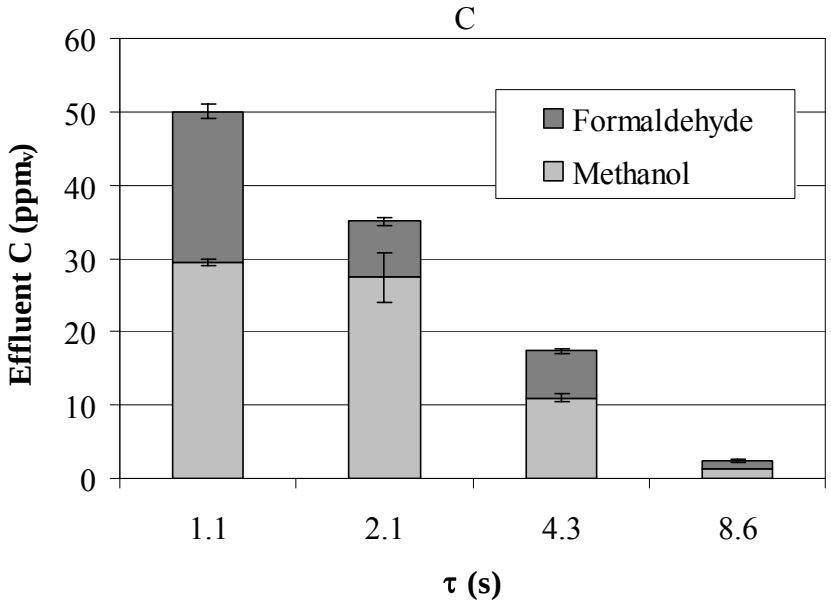

Figure 5-6. Continued.

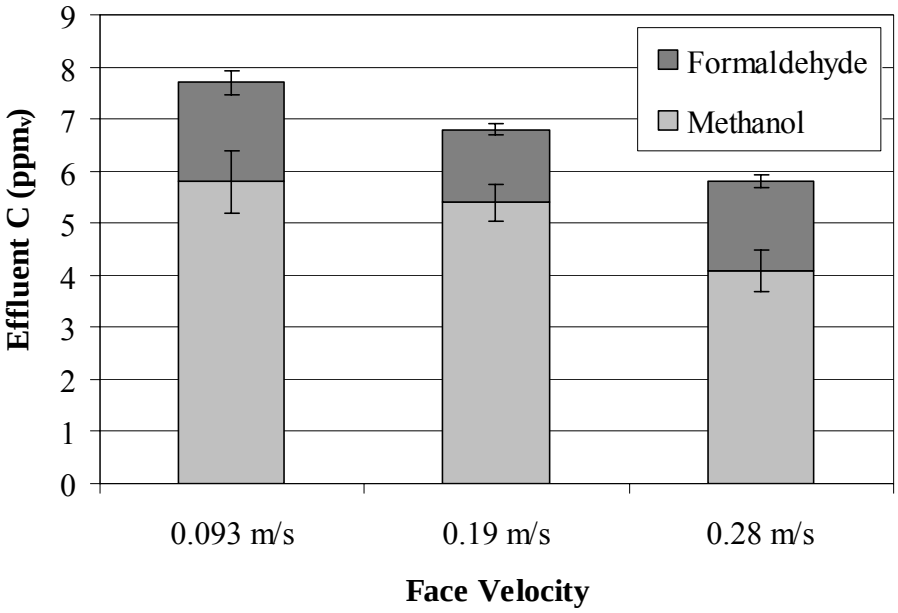

Figure 5-7. Effluent methanol and formaldehyde concentrations at steady state for variable face velocities and constant space time (4.3 s) for 50 Å 12% STC.

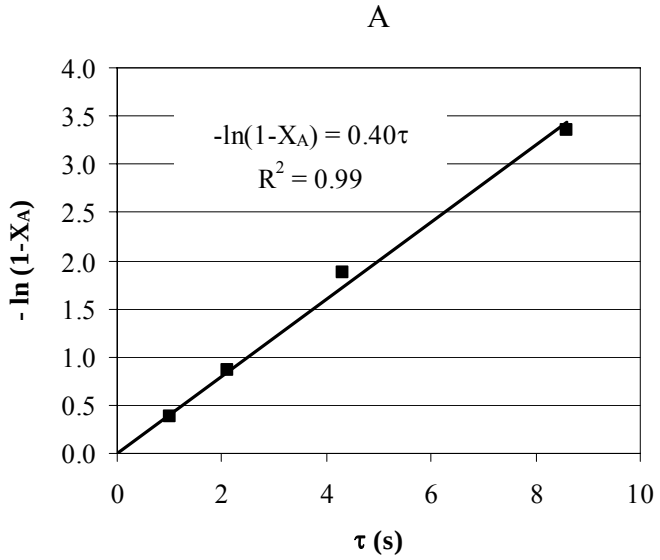

Figure 5-8. Linear regression of L-H model using mineralization rates achieved at various space times. A) 50 Å 12% STC. B) 120 Å 12% STC. C) 260 Å 12% STC.

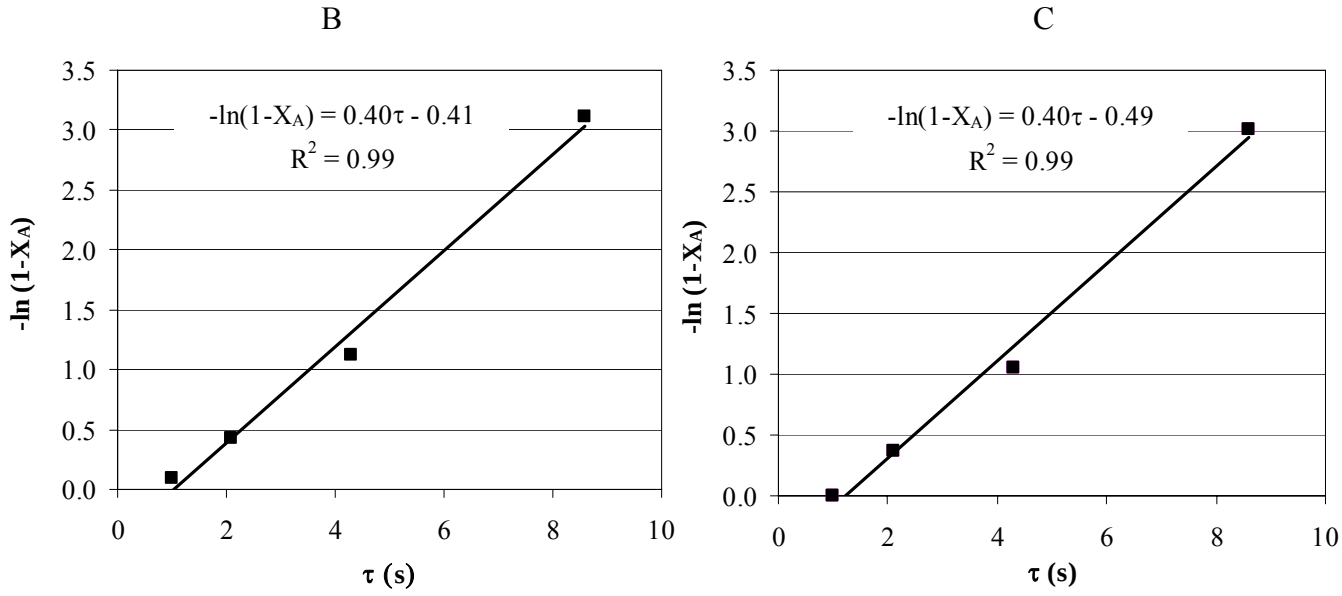

Figure 5-8. Continued.

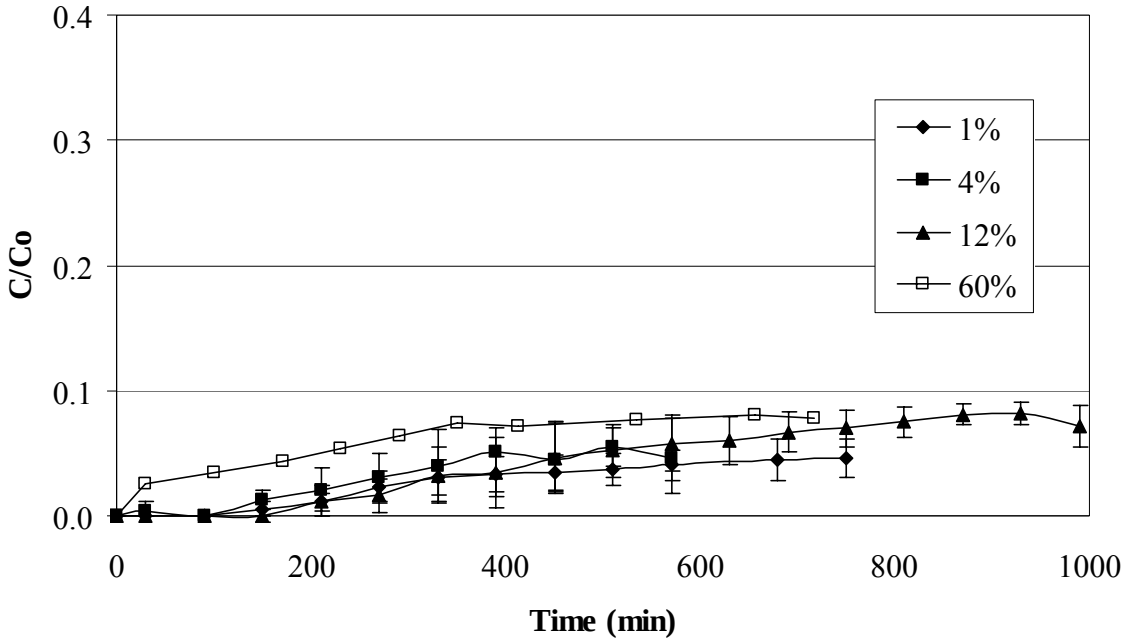

Figure 5-9. Effect of TiO_2 loading in 50 Å STC on methanol removal when illuminated with UVA light.

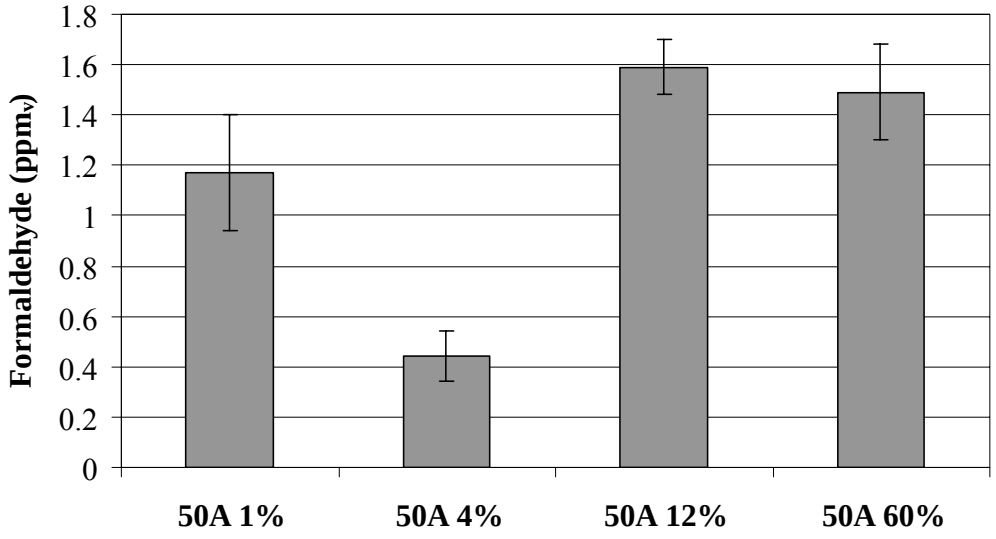

Figure 5-10. Effect of TiO_2 loading on formaldehyde production at steady state using 50 Å STC illuminated with UVA light.

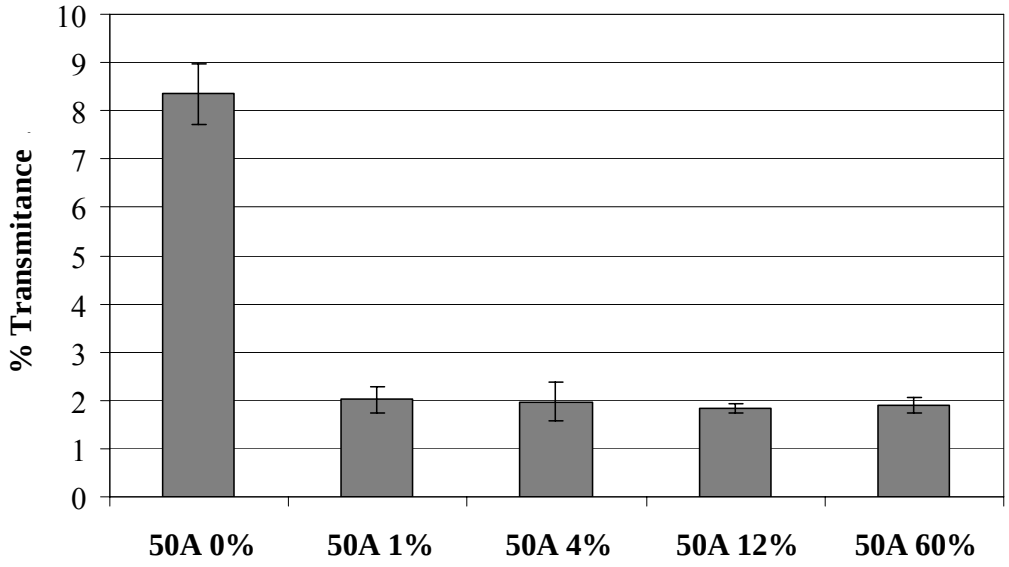

Figure 5-11. Percent transmittance of UVA light through 50 Å STC with various TiO_2 loadings.

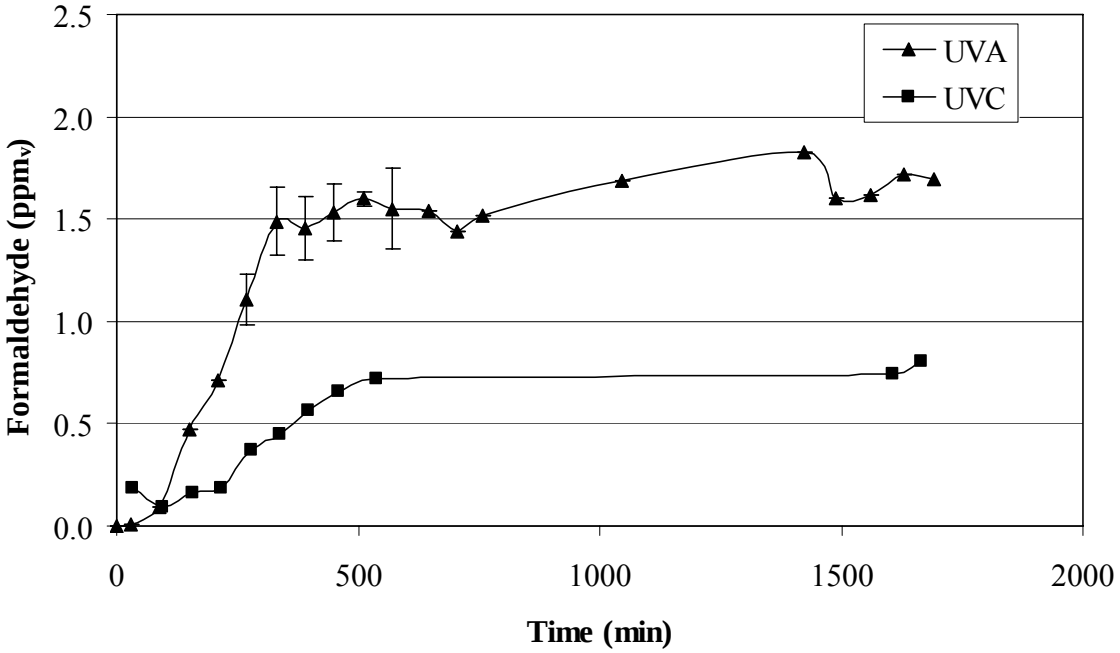

Figure 5-12. Effluent formaldehyde concentrations using 50Å 12% STC irradiated with UVA and UVC light.

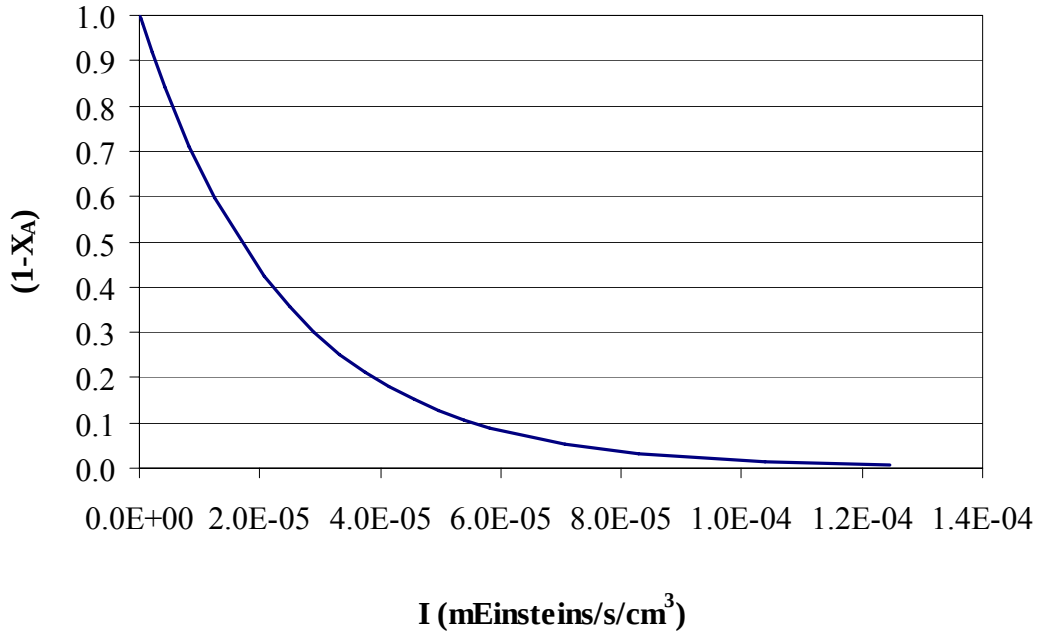

Figure 5-13. Predicted C/Co versus absorbed light flux for 50 Å 12% STC, 4.3 s residence time, Co = 50 ppm_v and 95% relative humidity.

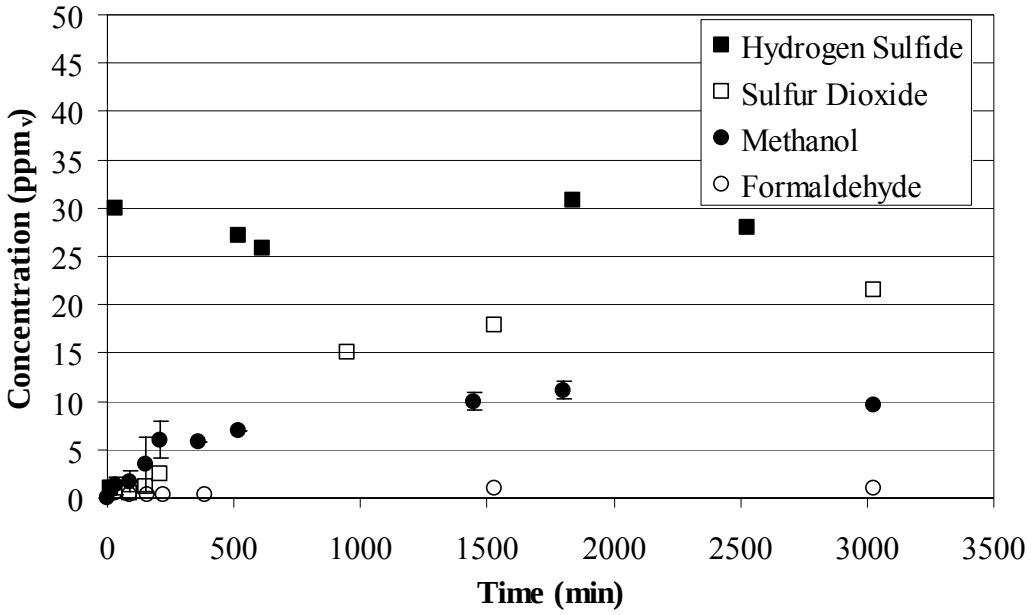

Figure 5-14. Effluent concentrations of H_2S, methanol and oxidation byproducts from 50 Å 4% STC illuminated with UVC light (Co methanol = 50 ppm_v, Co H_2S = 50 ppm_v).

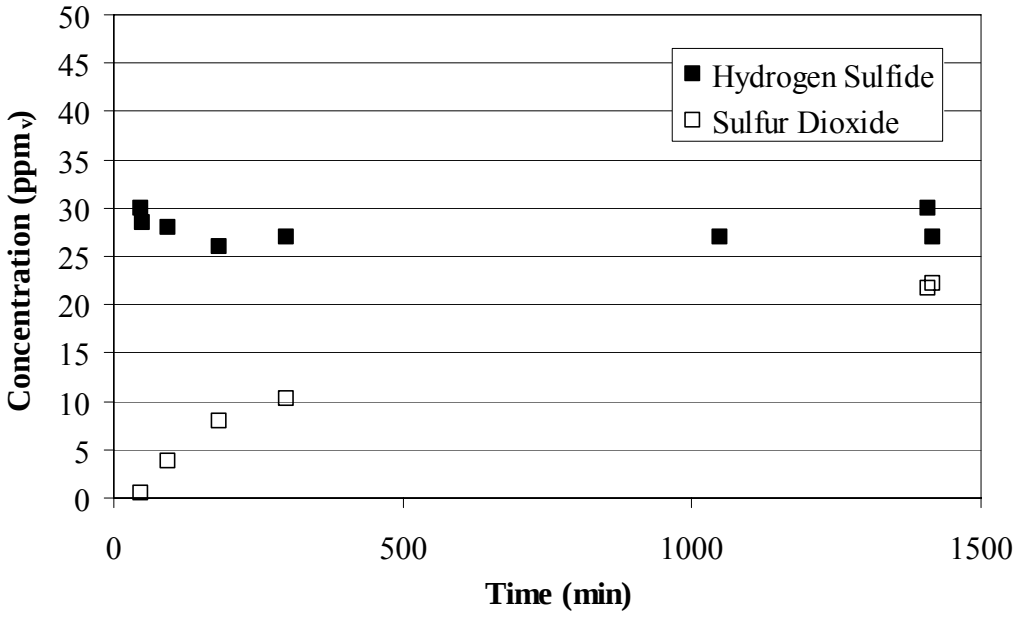

Figure 5-15. Effluent concentrations of H_2S and SO_2 from 50 Å 4% STC illuminated with UVC light (Co H_2S = 50 ppm_v).

CHAPTER 6
EFFECT OF CATALYST SUPPORT ON THE PHOTOCATALYTIC DEGRADATION OF METHANOL IN A PACKED-BED REACTOR

The objective of this study was to investigate the effect of the catalyst support on methanol oxidation efficiency using STC, TiO_2 coated on an opaque adsorbent material (i.e., activated carbon (AC)), and TiO_2 coated on a non-adsorbent material (i.e., 5 mm glass spheres). Preliminary scale-up was performed at the bench-scale by increasing the annulus size of the reactor from 8 mm to 25 mm in order to evaluate the efficacy of these materials for full-scale applications. In addition, the competitive effects of water vapor on methanol adsorption capacity and oxidation efficiency were evaluated.

The STC and TiO_2-coated AC were analyzed for BET surface area and total pore volume. The results of this analysis are shown in Table 6-1. A comparison of the total surface area and TiO_2 mass loading of the materials normalized for the reactor bed volume are shown in Table 6-2. Although the total specific surface area of the STC was less than half of that of the TiO_2-coated AC (617 m^2/g versus 1424 m^2/g), the surface area per reactor volume was more similar (308 m^2/cm^3 versus 380 m^2/cm^3) due to the higher bulk density of the STC. The bulk density of the STC and TiO_2-coated AC was about 0.53 and 0.26 g/cm^3, respectively. The TiO_2-coated glass spheres had the smallest total surface area per bed volume (0.43 m^2/cm^3) since the glass spheres were non-porous and only external surface area contributed to the total available surface area.

The TiO_2 mass loading per reactor volume was similar for the TiO_2-coated AC and TiO_2-coated glass spheres (9.9 and 10.5 mg/cm^3, respectively). The 50 Å 4% STC had a total TiO_2 mass loading of 26.7 mg/cm^3, which was about 2.5 times greater than the TiO_2-coated AC and TiO_2-coated glass spheres. The TiO_2 loading was calculated based on the amount of TiO_2 contained in each material and does not indicate the amount of TiO_2 that was available for

adsorption and photocatalytic reactions. For example, based on studies by Byrne et al. (2008), about 32% of the TiO_2 in the 50 Å 4% STC was inaccessible due to the formation of the SiO_2 matrix around the TiO_2 during synthesis. Therefore, the effective TiO_2 loading per bed volume would be 18.2 mg/cm^3. Based on the synthesis method for the TiO_2 coated AC and glass spheres, the majority of the TiO_2 should be accessible since TiO_2 particles were deposited on the external surface of the materials.

Methanol Adsorption and Oxidation in a Low Humidity Gas Stream

The TiO_2-coated materials were tested for methanol removal via adsorption (i.e., in the dark) at room temperature and simultaneous adsorption and oxidation (i.e., in the presence of UVC light) using a 4.3 s residence time, an influent methanol concentration of 50 ppm_v and a water vapor concentration of less than 65 ppm_v (typically 10 ppm_v), which was specified by the supplier of the compressed air used as the feed gas. A water vapor concentration of 65 ppm_v is equivalent to an RH of about 0.22% at 23 °C. As shown in Figure 6-1, the adsorption capacity of the TiO_2-coated glass spheres was low (ca. 0.1 mg/g) and initial breakthrough (i.e., effluent concentration greater than the MDL of 0.6 ppm_v or C/Co = 0.012) was achieved during the first sample. The TiO_2-doped adsorbent materials achieved extended periods of methanol removal (i.e., 1000 min for the AC and 3200 min for the STC) before breakthrough. The total methanol capacity of the STC (11 mg/g) was greater than that of the TiO_2-coated AC (6 mg/g). The adsorption capacity of the silica gel is a result of its surface chemistry, which is dominated by silanol functional groups (Si-OH) that serve as good adsorption sites for alcohols (e.g., methanol) via hydrogen bonding (Parida et al., 2006). In the presence of UV light, the effluent methanol concentrations for the TiO_2-coated glass spheres and STC were below the MDL (0.6 ppm_v or C/Co = 0.012). The effluent concentration of the TiO_2-coated AC reached a steady state concentration of about 2.5 ppm_v (C/Co = 0.05) after about 2500 min.

The effluent was tested for the presence of intermediate organic byproducts. As shown in Figure 6-2, TiO_2-coated glass spheres and TiO_2-coated AC created formaldehyde in the effluent, whereas the STC did not. According to TOC and GC analysis, other oxidation byproducts (e.g., formic acid, formates) were not identified in the effluent gas stream.

The formaldehyde concentration for the TiO_2-coated AC was low for the first 1000 min and then steadily increased until reaching a steady state concentration of about 6.3 ppm_v after 2000 min. The production of formaldehyde as an intermediate oxidation byproduct exceeded the adsorption capacity of the AC, thus causing the breakthrough profile shown in Figure 6-2. The effluent formaldehyde concentration for the TiO_2-coated glass spheres was about 0.3 ppm_v at steady state, which was achieved after about 500 min. For the STC system, effluent methanol concentrations were below the MDL and effluent formaldehyde concentrations were less than 0.1 ppm_v for the duration of the experiment. Thus, the STC resulted in the most efficient system for the mineralization of methanol. Several factors may have attributed to the enhanced efficiency of the STC system:

- The STC system had twice the amount of available TiO_2 surface area, which likely resulted in more active sites for oxidation leading to an increase in the overall efficiency.
- The STC exhibited a greater adsorption capacity for methanol compared to both the TiO_2-coated AC and the TiO_2-coated glass spheres. This enhanced adsorption capacity would concentrate the pollutant near the photocatalyst surface, potentially increasing the oxidation rate. Studies have shown that enhanced adsorption capacity has resulted in higher oxidation rates for organic compounds (Anderson and Bard, 1997; Tsumura et al., 2002; Vohra and Tanaka, 2003; Torimoto et al., 1996).
- The STC may have been less affected by the low water vapor concentration than both the TiO_2-coated AC and glass spheres. It has been suggested that SiO_2-TiO_2 materials use hydroxyl groups at the SiO_2-TiO_2 interface to produce hydroxyl radicals for the degradation of organic compounds thus enhancing the efficiency of the material (Yang and Chen, 2005).

Compared to the TiO_2-coated AC, both the STC and TiO_2-coated glass spheres were more efficient for methanol mineralization. This was likely due to the transparency of the silica gel and

glass spheres, which would allow for more efficient use of the UV radiation within the reactor. AC, which is opaque, does not allow transmission of UV light into or through the carbon matrix.

For the TiO_2-coated AC system at steady state, the effluent concentration of formaldehyde was about 6.3 ppm_v at steady state while the methanol concentration was about 1 ppm_v. This indicates that methanol was preferentially oxidized over formaldehyde in the TiO_2-coated AC system. The effluent concentration of formaldehyde from the TiO_2-coated glass spheres was 0.3 ppm_v while the effluent methanol concentration was non-detectable. Since the MDL for methanol was 0.6 ppm_v, it was unclear if methanol was preferentially oxidized in this case. The oxidation of methanol to formaldehyde can proceed by the direct oxidation of methanol in the electron hole in the absence of water vapor (Equations 2-9 through 2-11). However, the subsequent reaction from formaldehyde to formic acid requires a water molecule (Equation 2-13). The oxidation of formic acid to carbon dioxide and water can be accomplished by reaction with the electron hole in the absence of water vapor (Equations 2-14 and 2-15), which supports the absence of formic acid in the reactor effluent. Thus, the rate limiting step in the mineralization of methanol using TiO_2-coated AC was the oxidation of formaldehyde to formic acid. In the case of the STC, no formaldehyde was present in the effluent likely due to its higher overall efficiency (as discussed above). The availability of hydroxyl radicals at the SiO_2-TiO_2 interface may serve to increase the efficiency of formaldehyde oxidation to formic acid by allowing the indirect oxidation mechanism to proceed. In addition, the STC may have been able to adsorb the water vapor that was present in the gas stream better than the TiO_2-AC due to its surface functionality, which consists of silanol groups (Si-OH) that easily adsorb water via hydrogen bonding (Nawrocki, 1997; Morrow and Gay, 2000). This adsorbed water vapor could function to participate in direct oxidation or form hydroxyl radicals for indirect oxidation.

Methanol Adsorption and Oxidation in a High Humidity Gas Stream

In order to further elucidate the competitive effects of water vapor on the TiO_2-coated materials, they were tested for methanol adsorption and oxidation in a high humidity gas stream (RH_i = 95% at 23 °C). As shown in Figure 6-3, the adsorption breakthrough profiles were steeper and the adsorption capacities of the materials were reduced (1.2 mg/g for STC and 1.9 mg/g for AC). Although the AC broke through earlier than the STC, its adsorption capacity on a mg/g basis was greater than that of the STC due to the difference in bulk density between the two materials (i.e., 0.26 g/cm^3 for AC and 0.53 g/cm^3 for STC). The humid gas stream negatively affected the STC adsorption capacity more than that of the AC, indicating that the competitive effect of water vapor was more pronounced for STC than AC. This can be expected since the STC is dominated by silanol functional groups, which readily form hydrogen bonds with water, while the AC has a more heterogeneous surface chemistry (Puri, 1970).

In the presence of UV, the methanol removal efficiencies of the materials were about 95% for both the STC and TiO_2-coated AC. The systems reached steady state after approximately 250 min for AC and 400 min for STC. The TiO_2-coated glass spheres immediately achieved steady-state removal efficiency, which was between 80 and 90%. Steady state was quickly reached due to the low surface area and resulting low adsorption capacity of the TiO_2-coated glass spheres.

As shown in Figure 6-4, the increase in RH resulted in decreased formaldehyde production in the TiO_2-coated AC system (i.e., about 0.8 ppm_v at steady state). The reaction of formaldehyde to formic acid was no longer limited by the lack of water vapor, which may have resulted in lower formaldehyde concentrations in the effluent compared to the low RH case shown in Figure 6-2. In addition, Yamakata et al. (2003) showed that water vapor enhanced the

photocatalytic oxidation of methanol by preventing electron accumulation, which would otherwise cause defective sites on the TiO_2 surface and faster electron-hole recombination.

Although the water vapor increased the overall efficiency of the TiO_2-AC system, it resulted in a decrease in efficiency for the TiO_2-coated glass spheres and STC. The humid gas stream resulted in an increase in effluent formaldehyde concentrations for the TiO_2-coated glass spheres (about 1 ppm_v) and STC (0.5 ppm_v). The decrease in overall oxidation efficiency compared to that in dry conditions was likely a result of water competition for adsorption and reaction sites. The presence of higher effluent methanol concentrations in these systems indicates that the competition with water vapor was prevalent. It was hypothesized that the STC was more negatively affected by the increase in water vapor than the TiO_2-coated AC because the surface coverage of water vapor on the STC was greater than that on the AC. Water vapor adsorption studies confirmed this hypothesis and are discussed in more detail below.

Water Vapor Adsorption

In order to elucidate the effects of water vapor on the STC and TiO_2-coated AC systems, the water vapor adsorption profile was determined by measuring the effluent relative humidity of humid gas (influent RH = 95% at 23 °C) after passing through the reactor packed with TiO_2-coated AC or STC and illuminated with UV light. The results of these studies are shown in Figure 6-5. Note that the MDL for the hygrometer was 12% RH, so the lowest RH value plotted on the graph is 12% even though the actual effluent RH may have been lower. The total amount of water adsorbed by the STC and TiO_2-coated AC was 59 and 25 mg/g, respectively. For the STC system, this indicates that there were 3.7 water molecules adsorbed per nm^2 of STC, giving a surface coverage of about 0.26 m^2 of water per m^2 of STC (26%). For the TiO_2-coated AC, there were 0.58 water molecules adsorbed per nm^2, giving a surface coverage of about 0.05 m^2 of

water per m^2 (5%). Thus, the competition between water vapor and methanol on the STC surface would be much greater than that on the TiO_2-coated AC.

Capillary condensation within the pores was not evident for either the STC or TiO_2-coated AC. The Kelvin equation predicts that at 50°C, which is the approximate temperature of the bed with the UV light on, capillary condensation should only occur in pores less than 12 Å in diameter. For both the STC and TiO_2-coated AC, the majority of the pores were greater than 12 Å in diameter. For the STC, pores greater than 12 Å in diameter contributed to more than 95% of the total pore volume. According to Khan (2006), approximately 90% of the pore volume in BioNuchar AC, which was used in this study, resulted from pores greater than 12 Å in diameter.

In order to elucidate the effects UV light may have on the adsorption of water onto TiO_2-doped materials, the STC was tested for water adsorption in the dark at 50 °C. The results, also shown in Figure 6-5, indicate that there was no difference between the breakthrough profiles of the STC tested in the dark at 50°C or in the presence of UV light. Thus, the effect of UV light on water vapor adsorption was primarily a function of the heat generated by the lamp.

Reactor Scale-up using TiO_2-doped Materials

The TiO_2-doped materials were tested in a large annulus reactor (25 mm annulus) in order to evaluate the TiO_2-doped materials for potential use in full-scale applications, particularly for the treatment of HVLC gases emitted from pulp and paper mills. The TiO_2-doped sorbents were tested for methanol removal in a high humidity gas stream (RH = 95% at 23 °C). The high humidity case was chosen since HVLC gases are saturated with water vapor. The flow rate was adjusted such that the mass transfer characteristics (i.e., residence time and face velocity) were the same as those from the 8 mm annulus studies. As shown in Figure 6-6, the TiO_2-coated glass spheres achieved about 40% methanol removal over the duration of the study. The breakthrough profile for the STC was shallower than that of the TiO_2-coated AC, likely due to the greater

capacity for methanol adsorption by the STC, resulting in higher removal rates for the STC between about 100 and 1300 min. Both TiO_2-coated adsorbents achieved about 50% methanol removal at steady state. Note that error bars are present only for the experiments using STC in Figures 6-6 and 6-7 since experiments testing the TiO_2-coated AC and glass spheres were not replicated.

As shown in Figure 6-7, the effluent formaldehyde concentrations for the STC and TiO_2-coated AC were similar and increased steadily until reaching a steady state concentration of between 1.5 and 2.0 ppm_v. The TiO_2-coated glass spheres achieved steady state production of formaldehyde at about 1.6 ppm_v. According to TOC analysis, other oxidation byproducts (e.g., formic acid, formates) were not identified in the effluent gas stream.

The decrease in methanol oxidation efficiency in the large annulus reactor compared to that of the small annulus reactor was likely a result of inadequate UV light exposure within the entire packed bed. In the large annulus reactor, the TiO_2-doped adsorbents performed better than the TiO_2-coated glass spheres, indicating that adsorption of methanol onto a high surface area catalyst support resulted in higher oxidation rates. However, no difference was discerned between the silica gel, which is transparent, and AC, which is opaque, when used as the catalyst support in the large annulus reactor. The similar performance between the STC and the AC may be a function of the STC's affinity for water vapor, which resulted in a decrease in oxidation efficiency in the high humidity gas stream. It is expected that at lower RH, the efficiency of the STC system would improve as the competition of water vapor decreases.

Table 6-1. BET surface area and average pore volume of TiO_2-doped sorbents.

Material	BET surface area (m^2/g)	Pore volume (cc/g)
STC	616	0.79
TiO_2-coated AC	1424	1.06

Table 6-2. Surface area and TiO_2 loading per reactor volume.

Material	Total surface area per bed volume (m^2/cm^3)	TiO_2 loading per bed volume (mg/cm^3)
50 Å 4% STC	308	26.7
TiO_2-coated AC	380	10.5
TiO_2-coated glass spheres	0.43	9.9

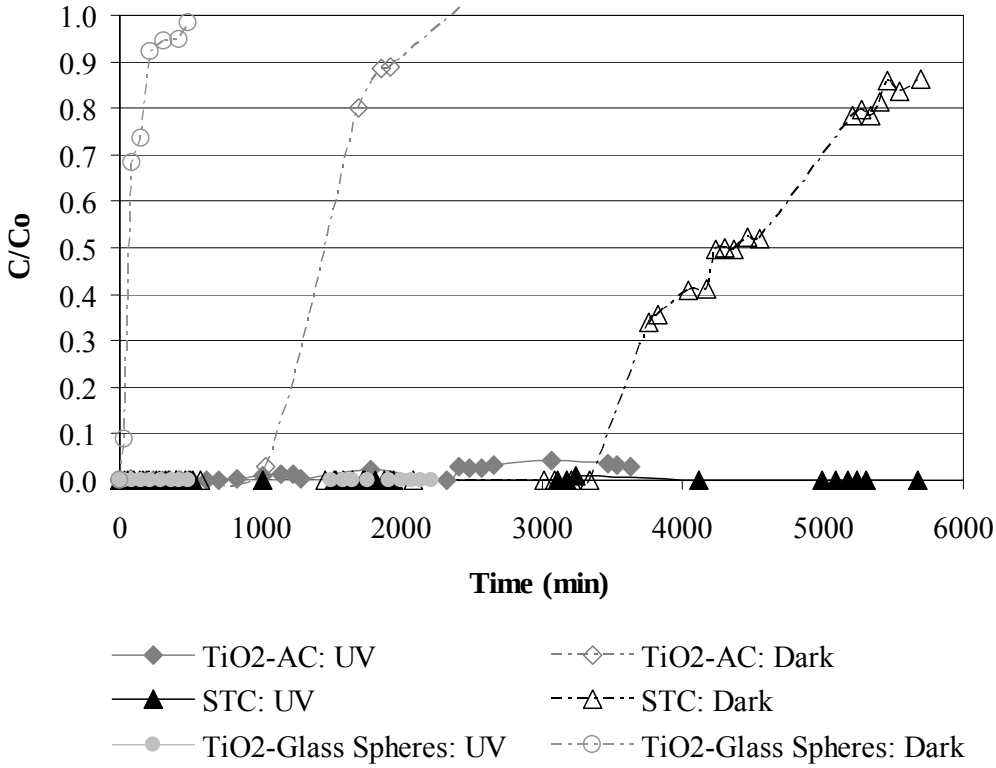

Figure 6-1. Normalized effluent methanol concentration for titania-doped materials used in the dark (adsorption only) and with UV light (adsorption and oxidation).

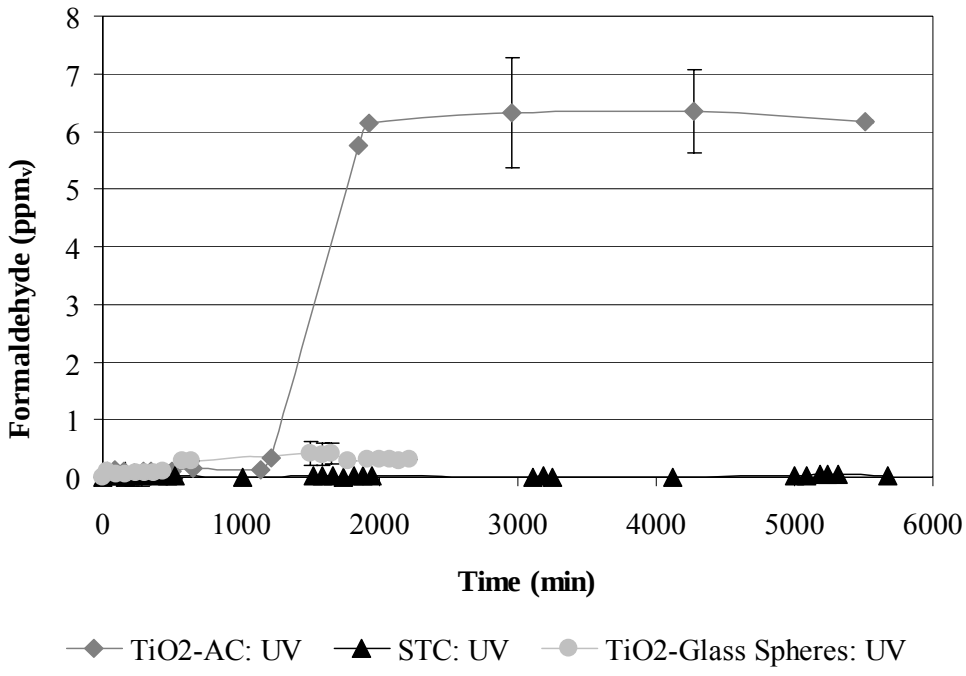

Figure 6-2. Intermediate byproduct (formaldehyde) formation by TiO_2-coated materials.

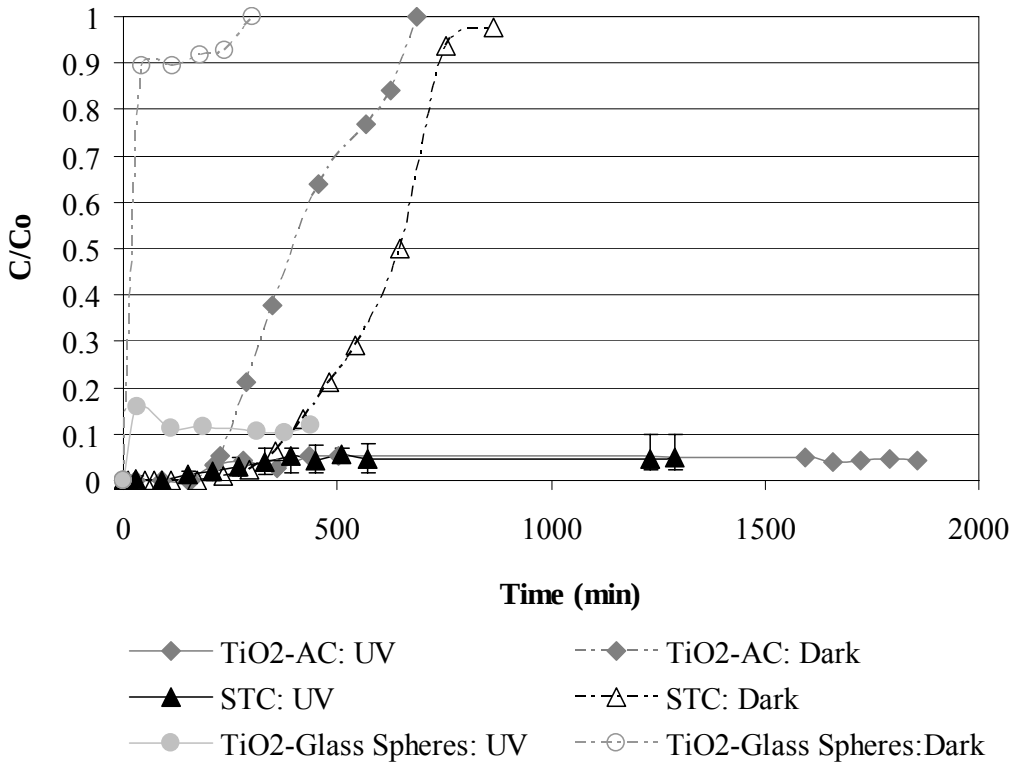

Figure 6-3. Normalized effluent methanol concentration for TiO_2-doped materials used in the dark and with UV light in a high humidity gas stream (RH = 95%).

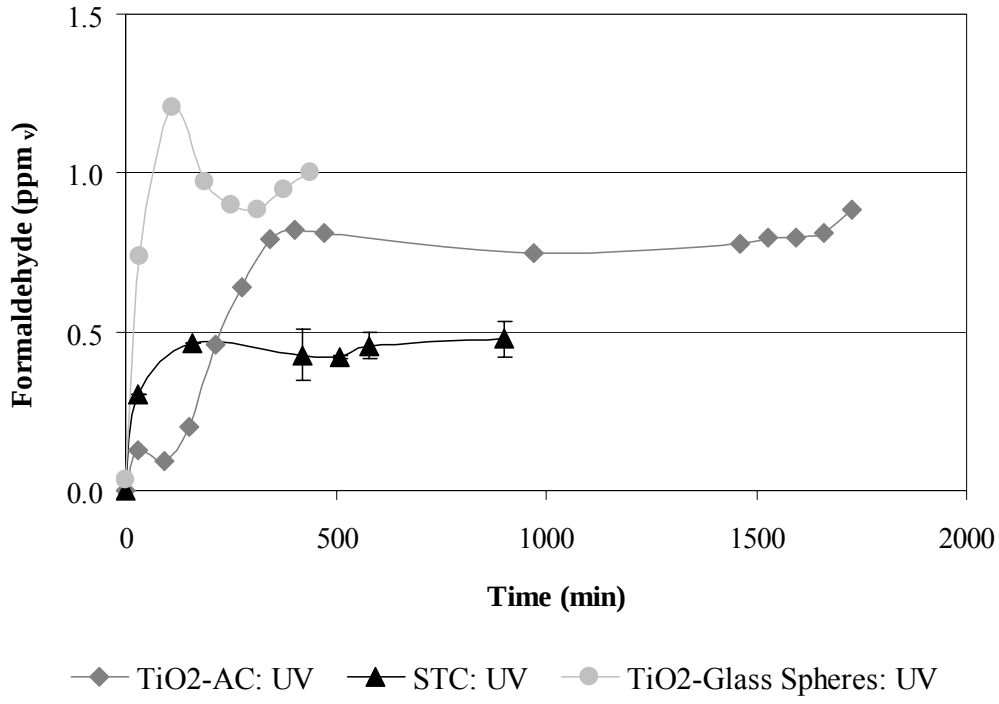

Figure 6-4. Intermediate byproduct (formaldehyde) formation by TiO_2-coated materials used in a high-humidity gas stream (RH = 95%).

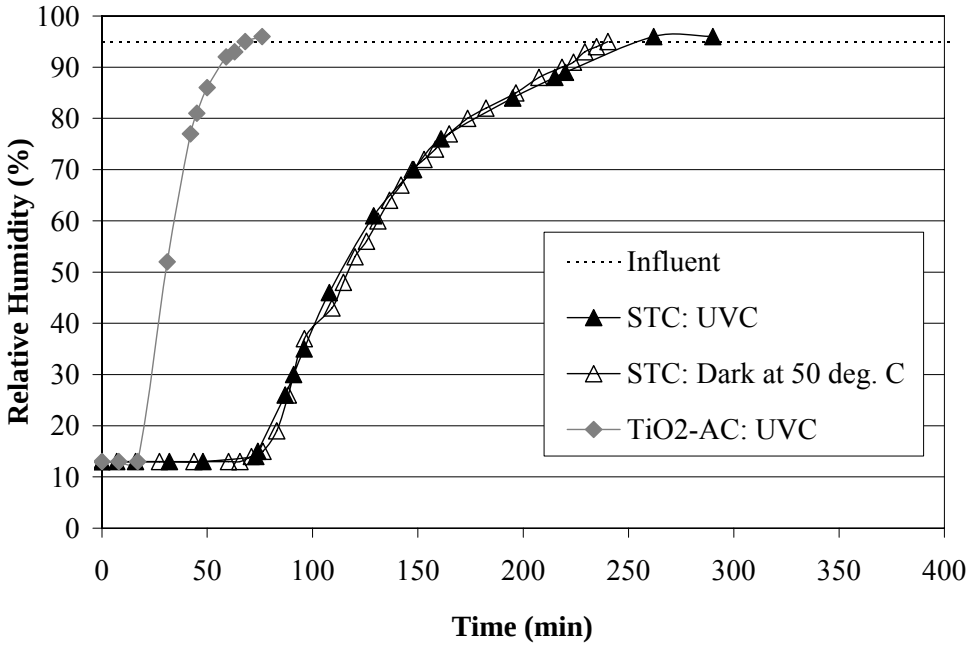

Figure 6-5. Water vapor adsorption breakthrough profile in a high humidity gas stream (RH = 95%).

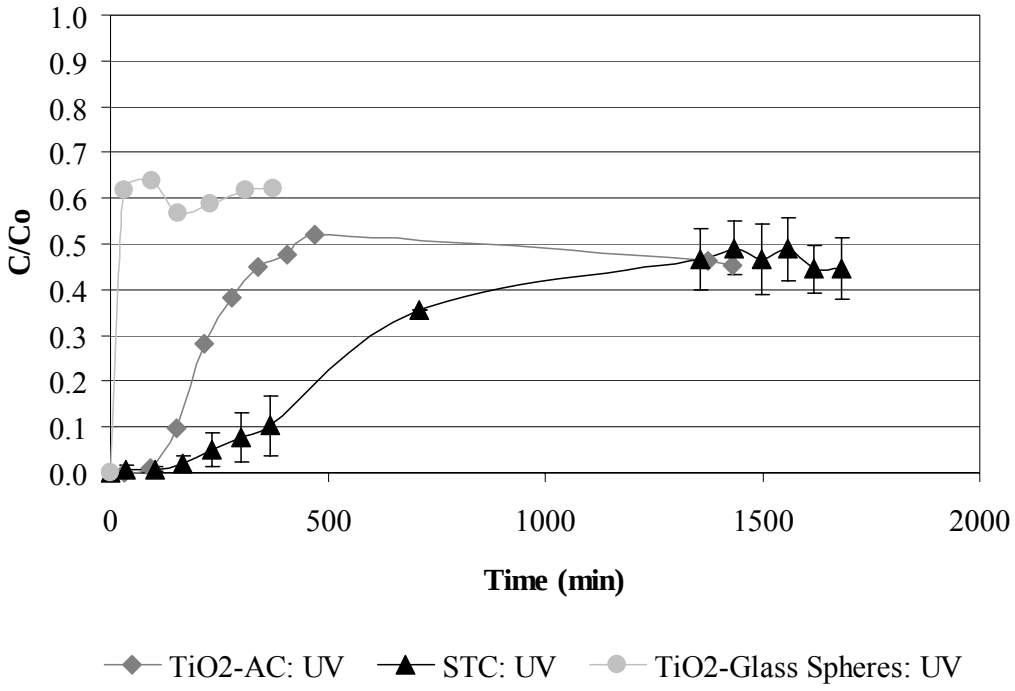

Figure 6-6. Normalized effluent methanol concentration for TiO_2-doped materials used in a large annulus reactor (25 mm) and high humidity gas stream (RHi = 95%).

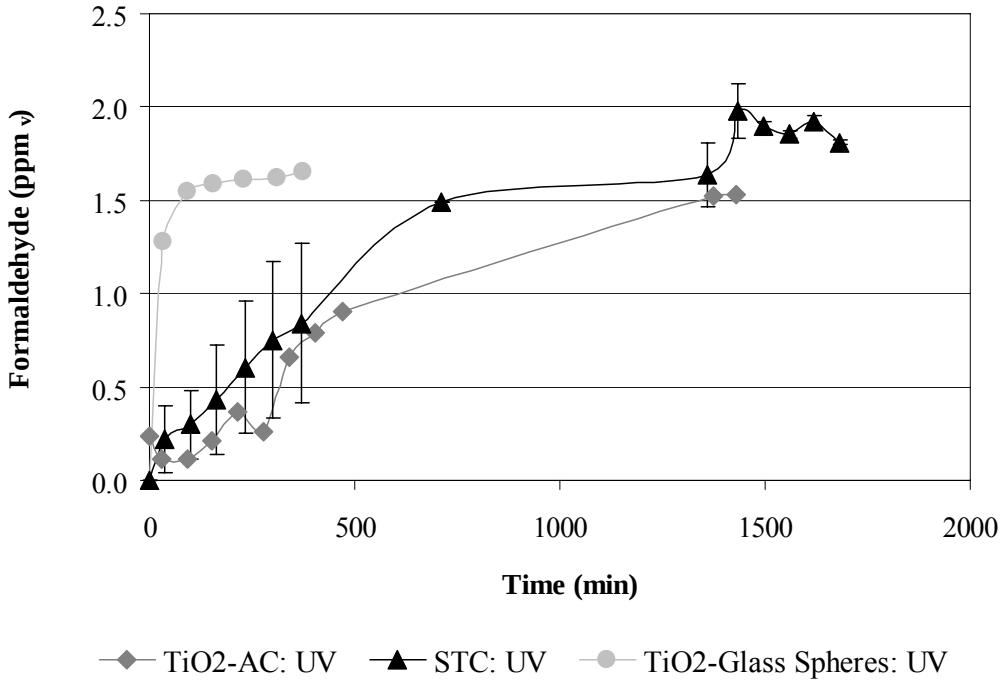

Figure 6-7. Intermediate byproduct (formaldehyde) formation by TiO_2-coated materials used in a 25 mm annular reactor and high humidity gas stream.

CHAPTER 7
PILOT STUDIES FOR METHANOL DEGRADATION

Based on the promising results and knowledge gained from bench-scale studies, a pilot-scale reactor was designed to treat 40 ACFM using 50 Å 4% STC pellets and UVC lamps. The laboratory-scale synthesis process for the STC pellets was scaled up to make the approximately 100 pounds of pellets needed for the studies. This scale-up process represented a substantial increase in production compared to the laboratory scale synthesis technique, which yielded several grams of pellets per batch. A novel test apparatus was designed and built to study the UV light distribution through a packed bed of STC pellets. Using this information as well as that learned during bench-scale studies, a pilot reactor was designed, fabricated, and tested for methanol degradation from an air stream saturated with water vapor.

STC Synthesis for Pilot-Scale Studies

In order to produce a sufficient quantity of STC pellets (50 Å 4%) for the pilot studies, the bench-scale synthesis method was modified to increase production efficiency while producing composites with similar characteristics (i.e., surface area and pore size). Silbond Condensed TEOS was chosen as the silica source. Silbond Condensed was chosen since it contained 94% TEOS with the balance comprised of ethanol and polysilicates. This TEOS source was chosen since it was economical and the balance of ingredients would not likely negatively affect the characteristics of the final STC product. The TEOS was added to water, ethanol, 1 N nitric acid, $3\%_{wt}$ hydrofluoric acid, and Degussa P25 TiO_2. The ingredients were stirred using a paddle mixer. Figure 7-1 shows an image of the mixing assembly used for blending the STC raw materials (mixing container is not shown to allow a view of the mixing paddle bars).

After mixing, the liquid STC was then transferred to molds, which were made from 5.1 cm thick polyethylene sheets drilled with 0.8 cm diameter holes. Each mold was approximately 40.6

cm by 61.0 cm and contained 2,750 holes. An image of one mold is shown in Figure 7-2. The molds were filled by pouring the liquid sol into the molds, which were sealed on the bottom and top with sheets of solid polyethylene. The STC pellets were aged at 65°C for 48 hours. The lids were then loosened and the pellets dried in the molds at 103°C in dual thermal chambers. The pellets were removed from the molds, transferred to Pyrex containers, and then heated to 180°C in the dual thermal chambers. After aging and drying, pellets were approximately 3 mm in diameter and 20 mm in length.

Since no heat transfer system was commercially available that was suitable for the STC preparation, a double-chamber heat transfer system was designed. This heat chamber provided a pneumatically sealed heat-generating source that was isolated from the STC materials. The system allowed the necessary temperature variations within the inner-chamber, where the pellet trays resided during aging and drying. The inner-chamber was equipped with a ventilation system that allowed any volatile gases to discharge away from any source of heat or flame. This gas could be passed through a heat exchanger for recovery of the ethanol. A photo of the heat chamber is shown in Figure 7-3.

The STC pellets were made in a series of batches, each of which yielded 7-8 pounds of pellets. A grab sample was taken from each batch and analyzed for surface area, total pore volume, and pore size. The results of this analysis are shown in Table 7-1. The STC synthesized for pilot studies used the same ratio of raw ingredients as the pellets used for bench-scale testing. However, the dried STC pellet had a higher BET surface area and smaller pore size than those synthesized in the lab (surface area was 723 m^2/g versus 617 m^2/g and pore size was 38 Å versus 49 Å). The differences between these measurements can be attributed to slight differences in the synthesis procedure that were inherent with scale-up. Since the bench-scale studies indicated

that STC with higher surface area and smaller pore sizes achieved better performance, there was no attempt to adjust the pilot-scale procedure to achieve STC with different characteristics.

UV Light Distribution in a Packed Bed of STC

In order to determine the spacing of UV lamps for the pilot reactor, a unique test system was developed to measure the UV light penetration through a packed bed of STC. A series of square boxes of the same height and varying length/width dimensions were manufactured from Alzak reflective material. A support stand was made to support a UVC lamp in the center surrounded by any one of the boxes. Each box had a ¼ inch port for UV measurements. A schematic of the test system (provided by the fabricator) is shown in Figure 7-4.

Each box was filled with the STC pellets and the UV lamp was illuminated. UV measurements were taken through the port on the side of the box to measure the amount of light penetrating through the packed bed. This was repeated for each box so that the UV light penetration through various bed depths could be measured. The results are shown in Table 7-2. The UV intensity decreased as the packed bed depth increased for two reasons: (1) the intensity of UV light decreases as a function of the inverse square route of the distance from the lamp; and (2) a deeper bed of STC would also serve to attenuate more light. No UV light was measured through a packed bed depth of 1 inch. Therefore, the maximum distance between any portion of the packed bed and a UV lamp should be less than 1 inch in order to avoid "dark spots" in the reactor.

Pilot Studies

Figure 7-5 shows a process flow diagram for the pilot studies. A variable frequency drive fan was used to push the gas stream through the pilot reactor. The space time was about 4.3 s, similar to that used in bench-scale studies. A water/methanol mixture was vaporized and injected into the gas stream so that the influent methanol concentration was about 50 ppm_v and relative

humidity between 95 and 99%. The static pressure and velocity pressure were monitored before the inlet to the pilot reactor. Thermocouples were used to measure inlet and outlet temperature.

The pilot reactor was fabricated by MicroEnergy Systems, Inc. (Oakland, MD). A general arrangement drawing for the pilot reactor, which was provided by MicroEnergy Systems, Inc., is shown in Figure 7-6. A photo of the reactor is shown in Figure 7-7. The dimensions of the reactor were approximately 17 in by 17 in by 8 ft tall. The gas flowed upwards into the bottom of the reactor and through a plenum, which supported the packed bed of STC pellets. The STC pellets were packed between 46 UVC lamps (American Ultraviolet Corporation), which were oriented in the reactor parallel to the air flow. The lamps were spaced 2.375 in. center to center such that 79% of the pellets were within 0.6875 in. of a UV lamp and no pellet was more than 1 in. from a UV lamp. The UV lamps were housed in 1 in. quartz sleeves, each of which included electrical connectors and wires, the latter of which passed through sealed stoppers. Top and bottom support racks (shown in section A-A of Figure 7-6) were designed to support each UV lamp assembly. A UV-Technik Electronic Ballast Power Center was installed in conjunction with the 46 UV bulbs, thus giving the capability to vary UV radiation in response to a variable voltage power input, which was controlled by the potentiometer setting. A UVP radiometer (Upland, CA) was used to measure the UV intensity through an observation window on the side of the reactor. The inside of the reactor was lined with Alzak UV reflective material. Initial studies performed with an empty reactor showed no photolysis of methanol and that adsorption of methanol to the reactor and its appurtenances was negligible.

Two tests were conducted with variable UV intensities controlled by varying the potentiometer setting, which controlled the voltage input. For the first test, the potentiometer was set to 22%. The UV intensity (as measured through an observation port located on the side of the

reactor) was about 6.5 mW/cm^2. For the second test, the potentiometer was set to 100% and the corresponding UV intensity was about 11 mW/cm^2. In both cases the breakthrough profile was similar to that seen in bench-scale studies. The effluent methanol concentration was non-detectable for the first 4-6 hours, due to adsorption on the virgin STC surface, and then increased until the steady state was reached (i.e., the rate of adsorption equaled the rate of oxidation). The results of the pilot tests are shown in Table 7-3. The methanol oxidation efficiency was dependent on the UV intensity at steady state, with the higher UV intensity resulting in about 66% removal while the lower UV intensity resulted in about 27.5% removal efficiency. The effluent formaldehyde concentration was minimal (i.e., less than 1 ppm_v) for both studies, thus indicating that the majority of methanol was oxidized to inert byproducts (i.e., carbon dioxide and water vapor). The effluent temperatures were significantly higher than the influent temperatures for both tests due to the heat generated by the high intensity lamps. When operated at their maximum intensity, the lamps require 60 W and output 16.2 W as UVC. Therefore, most of the input energy was lost as heat, which resulted in the elevated effluent temperatures.

The effluent temperatures suggest that the reactor operated under elevated temperatures compared to the temperature tested at the bench-scale, which was about 50°C (122°F). Elevated temperatures can result in a decrease in UV intensity since UV lamps operate most efficiently at 104°F. Based on manufacturer provided data, the UV lamps operate at about 70% efficiency at 139.3°F (low intensity setting) and 50% efficiency at 157.6°F (high intensity setting). This decrease in photon flux could yield a decrease in oxidation rate. In addition, a decrease in the adsorption affinity of methanol for the STC surface due to the higher temperatures could result in decreased oxidation rates. Therefore, improved results may be achieved by adding a cooling system to the UV lamps to transfer heat away from the lamps and packed bed.

In addition to temperature effects, the efficiency of the pilot reactor may have been dictated by the UV light distribution in the packed bed. The maximum distance between an STC pellet and a UV lamp in the reactor was 1 in. The reactor was designed so that the UV intensity approached zero as the distance away from the UV lamp increased to 1 in. However, the UV intensities achieved in the portions of the bed approaching 1 in. from the UV lamp may not have been sufficient to achieve higher oxidation rates. Thus, a minimum UV intensity across the entire bed may be necessary to increase oxidation efficiency.

Table 7-1. BET surface area, pore volume, and pore size analysis for pilot STC.

BET surface area (m^2/g)	Total pore volume (cc/g)	Actual pore size (Å)
723 ± 67	0.75 ± 0.12	38 ± 3

Table 7-2. UV intensity measurements through packed beds of STC of varying depths.

Box No.	Distance (in.)	UV intensity ($\mu W/cm^2$)
5	0.25	42
4	0.5	16
3	0.75	3
2	1.0	0
1	2.0	0

Table 7-3. Results of pilot studies with variable potentiometer settings.

Experiment	UV intensity (mW/cm^2)	Inlet temp (°F)	Outlet temp (°F)	Steady state methanol removal	Formaldehyde production (ppm_v)
Low Intensity (Setting = 22%)	6.5	75.6 ± 5.4	139.3 ± 3.0	27.5 ± 5.5%	0.28 ± 0.26
High Intensity (Setting = 100%)	11.5	72.6 ± 4.0	157.6 ± 6.0	66 ± 7%	0.74 ± 0.10

Figure 7-1. Mixing assembly for blending the raw ingredients for pilot-scale STC synthesis.

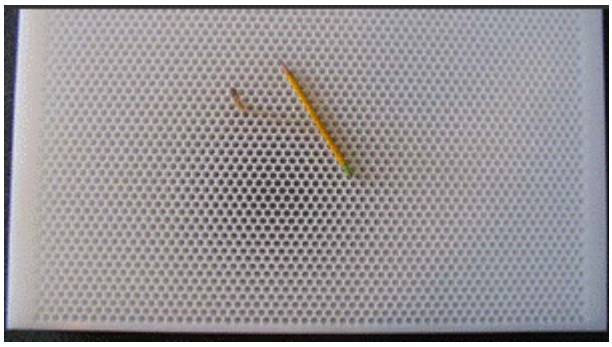

Figure 7-2. Pilot-scale molds for STC synthesis.

Figure 7-3. Specialty heat chamber for pilot-scale STC synthesis.

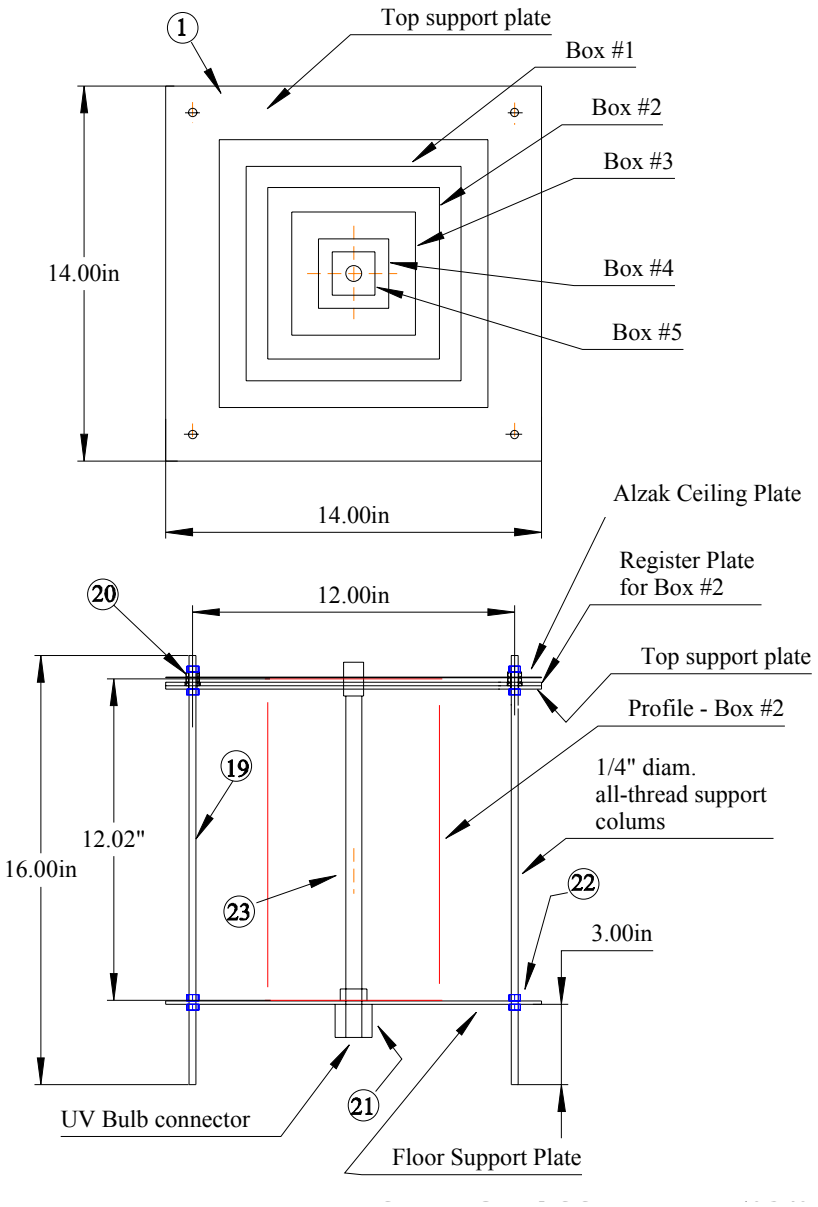

Figure 7-4. Alzak box test system for measuring UV light penetration through packed beds of various depths.

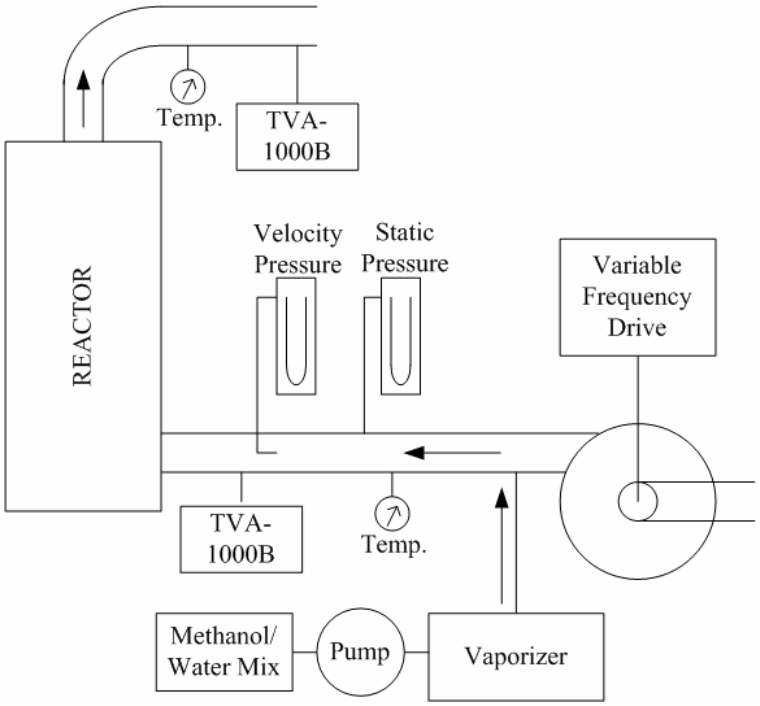

Figure 7-5. Process flow diagram for methanol degradation pilot studies.

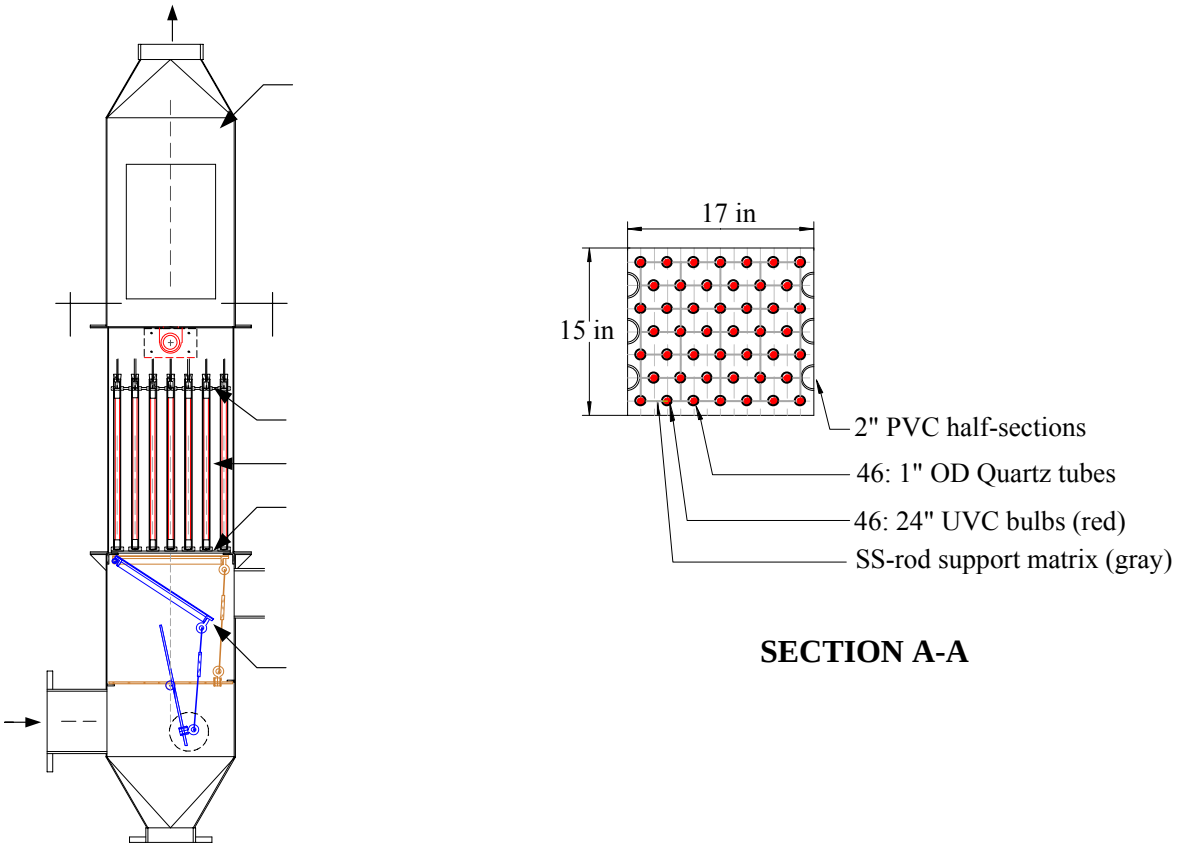

Figure 7-6. General arrangement drawing of the pilot reactor for methanol degradation.

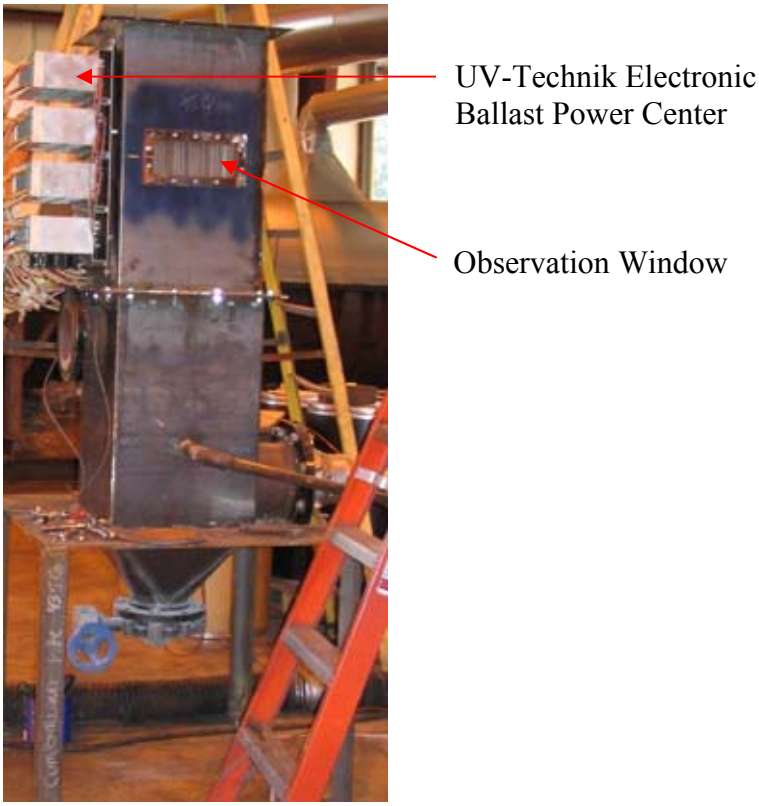

Figure 7-7. Photo of pilot reactor.

CHAPTER 8
DEVELOPMENT OF A REGENERABLE SYSTEM EMPLOYING STC PELLETS FOR MERCURY REMOVAL FROM END-BOX EXHAUST AT A CHLOR-ALKALI FACILITY

The STC technology may be advantageous for the removal of mercury from end-box exhaust in chlor-alkali facilities due to its high mercury adsorption capacity and ability to be regenerated with acid. The mercury-laden acid used for regeneration can be recycled into the mercury-cell process, thus closing the loop on mercury emissions. This chapter summarizes the design and performance of pilot- and full-scale reactors used to recover mercury from the end-box exhaust at a chlor-alkali facility. In addition, an economic analysis, which compares the costs of implementing this technology versus using activated carbon at the facility, is presented.

Pilot-Scale Packed Bed Reactor

A pilot reactor was fabricated and tested for mercury removal from end-box exhaust, which consisted of air and trace quantities of hydrogen (0.02%), contained elemental mercury vapor, and was saturated with water vapor. The total flow rate of the caustic exhaust system was about 350 ACFM during the pilot studies. The exhaust passed through a heat exchanger, which reduced the temperature to between 6 and 8 °C, and a series of knock-out pots to remove entrained water and mercury droplets. A slipstream of the exhaust was taken after the knock-out pots and passed through a blower, into the pilot reactor, and back into the vent for release into the atmosphere. A process flow diagram for this process is shown in Figure 8-1.

The pilot reactor contained a fixed bed of STC pellets packed around UV lamps. The STC pellets had an average BET surface area of 351 m^2/g, pore volume of 0.95 cm^3/g, and pore diameter of 109 Å. The reactor contained two chambers (Chamber A and Chamber B), which could be operated and sampled independently of each other. Two Teflon-coated UV lamps (American Ultraviolet Corporation), were positioned vertically in each chamber and on two external reactor walls (one wall of each chamber). The reactor walls were made up of Lucite

UVT material, which is transparent to UV light. The outer shell of the reactor was made of Alzak reflective metal in order to reflect light into the packed bed. The exhaust flowed upwards through the reactor while the STC pellets were continuously irradiated with the UV lamps. Each lamp was controlled individually such that any combination of lamps could be illuminated at one time. A schematic and photo of the pilot reactor are shown in Figures 8-2 and 8-3.

Pilot Study Results

The pilot-scale study treating mercury in a slipstream from caustic exhaust was conducted from February to May of 2005 at a chlor-alkali facility in the US. For all pilot studies, the UV lamps were operated continuously in order to maximize mercury removal efficiency to help meet this facility's goal of zero emissions. The objective of the pilot experiments was two-fold: (1) confirm the efficacy of the technology for mercury removal and recovery by regeneration with HCl; and (2) determine the factors that may limit mercury removal efficiency (e.g., residence time, mass transfer, and UV light distribution within the packed bed).

In order to confirm the efficacy of the technology and test the effectiveness of regeneration using HCl, a series of two experiments were conducted. In the first experiment, the reactor was packed with virgin STC pellets and continuously operated for 10 days using a flow rate of 10 ACFM and a space time of 0.53 s. As shown in Figure 8-4, the influent concentrations ranged between 400 and 1600 ug/ft^3 (or 1795 and 7180 ppb$_v$). Although the influent mercury concentration was highly variable, the effluent mercury concentration remained low (26 ± 17 ug/ft^3 for Chamber A and 31 ± 16 ug/ft^3 for Chamber B). The mercury removal rate achieved by the reactor over this 10 day period was 96 ± 3 %. Although the reactor ran continuously for the 10 day period, no samples were collected on days 3-5 since the chlor-alkali facility employees were not available to collect samples. Table 8-1, which refers to this experiment as "Test No. 1", shows a summary of results for the pilot data. The error is represented as the standard deviation.

After the 10 days of operation, the pellets were removed from the reactor and regenerated in HCl. The mercury concentration on the pellets was determined by digesting the pellets before and after regeneration. About 99% of the mercury was removed from the pellets using this regeneration procedure. In order to test the effect of regeneration on the performance of the STC pellets, a second experiment was conducted in which virgin pellets were packed in Chamber A and the regenerated pellets were packed in Chamber B. The reactor was operated using the same flow rate and space time (10 ACFM and 0.53 s) as the previous experiment. As shown in Figure 8-5, both the new and regenerated pellets performed similarly and achieved greater than 90% removal for at least 21 days. After 35 days of operation, the effluent mercury concentration approached that of the influent; thus, breakthrough was achieved. The mercury loading on the pellets was calculated by performing a mass balance on the reactor. After the first 21 days of operation (i.e., before breakthrough) the mercury loading on the virgin pellets was about 260 mg/g and the loading on the regenerated pellets was about 247 mg/g. Since these mass loadings are similar, this confirms that the regeneration procedure did not impact the performance of the STC pellets.

A series of tests were conducted in which the effects of space time, mass transfer, and UV irradiation were studied. For each experiment (shown as Test Nos. 2 through 4 in Table 8-1), virgin STC pellets were used in the pilot reactor. In order to hypothetically improve upon the performance of Test No. 1, the flow rate was decreased for Test No. 2, resulting in a longer space time and higher j-factor (i.e., improved mass transfer). The average effluent concentration for Test No. 2 was 11.5 ug/ft^3, which is significantly lower than the effluent concentrations from Test No. 1 ($P = 0.0248$ based on two-tailed t-test with 95% confidence interval). To test whether this improvement was a result of better mass transfer or the increase in space time, the bed height

was increased from 10 in. to 31 in. and approximately the same flow rate as Test No. 2 was used for Test No. 3A. This increase in space time from 0.67 to 2.3 s resulted in lower mercury effluent concentrations, which averaged 2.9 ug/ft^3. This suggests that the mercury removal rate is limited by the rate of photocatalytic oxidation, rather than mass transfer.

A factor that may limit the rate of photocatalytic oxidation in a packed bed is ineffective UV light distribution within the bed. Therefore, in Test No. 3B, the outer UV lamps positioned behind the transparent side wall of the reactor were illuminated to enhance the distribution and increase the intensity of UV light in the bed. This increased irradiation did not result in a decrease in effluent mercury concentration. Thus, the rate of photocatalytic oxidation did not increase with the increase in UV radiation within the bed. Therefore, the space time through the bed was further increased in attempts to achieve lower effluent mercury concentrations.

In Test No. 4, the flow rate was decreased to 3.6 ACFM in order to increase the space time to 4.6 s. The effluent mercury concentration from this test averaged 3.6 ug/ft^3, which was not significantly different than Test No. 3A ($P = 0.1646$). Thus, the increase in space time from 2.3 to 4.6 s did not enhance mercury removal as was seen with the increase in space times between 0.53 and 2.3 s. At space times greater than 2.3 s, the removal rate through the reactor was limited by factor(s) other than photocatalytic oxidation rate. For example, at low effluent mercury concentrations (i.e., 3-6 ug/ft^3), there may not be sufficient driving force for mass transfer and subsequent adsorption. Additionally, photocatalytic reduction of sorbed mercuric oxide (HgO) to elemental mercury may occur by the free electrons on the TiO_2 surface, which are generated by irradiation of this surface with UV light (Li and Wu, 2006). Although the photocatalytic oxidation of elemental mercury is the primary reaction pathway since oxygen serves as a stronger electron trap than HgO, a photocatalytic reduction effect was seen in the work of Li and

Wu (2006) while studying the use of STC for mercury removal from flue gas. Elemental mercury has a lower adsorption affinity for the STC surface; thus, desorption or restrained adsorption of elemental mercury from the gas stream may occur. Thus, photocatalytic reduction may inhibit the attainment of lower effluent mercury concentrations.

Full-scale Reactor

Based on the promising results from the pilot studies, two full-scale reactors were designed and installed. Each of these reactors was designed to treat up to 1200 ACFM and 1600 ug/ft^3 and have in-situ regeneration capabilities. Each unit was designed to handle the entire flow rate so that the other could be offline for regeneration. The footprint of each reactor was about 3 feet by 6 feet. Before entering the reactor, the exhaust passed through a heat exchanger and demister, which removed entrained liquid droplets greater than 4 μm in diameter. The temperature entering the online reactor was typically between 10 and 15°C. Regeneration was performed in-situ by soaking the pellets inside of the reactor with 37%$_{wt}$ HCl for 30 min. The mercury-laden acid was then drained from the reactor and the pellets were rinsed with water. Both the HCl and water were introduced into the reactor by a spray nozzle located inside the top of the reactor above the packed bed. A process flow diagram for this full-scale system is shown in Figure 8-6.

The design of the pilot reactor was scaled-up so that the space time and Colburn j-factor in the full-scale units were 0.63 s and 0.10, respectively, when treating the maximum design flow rate of 1200 ACFM. The UV light spacing was similar to that used in the pilot scale reactor. The reactors were filled with STC pellets with an average BET surface area of 453 m^2/g, pore volume of 1.04 cm^3/g, and pore diameter of 92 Å. Two full-scale reactors were installed in parallel so that one could be in operation while the other was regenerated. This also provides a level of

redundancy since regeneration requires only a short period of time (i.e., 4 hours) compared to the time that the other reactor will be online before regeneration is required (i.e., 30 days).

Data from the first three operation cycles for the reactors are shown in Table 8-2. The error is represented as the standard deviation of measurements taken over the operation time. For all studies, the effluent mercury concentration remained steady throughout the run (i.e., error is not associated with breakthrough). The cycles are designated using a letter (either A or B) followed by a number. The letter indicates which reactor was in operation and the number indicates the cycle number. For example, Run No. A-1 indicates the first operation cycle for Reactor A. For the three operation cycles shown, the average flow rate decreased with each run for unknown reasons. The flow rate in subsequent runs (results not shown) varied between 400 and 700 ACFM.

Run No. A-1 averaged slightly more than 50% removal over a 29 day period. This poor performance was due to the lack of water entering the bed. The influent water loading into the pilot was about 3 lbs of water/1000 ft^3 of air; however, the loading into the full-scale reactor was about 0.45 lbs/1000 ft^3. This is a result of changes made to the exhaust system (including the addition of a new heat exchanger and demister) during the time between the pilot reactor testing and the installation of the full-scale reactors. During Run No. A-2, the demister was initially bypassed in order to increase the influent water loading and test this hypothesis. After 15 days of operation, the demister was brought online and water was added into the reactor through the nozzle in the top of the reactor above the packed bed. About 60 gallons of water were added to the reactor once per day for the remainder of the cycle.

Figure 8-7 shows the influent and effluent mercury concentrations for this run (No. A-2). During the first 15 days, while the demister was offline, the effluent mercury concentrations

were low. However, the influent mercury concentrations were highly variable, ranging between about 400 and 1800 ug/ft^3. Since the demister typically removed some of the elemental mercury that was entrained as small droplets in the exhaust, it was brought back online on Day 15 in order to decrease the influent mercury loading to the bed, thus increasing bed life and time between regenerations. Therefore, water was added through a nozzle positioned in the top of the reactor after the demister was brought back online. This proved equally as effective at reducing the effluent mercury concentration. During the entire 43-day cycle, the actual flow rate through the reactor was 560 ± 140 ACFM. The average effluent concentration was 21.5 ± 23.8 ug/ft^3, which corresponds to a mercury removal rate of 95 ± 5%. The mercury loading on the pellets at the end of this operational cycle was about 190 mg/g.

Some of the water, which was added through the nozzle to saturate the bed during Run No. A-2, passed through the packed bed and was drained from the reactor. During Run No. B-1, the demister was online and water was added through the top nozzle. However, the water loading rate was optimized so that 15 gallons of water were added every 2 hours. This water application rate did not result in excess water passing through the packed bed and yielded low effluent mercury concentrations, which averaged 10.8 ug/ft^3.

The addition of water to the full-scale reactor was necessary to provide sufficient hydroxyl radicals on the TiO_2 surface. This indicates that mercury was not directly oxidized by the electron holes on the TiO_2 surface, but was indirectly oxidized by hydroxyl radicals, which are powerful oxidants. These hydroxyl radicals are created by the oxidation of adsorbed water vapor. Due to the low influent water concentration and the rise in temperature through the reactor caused by heat generated by the UV lamps, adsorption of water vapor to the STC surface was

low. Therefore, constant water addition was necessary to maintain a sufficient quantity of water on the surface of the STC.

Economic Analysis

An economic analysis was performed to assess the feasibility of the STC technology compared to treated (e.g., sulfur or iodine impregnated) activated carbon. The design for both technologies was based on the maximum design flow rate and influent mercury concentration of 1200 ACFM and 1600 ug/ft^3, respectively. This corresponds to an influent mercury loading of 2765 g/day. The cost per pound of mercury removed was based on capital and O&M (operation and maintenance) costs over a 20 year period. This analysis assumes a mercury removal rate of 95% and continuous operation for both technologies and is solely based on economics. No attempt was made to assign a value to the risk associated with the handling, transport, and offsite disposal of mercury-laden waste for the case of activated carbon.

The costs associated with the STC technology are based on the actual full-scale installation described above. The costs associated with the activated carbon installation include a pre-heater and two beds of sulfur-impregnated activated carbon. The function of the pre-heater is to increase the temperature of the exhaust to about 100 °F in order to enhance mercury adsorption. The beds should be installed in series with provisions for bypass or reversal of flow to provide maximum utilization and reliability of the adsorption system (Anastas, 1976). The design of the carbon beds was based on a face velocity of 1 ft/s and space time of 8 s (Anastas, 1976; Klett, 2002). Thus, each carbon bed would be approximately 5 ft in diameter and 8 feet in height.

Capital Costs

The capital cost associated with the STC technology was based on the actual fabrication cost (in 2006 dollars) of the two full-scale reactors. This cost included support stands for the

reactors, associated electrical equipment (e.g., ballasts for UV lamps), and a PLC system, which allows the control room to remotely monitor the status of the reactor.

The capital cost for the carbon installation was based on the modular approach (Guthrie, 1974). This approach enables estimation of components of a chemical processing unit from known equipment costs using multipliers to adjust for design variations such as equipment configuration, material of construction and design pressure. A Marshall and Swift Index of 1250 was used to scale the cost data to 2006 dollars. Using this approach, the capital cost for the pre-heater and two carbon beds were estimated to be about $100,000.

O&M Costs

The operation and maintenance costs include those incurred annually for the following: (1) utilities (i.e., electricity), (2) operating labor, (2) maintenance materials and labor, and (3) taxes and insurance. The only utility needed for both technologies was electricity ($0.10/KWh). Labor cost was based on the 2006 Construction Cost Index wage of $31/hour. Maintenance materials and labor for operation and maintenance were based on reasonable assumptions for both technologies. Taxes and insurance were estimated to be 2.5% of the capital cost (Anastas, 1976).

The maintenance material costs for the STC technology were based on the cost to replace: (1) UV lamps and gaskets annually and (2) ballasts and STC pellets once every five years. Forty labor hours per year were included for maintenance. Operation costs included energy consumed by the UV lamps and blower. The number of regenerations per year, which varies based on influent mercury loading, was based on an STC capacity of 200 mg/g. The cost of acid and water was considered negligible since both are readily available at the facility. Four labor hours per regeneration were included in the operation costs. Costs associated with recycling the mercury back into the process was not incorporated into the analysis. Similarly, credit for mercury recovery was not included.

Replacement frequency of the carbon was based on an operational capacity of 100 mg/g (EPA, 1997b). Carbon replacement costs were estimated at $6.43 per pound and disposal was estimated to be $500 per ton (Klett et al., 2002). Operation costs for the carbon included that for the energy to power the blower. Maintenance materials and labor was estimated to be 2% of the capital cost per year (Anastas, 1976).

Economic Feasibility

The cost per pound of mercury removed was estimated for both technologies as a function of influent mercury loading, as shown in Figure 8-8. The cost per pound for the STC technology was lower than that for the activated carbon technology at influent mercury loadings greater than 149 g/day, which is the loading at which the STC and activated carbon cost curves intersect. Due to the uncertainty of the actual cost and performance associated with activated carbon installations, the error associated with the activated carbon costs may be as high as ± 30% (Anastas, 1976). Therefore, the difference in cost between the two technologies can only be considered significant for influent mercury loadings greater than about 470 g/day (i.e., the influent mercury loading at which the cost for the STC technology is more than 30% different that the cost for the activated carbon technology). At the design influent mercury loading of 2765 g/day, the cost per pound of mercury removed is about $20 for the STC technology and $84 for activated carbon. Thus, the STC technology is economically feasible at the design influent mercury loading. For the full-scale operation data presented in Table 8-2, the average influent mercury loading of the three runs was 357 g/day. At this loading rate, the economically favorable technology cannot be determined due to the uncertainty associated with the estimated cost of the activated carbon installation.

The shape of the cost curves is similar for the STC and activated carbon technologies. However, the dominate cost for the STC technology is that for the capital while, at influent

mercury loadings greater than about 300 g/day, O&M costs comprise a majority of the activated carbon costs. The cost of activated carbon replacement (material replacement and disposal fees only) is constant at $70 per pound of mercury removed. At low influent mercury concentrations, the activated carbon costs increase rapidly. This is because the fixed costs are not diluted with high mercury removal rates. Thus, the total cost per pound of mercury removed becomes highly dependent on the capital cost at lower influent loading rates.

Table 8-1. Summary of pilot experiments.

Test No.	Flow (ACFM)	Colburn j	Space time (s)	Influent (ug/ft^3)	Effluent (ug/ft^3)
1	10	0.106	0.53	762 ± 286	28 ± 16.3
2	8	0.122	0.67	652 ± 328	11.5 ± 7
3A	7.2	0.129	2.3	817 ± 203	2.9 ± 0.3
3B	7.2	0.129	2.3	817 ± 203	3.5 ± 1.2
4	3.6	0.183	4.6	550 ± 208	5.8 ± 4.5

Table 8-2. Full-scale performance data for three operation cycles.

Run No.	Operation Time (days)	Flow Rate (ACFM)	Influent (ug/ft^3)	Effluent (ug/ft^3)
A-1	29	682 ± 22	445 ± 75	204 ± 132
A-2	43	560 ± 140	595 ± 451	21.5 ± 23.8
B-1	28	400 ± 64	234 ± 116	10.8 ± 5.6

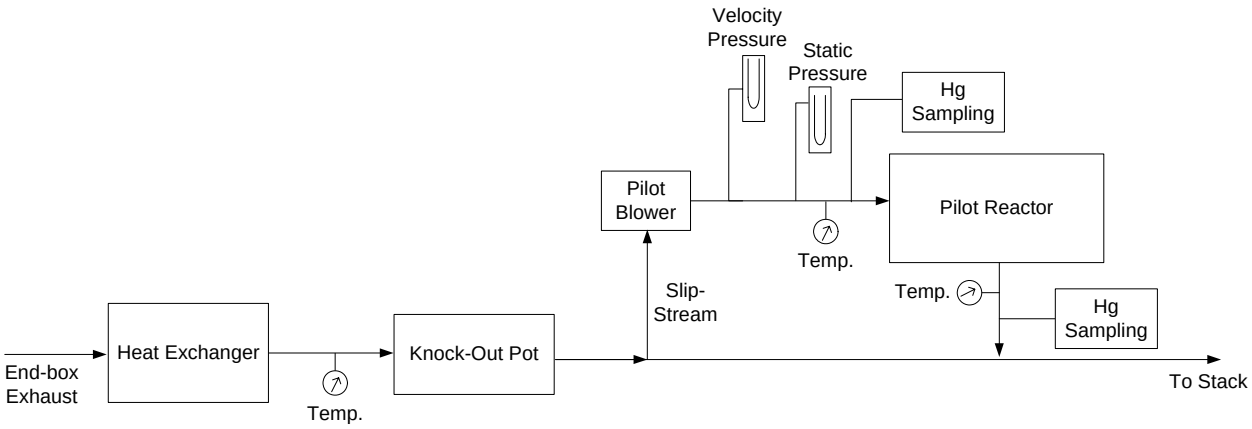

Figure 8-1. Process flow diagram for mercury recovery pilot studies.

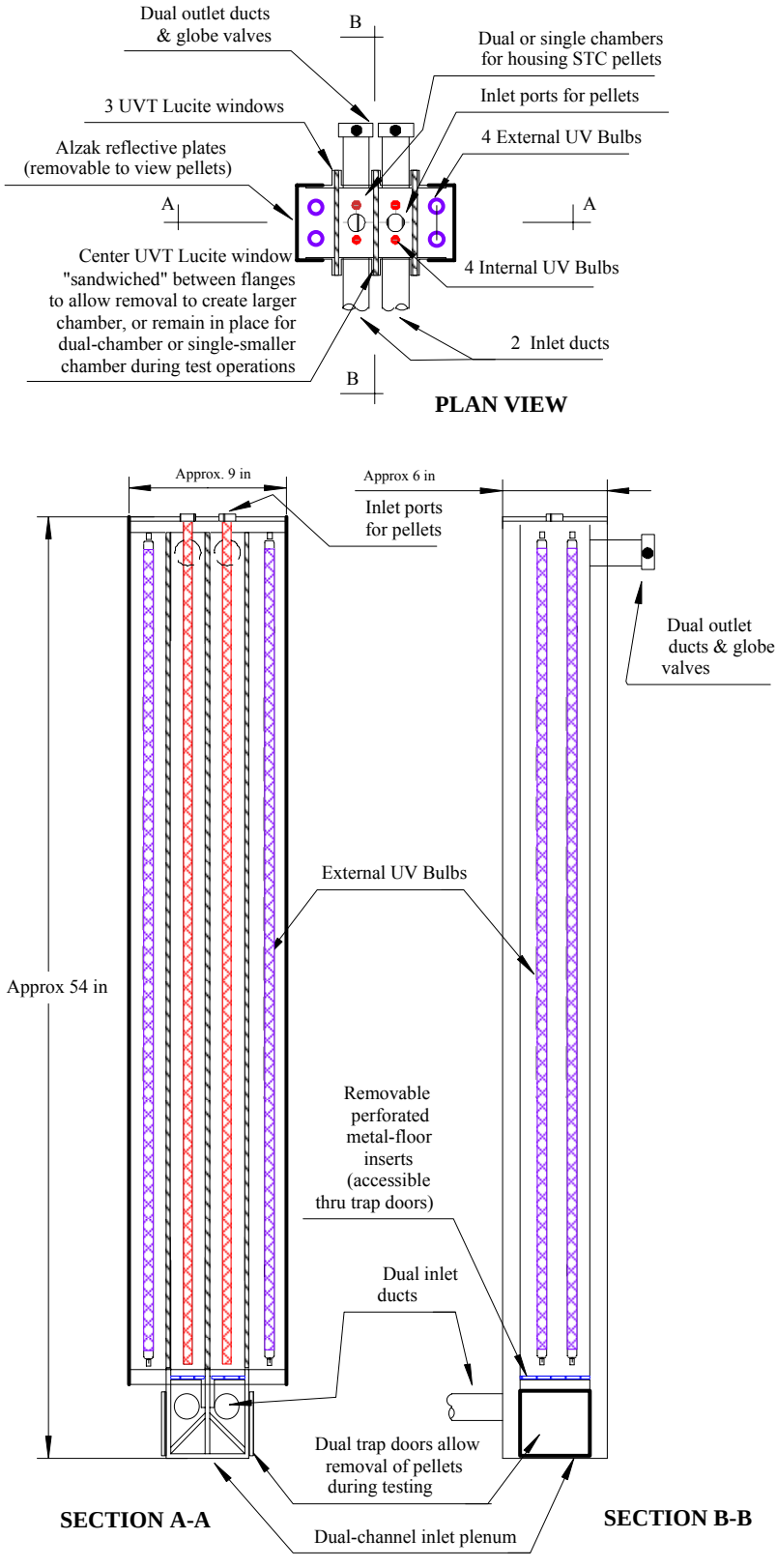

Figure 8-2. Schematic of pilot reactor for mercury recovery.

Figure 8-3. Photo of pilot reactor with UV lights illuminated.

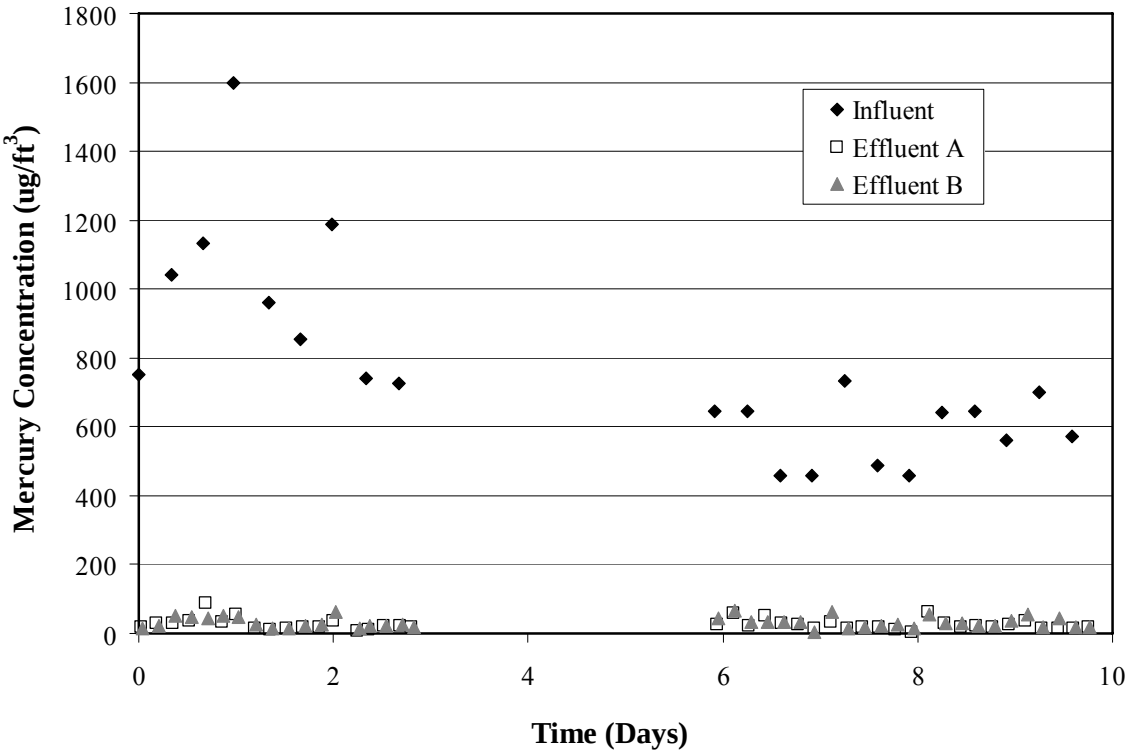

Figure 8-4. Influent and effluent mercury concentrations for the pilot reactor packed with virgin STC pellets (Test No. 1).

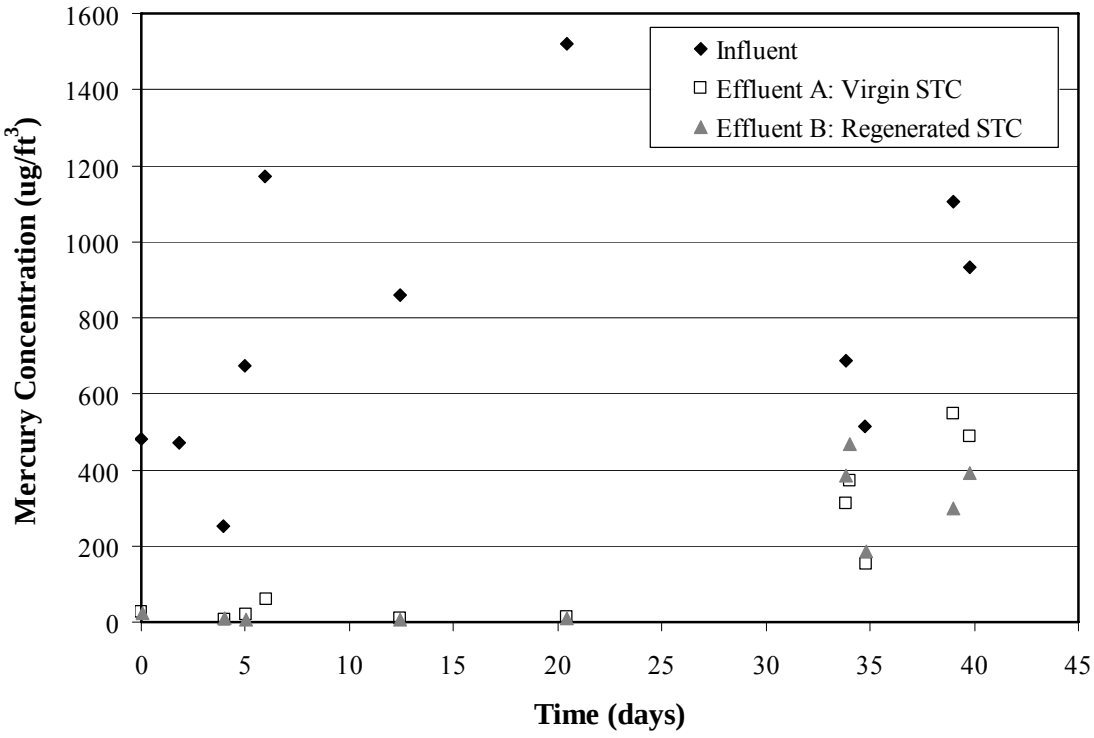

Figure 8-5. Influent and effluent mercury concentrations of the pilot reactor packed with virgin pellets (Chamber A) and regenerated pellets (Chamber B).

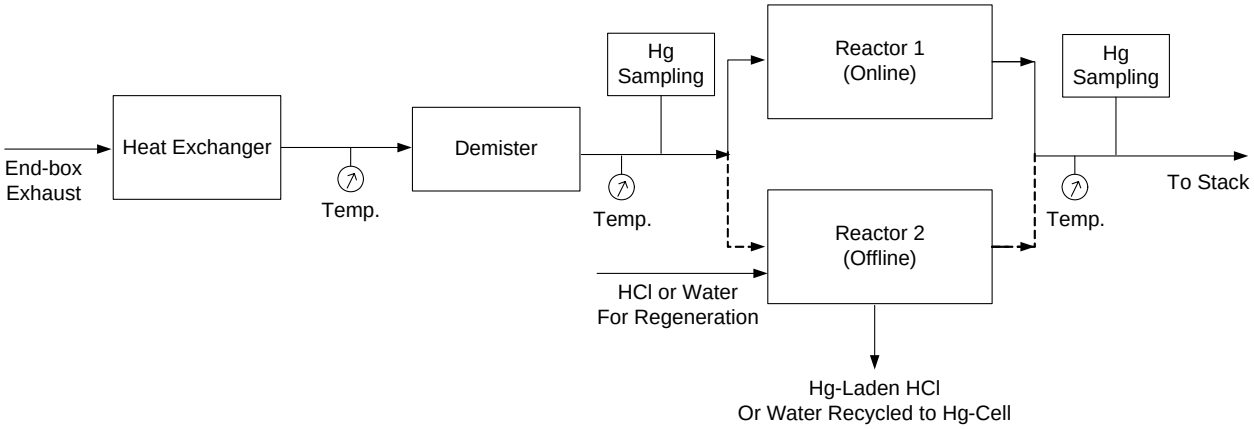

Figure 8-6. Process flow diagram for full-scale installation of mercury recovery units.

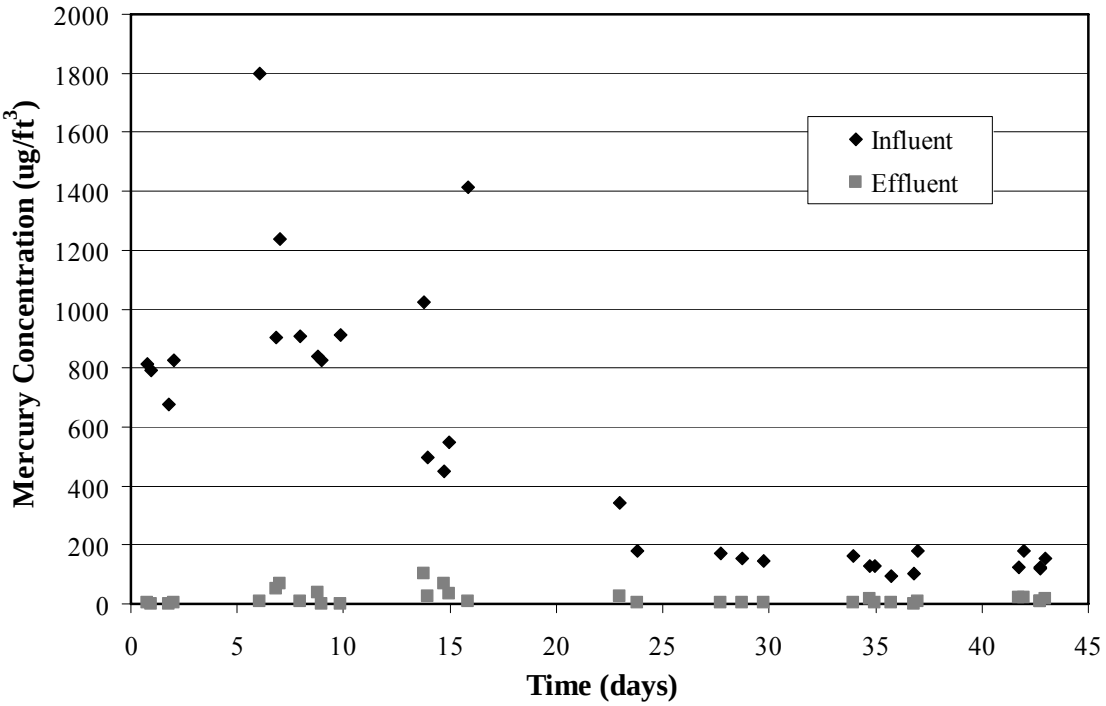

Figure 8-7. Influent and effluent concentrations for the full-scale reactor during its second adsorption cycle.

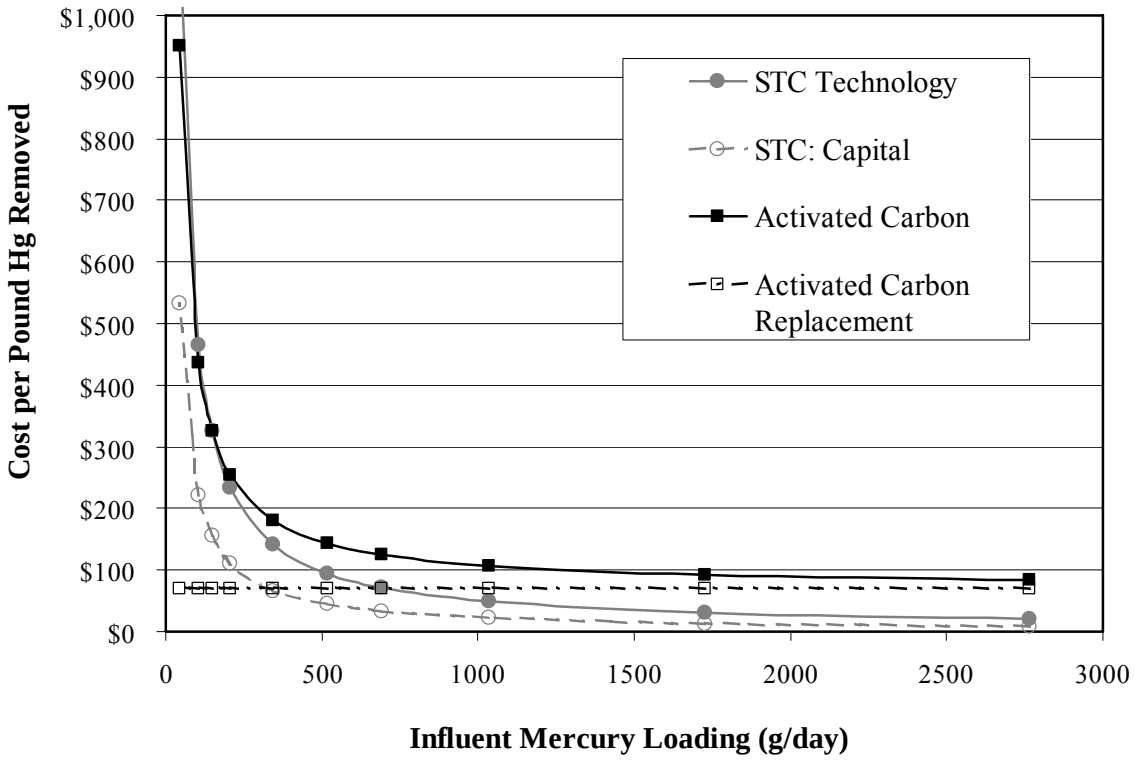

Figure 8-8. Comparison of cost per pound of mercury removed for activated carbon and STC as a function of influent mercury loading (for systems designed to treat up to 2765 g/day).

CHAPTER 9
CONCLUSIONS

STC pellets were synthesized using a sol-gel method with varying concentrations of HF and TiO_2. Mesoporous STC with varying pore volumes and surface areas were created. The performance of these STC for methanol removal was found to be a function of the surface area of the STC and space time of the gas in the reactor. The reaction kinetics were not limited by external or internal resistances to mass transfer. The 120 Å 12% and 260 Å 12% STC exhibited a lag time before achieving methanol mineralization, while the 50 Å 12% STC did not. All STC exhibited pseudo-first order reaction kinetics with a similar rate constant of 0.40 s^{-1}. The 50 Å STC were synthesized with varying TiO_2 loadings and the optimum loading was found to be 4%. Methanol oxidation was enhanced with the higher photon flux associated with using a UVC lamp rather than a UVA lamp. The bench-scale system reached steady state removal and was able to remove about 90% of the influent methanol with little byproduct formation (less than 1 ppm_v formaldehyde). When H_2S was introduced into the system, the H_2S competed with methanol resulting in a decrease in methanol removal efficiency to about 80%. Although the H_2S did not adsorb well to the STC surface, the H_2S was oxidized by the STC when illuminated with UV light to SO_2 and SO_4^{2-}. A pilot-scale reactor was designed and fabricated to treat 40 ACFM of humid air laden with 50 ppm_v of methanol. Pilot-scale studies showed about 66% methanol removal efficiency at steady state when the space time of the gas through the packed bed was 4.3 s. The methanol removal efficiency achieved in the pilot studies was less than that in the bench-scale studies because the UV light distribution within the packed bed was limited and elevated reaction temperatures likely inhibited the oxidation rate by decreasing the adsorption of methanol onto the STC and the efficiency of the UV lamps.

STC and TiO_2-coated AC were compared to TiO_2-coated glass spheres for the removal of methanol. In a low humidity environment (RH = 0.22%), the adsorption capacity of the STC (11 mg/g) was greater than that of TiO_2-coated AC (6 mg/g) and TiO_2-coated glass spheres. The silanol groups (Si-OH) on the STC surface promoted methanol adsorption in a low humidity gas stream, where competition with water vapor was low. When STC was irradiated with UV light, no methanol or oxidation byproducts were detected in the effluent. Formaldehyde, an oxidation byproduct of methanol, was detected in the effluent using TiO_2-coated AC and TiO_2-coated glass spheres. The TiO_2-coated AC showed that the limiting reaction in the mineralization of methanol was the oxidation of formaldehyde to formic acid. In a high humidity gas stream (RH = 95%), the adsorption capacity of the STC (1.2 mg/g) and TiO_2-coated AC (1.9 mg/g) was reduced due to the competition with water vapor for adsorption sites. The overall efficiency of the TiO_2-coated AC increased likely due to the presence of water vapor, which is required for the oxidation of formaldehyde to formic acid. The methanol adsorption capacity of the AC was greater than the STC in the high humidity gas stream since the surface chemistry of the AC was more heterogeneous than that of the STC, which was dominated by silanol groups that strongly adsorb water via hydrogen bonding. In the presence of UV light, the STC and TiO_2-coated AC reached a steady state methanol removal efficiency of 95%. Water vapor adsorption studies found that the surface coverage of water on the STC surface was greater than that on the TiO_2 surface and that the adsorption of water vapor on the STC was solely affected by the heat generated from the UV lamp. In a high humidity gas stream with a large annulus reactor, the STC and TiO_2-coated AC performed similarly, achieving 50% methanol removal compared to the TiO_2-coated glass spheres, which achieved 40% methanol removal. Thus, using an adsorbent material as a catalyst support in larger scale systems was beneficial. However, the use of silica

gel, which was transparent, versus AC, which was opaque, did not result in a difference in the photocatalytic oxidation rate in the 25 mm annulus reactor. This was likely due to the decrease in degradation efficiency associated with water competition on the STC surface, which was not as prevalent for the TiO_2-coated AC.

The series of pilot experiments performed a chlor-alkali facility confirmed the efficacy of the scale up of the STC technology for the removal of elemental mercury from end-box exhaust. The experiments showed that the reactor was able to consistently achieve 96% mercury removal in a variety of system conditions, including highly variable influent conditions (400 to 1600 ug/ft^3). In the range of flow rates tested, mercury removal rate was limited by space time and not mass transfer. An increase in space time between 0.53 s and 2.3 s yielded slight increases in mercury removal. However, longer space times did not result in a change in mercury removal. Regeneration with concentrated HCl was performed and proved to be effective. The regenerated pellets were successfully brought back online and performed similarly to virgin pellets. Two full-scale reactors were installed and performed similarly to the pilot-scale reactors. An economic analysis showed that the cost per pound of mercury removed was less for the STC technology than for sulfur impregnated activated carbon at influent mercury loading rates greater than 470 g/day. At lower influent loading rates, neither technology could be deemed economically favorable due to the uncertainty associated with the activated carbon cost estimate. Thus, the STC proved to be both technologically and economically feasible for this application.

Recommendations for future work are listed below:

- The competitive effects of adsorption and oxidation of VOCs in a multi-component system employing STC should be modeled since these systems will be more indicative of real-world applications;

- The transparency of STC containing various TiO_2 loadings should be quantified to better understand the relationship between the quantity of TiO_2 that is irradiated and oxidation efficiency;

- The effects of adsorption on H_2S oxidation efficiency should be studied in order engineer a composite that promotes the oxidation of H_2S to SO_4^{2-} rather than SO_2, which would need to be scrubbed from the gas before being released to the atmosphere.

As a result of this work, the following contributions to science were made:

- First to demonstrate that the oxidation efficiency of photocatalyst pellets for the degradation of a gaseous organic compound (methanol) was affected by material properties of the pellets (i.e., pore size and TiO_2 loading), photon flux, and space time of the gas through the reactor;

- First to model the rate of photocatalytic oxidation of gaseous methanol by photocatalyst pellets of various pore sizes using pseudo-first order equations and demonstrate that a lag time existed before mineralization proceeded, which was dependent on the internal surface area of the pellets;

- First to demonstrate that the limiting step in the mineralization of methanol differed depending on both the type of catalyst support and the humidity of the gas entering the reactor;

- Supported evidence that both SO_2 and SO_4^{2-} were formed as byproducts as a result of the photocatalytic oxidation of H_2S, which contrasts some studies that reported the formation of only SO_4^{2-};

- First to demonstrate that the oxidation efficiency of methanol decreased as a result of the competitive oxidation of H_2S in a humid gas stream and that the oxidation of H_2S was unaffected by the presence of methanol;

- First to implement a full-scale technology employing photocatalysis for the removal of mercury from gas-phase emissions in the chlor-alkali industry.

LIST OF REFERENCES

Al-Ekabi, H., Serpone, N., 1988. Kinetic studies in heterogeneous photocatalysis. 1. Photocatalytic degradation of chlorinated phenols in aerated aqueous solutions over TiO_2 supported glass matrix. J. Phys. Chem. 92, 5726-5731.

Alberici, R.M., Jardim, W.F., 1997. Photocatalytic destruction of VOCs in the as-phase using titanium dioxide. Appl. Catal. B – Environ. 14, 55-68.

Anastas, Y., 1976. Molecular sieve mercury control processes in chlor-alkali plants, EPA-600/2-76-014. U.S. Government Printing Office, Washington D.C.

Anderson, C., Bard, A., 1997. Improved photocatalytic activity and characterization of mixed TiO_2/SiO_2 and TiO_2/Al_2O_3 Materials. J. Phys. Chem. 101, 2611-2616.

Arana, J., Dona-Rodriguez, J., Cabo, C., Gonzalez-Diaz, O., Herrara-Melian, J., Perez-Pena, J., 2004. FTIR study of gas-phase alcohols photocatalytic degradation with TiO_2 and AC-TiO_2. Appl. Cataly. B – Environ. 53, 221-232.

Byrne, H., Kostedt, W., Stokke, J., Mazyck, D., 2008. Characterization of HF-catalyzed silica gels doped with Degussa P25 Titanium Dioxide. Submitted to J. Non-Cryst. Solids.

Canela, M., Alberici, R., Jardim, W., 1998. Gas-phase destruction of H_2S using TiO_2/UV-Vis. J. Photochem. Photobiol. A 112, 73-80.

Chang, H., Wu, N., Zhu, F., 2000. A kinetic model for photocatalytic degradation of organic contaminants in a thin-film TiO_2-catalyst. Wat. Res. 34, 407-416.

Chen, J., Ollis, D., Rulkens, W., Bruning, H., 1999. Photocatalyzed oxidation of alcohols and organochlorides in the presence of native TiO_2 and metallized TiO_2 suspensions. Part (II): Photocatalytic mechanisms. Wat. Res. 33, 669-676.

Chu, W., Wong, C., 2004. Study of herbicide alachlor removal in a photocatalytic process through the examination of the reaction mechanism. Ind. Eng. Chem. Res. 43, 5027.

D'Itri, F., Andren, A., Doherty, R., Wood, J., 1978. An Assessment of Mercury in the Environment. National Academy of the Sciences, Washington, D.C.

Devilliers, D., 2006. Semiconductor photocatalysis: Still an active research area despite barriers to commercialization. Energia, 17, 1-3.

Dijkstra, M., Panneman, H., Winkelman, J., Kelly, J., Beenackers, A., 2002. Modeling the photocatalytic degradation of formic acid in a reactor with immobilized catalyst. Chem. Eng. Sci. 57, 4895-4907.

Doucet, N., Bocquillon, F., Zahraa, O., Bouchy, M., 2006. Kinetics of photocatalytic VOCs abatement in a standardized reactor. Chemosphere 65, 1188.

Ferguson, M., Hoffmann, M., Hering J., 2005. TiO_2-photocatalyzed As(III) oxidation in aqueous suspensions: reaction kinetics and effects of adsorption. Environ. Sci. Technol. 39, 1880-1886.

Gao, X., Wachs, I., 1999. Titania-silica as catalysts: molecular structural characteristics and physico-chemical properties. Catal. Today 51, 233-254.

Garner, J., 2001. Air emission control regulations pose new challenges for mills. Pulp and Paper 75, 44-46.

Garton, M.J., 2005. Photocatalytic oxidation of selected organic contaminants and inactivation of microorganisms in a continuous flow reactor packed with titania-doped silica. Masters Thesis, University of Florida.

Guthrie, K., 1974. Process plant estimating, evaluation, and control. Craftsman Book Co. of America, Solana Beach, CA. pp 1-604.

Hoffmann, M.R., Martin, S.T., Choi, W., Bahnemann, D.F., 1995. Environmental applications of semiconductor photocatalysis. Chem. Rev. 95, 69-96.

Holmes, F., 2003. The performance of a reactor using photocatalysis to degrade a mixture of organic contaminants in aqueous solution. Masters Thesis, University of Florida.

Huang, M., Tso, E., Datye, E., Prairie, M., Stange, B., 1996. Removal of silver in photographic processing waste by TiO_2-based photocatalysis. Environ. Sci. Technol. 30, 3084-3088.

Hurum, D., Agrios, A., Gray, K., Rajh, T., Thurnauer, M., 2003. Explaining the enhanced photocatalytic activity of Degussa P25 mixed-phase TiO_2 using EPR. J. Phys. Chem. B 107, 4545-4549.

Kataoka, S., Lee, E., Tejedor-Tejedor, I., Anderson, M., 2005. Photocatalytic degradation of hydrogen sulfide and in situ FT-IR analysis of reaction products on surface TiO_2. Appl. Catal. B – Environ. 61, 159-163.

Kato, S., Hirano, Y., Iwata, M., Sano, T., Takeuchi, K., Matsuzawa, S., 2005. Photocatalytic degradation of gaseous sulfur-deposited titanium dioxide. Appl. Catal. B – Environ. 57, 109-115.

Khan, A., 2006. Modification of activated carbon to improve aqueous manganese removal. PhD Dissertation, University of Florida.

Kim, B.S., Hong, C.S., 2002. Kinetic study for photocatalytic degradation of volatile organic compounds in air using thin film TiO_2 photocatalyst. Appl. Catal. B – Environ. 35, 305-315.

Klett, M., Maxwell, R., Rutkowski, M., 2002. The cost of mercury in an IGCC Plant (final report). Prepared for The United States Department of Energy National Energy Technology Laboratory.

Knudsen, J., Hottel, H., Sarofim, A., Wankat, P., Knaebel, K., 1999. Mass transfer. In: Green, D., Maloney, J., Perry, R. (Eds.), Perry's Chemical Engineer's Handbook. McGraw Hill, New York. pp 72-74.

Lee, T., Biswas, P., Hedrick, E., 2001. Comparison of Hg^o capture efficiencies of three in situ generated sorbents. Env. Energy Eng. 47, 954-961.

Lee, T., Biswas, P., Hedrick, E., 2004. Overall kinetics of heterogeneous elemental mercury reactions on TiO_2 sorbent particles with UV irradiation. Ind. Eng. Chem. Res. 43, 1411-1417.

Levenspiel, O., 1999. Pore diffusion resistance. In: Chemical Reaction Engineering, third ed. John Wiley & Sons, New York, pp. 470-477.

Li, Y., Wu, C.Y., 2007. Kinetic study for photocatalytic oxidation of elemental mercury on a SiO_2-TiO_2 nanocomposite. Environ. Eng. Sci. 24, 3-12.

Li, Y., Wu, C.Y., 2006. Role of moisture in adsorption, photocatalytic oxidation, and reemission of elemental mercury on a SiO_2-TiO_2 nanocomposite. Environ. Sci. Technol. 40, 6444-6448.

Lichtin, N., Avudaithai, M., Berman, E., Dong, J., 1994. Photocatalytic oxidative degradation of vapors of some organic compounds over TiO_2. Res. Chem. Intermed. 20, 755-781.

Londeree, D., 2002. Silica-titania composites for water treatment. Masters Thesis, University of Florida.

Lu, M., Chen, J., Chang, K., 1999. Effect of adsorbents coated with titanium dioxide on the photocatalytic degradation of propoxur. Chemosphere 38, 617-627.

Ludwig, C., Mazyck, D., Chadik, P., Stokke, J., 2008. The performance of silica-titania carbon composites for photocatalytic degradation of gray water. Submitted to J. Env. Eng.

Minero C., Catozzo, F., Pelizzetti, E., 1992. Role of adsorption in photocatalyzed reactions of organic molecules in aqueous TiO_2 suspensions. Langmuir 8, 481-486.

National Council for Air and Stream Improvement, Inc. (NCASI), 1998. Method CI/SG/PULP 94.02 chilled impinger/silica gel tube test method at pulp mill sources for methanol, acetone, acetaldehyde, methyl ethyl ketone and formaldehyde, methods manual (03.B.003). NCASI, Research Triangle Park, NC.

Nguyen, V., Amal, R., Beydoun, D., 2003. Effect of formate and methanol on photoreduction/ removal of toxic cadmium ions using TiO_2 semiconductor as photocatalyst. Chem. Eng. Sci. 58, 4429-4439.

Nguyen, V., Beydoun, D., Amal, R., 2004. Photocatalytic reduction of selenite and selenate using TiO_2 photocatalyst. J. Photochem. Photobiol. A 171, 117-124.

Morrow, B., Gay, I., 2000. Infrared and MNR characterization of the silica surface. In: Papirer, E. (ed.), Adsorption on Silica Surfaces. Marcel Dekker, Inc., New York, pp. 9-61.

Murov, S., Carmichael, I., Hug, M., 1993. Potassium ferrioxalate actinometry. In: Handbook of Photochemistry. Mercel Dekker, New York, pp. 299-305.

Noguchi, T., Fujishima, A., Sawunyama, P., Hashimoto, K., 1998. Photocatalytic degradation of gaseous formaldehyde using TiO_2 film. Environ. Sci. Technol. 32, 3831-3833.

Nawrocki, J., 1997. The silanol group and its role in liquid chromatography. J. Chromatogr. A 779, 29-71.

Obee, T., Brown, R., 1995. TiO_2 photocatalysis for indoor air applications: Effect of humidity and trace contaminant levels on oxidation rates of formaldehyde, toluene, and 1,3-butadiene. Environ. Sci. Technol. 29, 1223-1232.

Ollis, D., Pelizzetti, E., Serpone, N., 1991. Destruction of water contaminants. Environ. Sci. Technol. 25, 1523-29.

Parida, S., Dash, S., Patel, S., Mishra, B., 2006. Adsorption of organic molecules on the silica surface. Adv. Colloid Interfac. 121, 77-110.

Pavlish, J., Sondreal , E., Mann, M., Olson, E., Galbreath, K., Laudal, D., Benson, S., 2003. Status Review of Mercury Control Options for Coal-fired Power Plants. Fuel Process. Technol. 82, 89-165.

Peral, J., Domenech, X., Ollis, D., 1997. Heterogeneous photocatalysis for purification, decontamination and deodorization of air. J. Chem. Technol. Biotechnol. 70, 117-140.

Pitoniak, E., Wu, C. Y., Londeree, D., Mazyck, D., Bonzongo, J.D., Powers, K., Sigmund, W., 2003. Nanostructured silica-gel doped with TiO_2 for Hg vapor control. J. Nanopart. Res. 5, 282-292.

Pitoniak, E., 2004. Evaluation of nanostructured silica-titania composites in an adsorption/ photocatalytic oxidation system for elemental mercury vapor control. Master of Engineering Thesis, University of Florida.

Pitoniak, E., Wu, C. Y., Powers, K. W., Sigmund, W., 2005. Adsorption enhancement mechanisms of silica-titania nanocomposites for elemental mercury vapor removal. Environ. Sci. Technol. 39, 1269-1274.

Portela, R. Sanchez, B., Coronado, J., Candal, R., Suarez, S., 2007. Selection of TiO_2-support: UV transparent alternatives and long-term use limitations for H_2S removal. Catal. Today 129, 223-230.

Puri, B., 1970. Surface complexes on carbons. In: Walker, P. (Ed.), Chemistry and Physics of Carbon. Marcel Dekker, New York, pp. 194-247.

Rodriguez, S., Almquist, C., Lee, T., Furuuchi, M., Hedrick, E., Biswas, P., 2004. A mechanistic model for mercury capture with in situ-generated titania particles: Role of water vapor. J. Air & Waste Manage. Assoc. 54, 149-156.

Satterfield, C., 1970. Mass transfer in heterogeneous catalysis. MIT Press, Cambridge, MA.

Schettler, T., 2001. Toxic threats to neurological development of children. Environ. Health Persp. Supplements 109, 813-817.

Serpone, N., 1995. Brief introductory remarks on heterogeneous photocatalysis. Sol. Energ. Mat. Sol. C. 38, 369-379.

Shul, Y., Kim, H., Haam, S., Han, H., 2003. Photocatalytic characteristics of TiO_2 supported on SiO_2. Res. Chem. Intermed. 29, 849-859.

Sing, K., Everett, D., Haul, R., Moscou, L., Pierotti, R., Rouquerol, J., Siemieniewska, T., 1984. Reporting physisorption data for gas/solid systems. Pure Appl. Chem. 57, 603-619.

Someshwar, A., 1994. NCASI technical bulletin 678: Volatile organic emissions from pulp and paper mill sources part IV – kraft brownstock washing, screening, and rejects refining sources. National Council for Air and Stream Improvement, Research Triangle Park, NC.

Sopyan, I., 2007. Kinetic analysis on photocatalytic degradation of gaseous acetaldehyde, ammonia and hydrogen sulfide on nanosized porous TiO_2 films. Sci. Technol. Adv. Mat. 8, 33-39.

Southworth, G.R., Lindberg, S.E., Zhang, H., Anscombe, F.R., 2004. Fugitive mercury emissions from a chlor-alkali factory: sources and fluxes to the atmosphere. Atmos. Environ. 38, 597-611.

Thommes, M., 2004. Physical adsorption characterization of ordered and amorphous mesoporous materials. In: Lu, G., Zha, X. (Eds), Nanoporous Materials: Science and Engineering. Imperial College Press, London, pp. 317 – 364.

Torimoto T, Ito S, Kuwabata S, Yoneyama H., 1996. Effects of adsorbents used as supports for titanium dioxide loading on photocatalytic degradation of propyzamide. Environ. Sci. Technol. 30, 1275-1281.

Travert, A., Manoilova, O., Tsyganenko, A., Mauge, F., Lavalley, J., 2002. Effect of hydrogen sulfide and methanethiol adsorption on acidic properties of metal oxides: An infrared study. J. Phys. Chem. B 106, 1350-1362.

Tsumura, T., Kojitani, N., Umemura, H., Toyoda, M., Inagaki, M., 2002. Composites between photoactive anatase-type TiO_2 and adsorptive carbon. Appl. Surface Sci. 196, 429-436.

Tsuru, T., Kan-no, T., Yoshioka, T., Asaeda, M., 2003. A photocatalytic membrane reactor for gas-phase reactions using porous titanium oxide membranes. Catal. Today 82, 41-48.

Turchi, C., Ollis, D., 1989. Mixed reactant photocatalysis: Intermediates and mutual rate inhibition. J. Catal. 119, 483-496.

Turchi, C., Ollis, D., 1990. Photocatalytic degradation of organic water contaminants: Mechanisms involving hydroxyl radical attack. J. Catal. 122, 178-192.

Uchiyama, H., Suzuki, K., Oaki, Y., Imai, H., 2005. A novel adsorbent photocatalyst consisting of titania and mesoporous silica nanoparticles. Mat. Sci. Eng. B - Solid 123, 248-251.

U.S. Environmental Protection Agency, 1997a. Mercury Study Report to Congress Volume IV: An Assessment to Exposure to Mercury in the United States, EPA-452/R-97-006. U.S. Government Printing Office, Washington D.C.

U.S. Environmental Protection Agency, 1997b. Mercury Study Report to Congress Volume VIII: Evaluation of Mercury Control Technologies and Cost, EPA-452/R-97-010. U.S. Government Printing Office, Washington D.C.

Varma, V., 2003. Experience with the collection, transport, and burning of kraft mill high volume low concentration gases, Technical bulletin 03-03. National Council for Air and Stream Improvement, Gainesville, FL.

Vohra, M., Tanaka, K., 2003. Photocatalytic degradation of aqueous pollutants using silica-modified TiO_2. Water Res. 37, 3992-3996.

Wu, C.Y., Lee, T.G., Tyree, G., Arar, E., Biswas, P., 1998. Capture of mercury in combustion systems by in situ generated titania particles with UV irradiation. Environ. Eng. Sci. 15, 137-148.

Xu, Y., Zheng, W., Liu, W., 1997. Enhanced photocatalytic activity of supported TiO_2: dispersing effect of SiO_2. J. Photochem. Photobiol. A 122, 57-60.

Yang, C., Chen, C., 2005. Synthesis and characterization of silica-capped titania nanorods: An enhanced photocatalyst. Appl. Catal. A – General 294, 40-48.

Yamakata, A., Ishibashi, T., Onishi, H., 2003. Effects of water addition on the methanol oxidation on Pt/TiO_2 photocatalyst studied by time-resolved infrared absorption spectroscopy. J. Phys. Chem. B 107, 9820-9823.

Yong, T., Schwartz, S., Wu, C.Y., Mazyck, D.W., 2005. Development of TiO_2/AC composite by dry impregnation for the treatment of methanol from humid air streams. Ind. Eng. Chem. Res. 44, 7366-7372.

BIOGRAPHICAL SKETCH

Jennifer Stokke was born to Susan and Wayne Stokke on August 26, 1981. She grew up in Tarpon Springs, FL and graduated from East Lake High School in 1999. She then moved to Gainesville in 1999 to attend the University of Florida, where she studied environmental engineering and graduated with highest honors in December of 2003. During her last year as an undergraduate, Jennifer began a research project focusing on the purification of gaseous emissions. She continued this work during her graduate studies at the University of Florida under the guidance of Dr. David Mazyck.